National Library of Canada
Acquisitions and Bibliographic Services Branch
395 Wellington Street
Ottawa, Ontario
K1A 0N4

Bibliothèque nationale du Canada
Direction des acquisitions et des services bibliographiques
395, rue Wellington
Ottawa (Ontario)
K1A 0N4

Your file Votre référence

Our file Notre référence

NOTICE

The quality of this microform is heavily dependent upon the quality of the original thesis submitted for microfilming. Every effort has been made to ensure the highest quality of reproduction possible.

If pages are missing, contact the university which granted the degree.

Some pages may have indistinct print especially if the original pages were typed with a poor typewriter ribbon or if the university sent us an inferior photocopy.

AVIS

La qualité de cette microforme dépend grandement de la qualité de la thèse soumise au microfilmage. Nous avons tout fait pour assurer une qualité supérieure de reproduction.

S'il manque des pages, veuillez communiquer avec l'université qui a conféré le grade.

La qualité d'impression de certaines pages peut laisser à désirer, surtout si les pages originales ont été dactylographiées à l'aide d'un ruban usé ou si l'université nous a fait parvenir une photocopie de qualité inférieure.

Canada

Sieving of Spherical Particles during Gel Electrophoresis: A New Computer Simulation Algorithm

by

Hong L. Guo

Thesis submitted to
The School of Graduate Studies and Research of
The University of Ottawa
in partial fulfilment of the requirements for the degree of

Master of Science in Physics

Department of Physics
Faculty of Science
University of Ottawa

ISBN 0-612-00532-1

Canada

UNIVERSITÉ D'OTTAWA
UNIVERSITY OF OTTAWA

Acknowledgements

First of all, I would like to express my sincere thanks to my supervisor, Dr. Gary W. Slater, for introducing me to the exciting field of the computer simulation of electrophoretic sieving, for his skilled, patient and systematic guidance, and for his painstaking arrangement of the financial support. I highly enjoy having the opportunity to work with Gary, whose superb intuition to physics and unremitting pursuit of knowledge extremely impress me, and whose professionalism and enthusiasm are for me a model.

Thanks go to Yang Cai and her family for their disinterested assistance in both physics and daily life. Yang has set up an example of being modest, forbearing and tenacious.

Thanks go to Zi-Cong Zhou from whom I learn a lot, not only about mathematics, physics and computer language, but also about what a scientist should possess.

Thanks go to my friend and colleague Grant I. Nixon, for taking time to polish the English of this thesis, for his valuable discussions about chain dynamics, and for his help with many other things. As a good researcher, Grant is very enthusiastic and easy to get along with.

Thanks go to my friend and colleague Sylvain Hubert, for his significant help in solving the Fokker-Planck equation.

Thanks go to my friend and colleague Claude Desruisseaux for his discussion and explanation about streptavidin-DNA electrophoresis, and for his excellent teaching of English.

Thanks go to my friend Robert Parent, for his useful discussions about diffusion problems.

Acknowledgements

Besides, I would like to take this opportunity to thank the School of Graduate Stdudies and Research of the University of Ottawa for awarding me the Tuition Fee Waiver scholarship for the 1992-93 academic year.

Finally, I would like to thank my wife Yu-Ye Li. Without her deep love and constant support, I would not have been able to reach the end of this work.

Abstract

A new computer simulation algorithm is developed to study the behavior of a hard sphere during gel electrophoresis. The electrophoretic mobility and the diffusion coefficients are presented to show the effects of the field intensity, of the gel concentration, and of the randomness of the gel. The results indicate that previous models are not applicable for either the periodic or the random gel, and that the Einstein relation does not hold because the gel molecules affect the dynamics of the hard sphere. Moreover, the randomness of sieving gels lead to a trapping effect where the longitudinal diffusion coefficient is much larger than expected when the gel is dense and the field intensity is non-negligible. This trapping effect predicts a limit to both the field intensity and the gel concentration that one can use for the separation of particles during gel electrophoresis. Our new algorithm thus opens a door to a detailed study of the process of electrophoretic sieving with potential applications in biology and biotechnology.

Contents

Acknowledgements i

Abstract iii

Contents iv

Chapter 1 Introduction 1

1.1 Electrophoresis of spheres 1

1.2 Migration of spheres 3

1.3 Diffusion during electrophoresis 3

1.4 Trapping 6

1.5 A new algorithm 10

Chapter 2 Theory and algorithm 12

2.1 The Ogston model 12

2.2 The Einstein relation 12

2.3 One-dimensional biased random walks 13

2.3.1 Free motion 14

2.3.2 With obstacles 19

2.4 The new algorithm 20

2.5 Implementation to computer simulations 28

Chapter 3 Simulation of periodic systems 30

3.1 Implementation 31

3.2 Drift in a free solution 33

3.3 Zero-field diffusion: with obstacles 36

3.4 Effect of electric fields 38

3.5 Effect of obstacles 41

Chapter 4 Simulation of random systems 50

4.1 Implementation 51

4.2 Zero-field diffusion 52

4.3 Effect of electric fields 57

4.4 Effect of obstacles 66

Chapter 5 Conclusions and Discussions 74

Appendix One-Dimensional Brownian Motion 76

A.1 Two absorbing walls 76

A.2 One absorbing and one reflecting wall 84

References 89

Chapter 1

Introduction

1.1 Electrophoresis of Spheres

Gel electrophoresis was initially developed to fractionate protein molecules. It is generally assumed that proteins, like bacteriophages and viruses, are usually ball-like and have an effective radius, provided they are not fibrous. To seperate those proteins by gel electrophoresis, mixtures of different kinds of proteins are layered within a narrow zone on the surface of a gel (such as a polyacrylamide gel). After layering, an electric field is used to drive the proteins through the gel.

During electrophoresis, each protein forms a separate band which is broadened by diffusion (see Fig. 1.1). The speed of migration is determined primarily by the average electric charge of the protein and the kinetic resistance of the gel to the motion (the later is called sieving). In principle, one can determine the radius of a protein by obtaining the electrophoretic mobility of migration which is defined as the drift velocity of proteins (caused by the electric field) divided by the intensity of the field applied. Alternatively, from the radius of the protein, one can deduce the effective pore size of the gel, estimate the structure of the gel, and furthermore, understand the dynamics of the motion of macromolecules in fibrous gel networks.

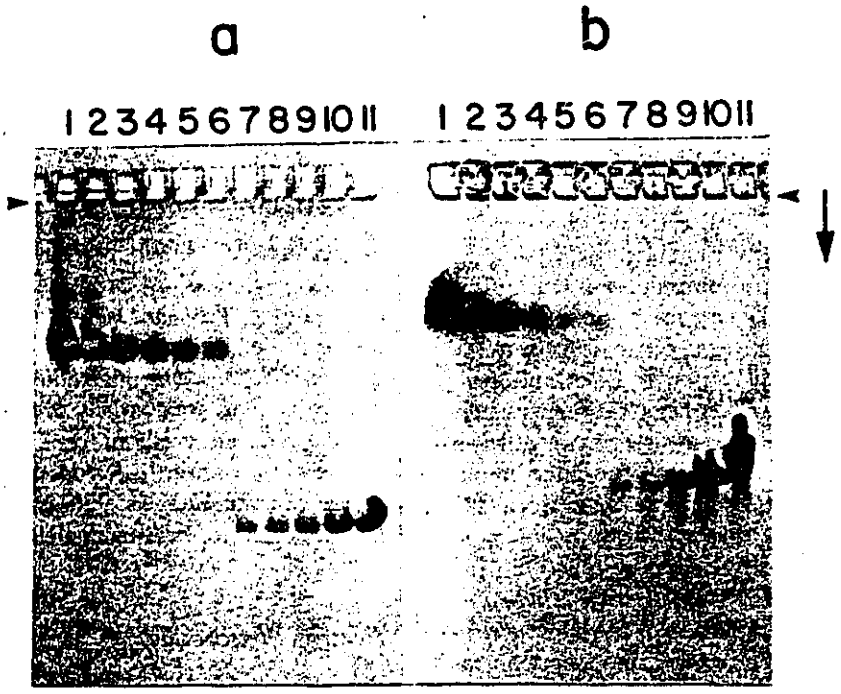

Figure 1 Agarose gel electrophoresis of bacteriophages fd-WT and T3 as a function of sample concentration and agarose percentage. Twenty microliter amounts of bacteriophages T3 and fd-WT were subjected to electrophoresis in agarose gels with an agarose percentage value of (a) 1.8 and (b) 0.4, as described in the Materials and Methods. The times of electrophoresis for (a) and (b) were, respectively, 26 and 10 h. The concentrations of sample were as follows (bacteriophage, followed by μg of protein/cm^2): (1) T3, 440; (2) T3, 220; (3) T3, 110; (4) T3, 54; (5) T3, 26; (6) T3, 16; (7) fd-WT, 16; (8), fd-WT, 26; (9) fd-WT, 54; (10) fd-WT, 110; and (11) fd-WT, 220. The arrow indicates the direction of electrophoresis; the arrowheads indicate the origins of electrophoresis. The cathode is at the top. Minor bands observed for both T3 and fd-WT are presumed to be aggregates (see the text).

Figure 1.1 Agarose gel electrophoresis of spheres[8]

1.2 Migration of Spheres

The separation mechanisms of gel electrophoresis are not fully understood at the microscopic level. For spherical macromolecules or objects, the controlling mechanism is often referred to as sieving, a concept developed for the pore size distributions in random arrays of long fibres. Based on the Poisson distribution, Ogston[18, 34] derived the probability that a sphere can be placed in a random fibre network. This probability yields an exponential function of the concentration of fibres. Morris[14], Rodbard and Chrambach assumed[21, 36] that the sieving reduces the magnitude of a sphere's electrophoretic mobility by a factor equal to the Ogston probability. If the fibres are assumed to be cylindrical, randomly oriented, and longer than the object sieved, the consequence of this assumption is that the Ferguson plot (logarithmic mobility vs. gel concentration) is linear.

Experimental data are frequently analyzed by using Ferguson plots to get a satisfactary description of the electrophoretic mobility. However, Ferguson plots are found to be, according to Serwer's results[7, 8], rarely linear (see Fig. 1.2). Based on their computer simulation results, Slater and Guo[32] indeed reported that the mobility is no longer a simple function of the fractional volume available to the particle even in a simple "periodic" gel.

1.3 Diffusion during Electrophoresis

The problem of a large particle diffusing in solution was originally studied by Einstein[3] at infinite dilution. In this limit, the interactions between the large particles can be neglected and

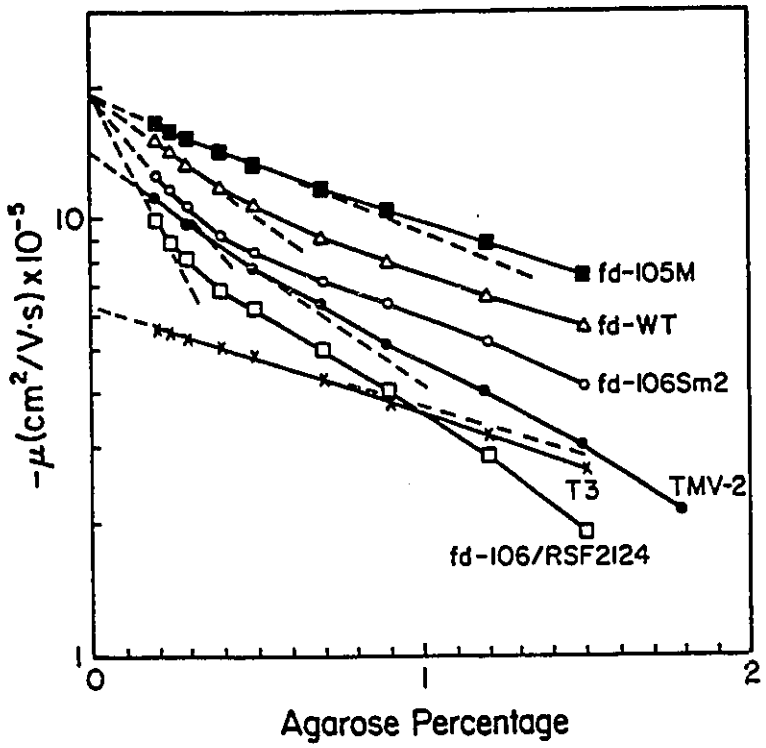

Figure 4 Ferguson plots. Ferguson plots for the particles indicated at the right were made by procedures described in Materials and Methods. All particles, except fd-105M and TMV-2, were analyzed in the same multigel. The data for fd-105M and TMV-2 were obtained from independent multigels.

Figure 1.2 Mobility vs. concentration[8] (Ferguson plots)

the interaction between a large particle and solvent molecules can be replaced by a randomly fluctuating force. The problem can then be solved by the Fokker-Planck equation (which reduces to the Fick diffusion equation in the absence of external fields), or by the Langevin equation. The well-known Einstein relation between the friction coefficient and the diffusion coefficient was thus deduced from Fick's and Langevin's equations.

To separate proteins or other macromolecules, a gel is then added to the solvent. One must then study the diffusion of a large particle among other large particles (or among the network of worm-like fibres, if a gel molecule does not form a coil) in addition to the small solvent molecules. In this case, a rigorous solution to the Smoluchowsky equation, which is effective in dealing with interactions between large particles, proves to be very difficult[10]. (This is mainly why we need to carry on computer simulations). Several gel models[1] (hard sphere, thin rod, flexible chain, etc.) have been proposed in order to calculate the electrophoretic mobility and the diffusion coefficient. In this thesis, we focus on a two-dimensional version of the hard sphere gel model.

Theoretical[15], experimental[19] and computational[23-26, 11, 12, 20, 16] works on diffusion have been done when there are no external fields. Nieuwenhuizen's theoretical calculation[15] indicates that the diffusion coefficient is related to the gel concentration through a quadratic function if the obstacles are randomly distributed (percolation lattice of obstacles). Phillies[19] fits his experimental data to a stretched exponential, i.e. to an exponential function of the concentration of obstacles to some fractional exponential power. Saxton's Monte-Carlo simulation results[23-26] gave different relationships between the diffusion coefficient and the concentration, depending

on the choice of model and type of lattice used (see Fig. 1.3).

In gel electrophoresis, where an external electric field is applied, one wishes to get sharp molecular bands (i.e., a large value of migration distance which is due to the electric field, but a small band brodening which is due to the thermal diffusion) in order to get a good molecular separation. However, the experimental determination of the diffusion coefficient during gel electrophoresis is very difficult. Scientists instead measure the mobility, which is easier to obtain, and then assume that the Einstein relation, a linear relationship between the diffusion coefficient and the mobility, holds during gel electrophoresis.

Recently, Slater[31] reported that the Einstein relation does not apply to DNA gel electrophoresis since it is intrinsically a non-equilibrium process. Slater and Guo[32] also reported that, for the electrophoretic seiving of spheres through a simple "periodic" gel, the Einstein relation is invalid even if the field intensity is very small.

1.4 Trapping

The gel molecules may form geometric structures such as fjords, bays, lakes, straits, ..., and so on (see Fig. 1.4). Such structures affect both the migration and the diffusion (both parallel and perpendicular to the direction of the field) of the particles to be sieved. A significant effect is due to trapping: an electric field may cause those large particles to be sterically trapped in the gel[27] (see Fig. 1.5). In such a case, the only means by which the trapped particle may get out of the trap is through Brownian thermal motion, but the probability of escape is small due to the existence of the electric field, especially for high field intensities. Similar phenomena occur in

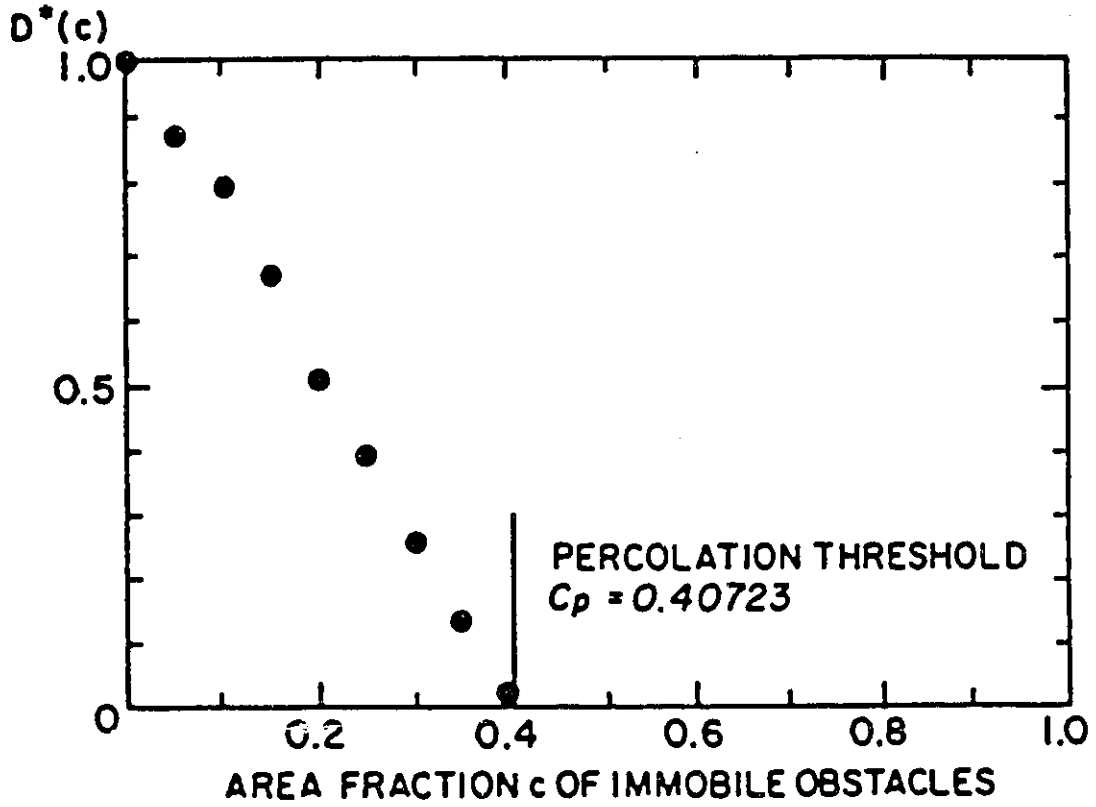

FIGURE 2 Diffusion constant $D^*(c)$ of point tracers as a function of area fraction c of point immobile obstacles on the square lattice.

Figure 1.3 Diffusion coefficient vs. concentration[23]

FIGURE 2 Electron microscopy at higher magnification. Electron microscopy of a 2.5% underivatized agarose gel was performed by procedures described under Materials and Methods. The length of the bar is 1000 nm.

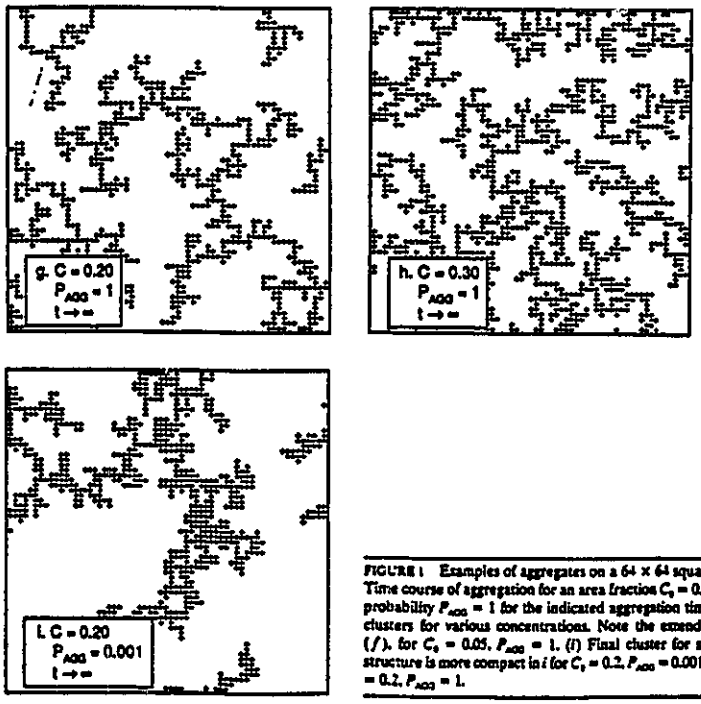

FIGURE 1 Examples of aggregates on a 64 × 64 square lattice. (*a–e*) Time course of aggregation for an area fraction $C_0 = 0.1$ and a sticking probability $P_{AGG} = 1$ for the indicated aggregation times. (*f–h*) Final clusters for various concentrations. Note the extended structure in (*f*), for $C_0 = 0.05$, $P_{AGG} = 1$. (*i*) Final cluster for small P_{AGG}. The structure is more compact in *i* for $C_0 = 0.2$, $P_{AGG} = 0.001$ than in *g* for $C_0 = 0.2$, $P_{AGG} = 1$.

Figure 1.4 (a) Electron micrographs of agarose gels[91] (b) Aggregates[24]

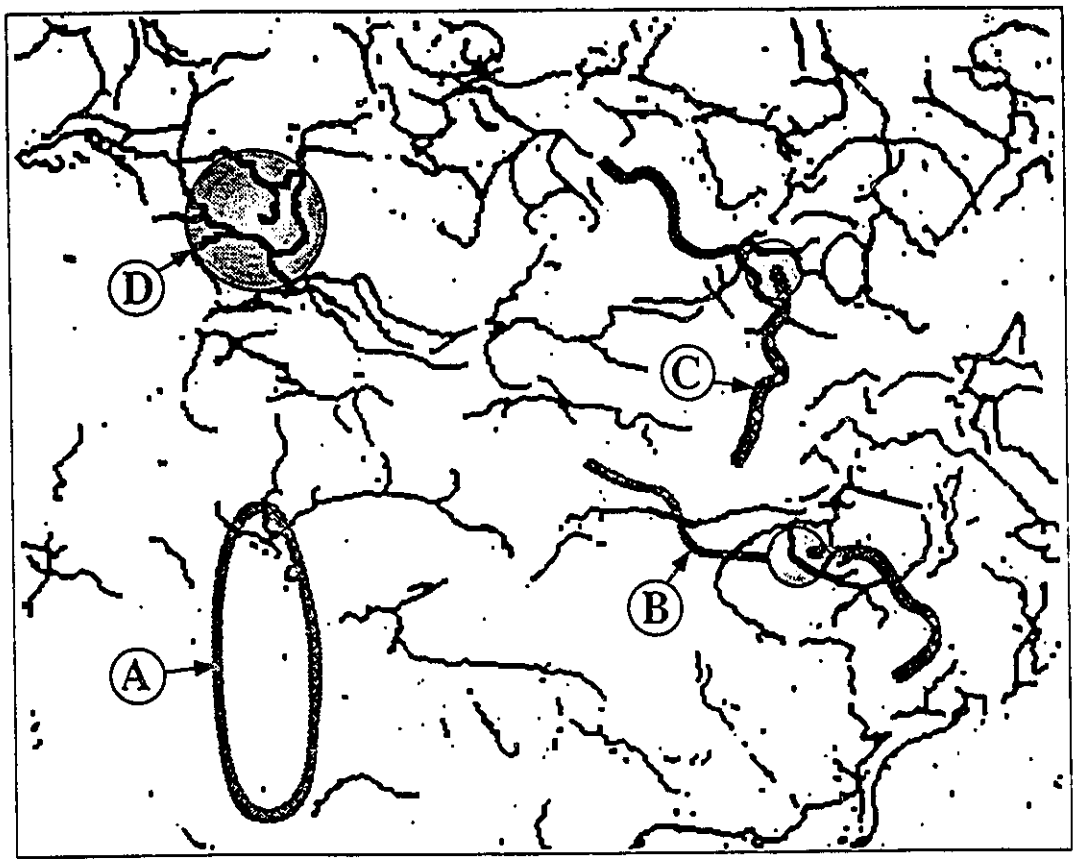

Fig 3. Trapping during gel electrophoresis. (A) Threading of a circular DNA by a projection from the network of fibers that formed the gel.(B, C) Passage of DNA molecules into pores that were too narrow to permit passage of a sphere that was attached to the DNA. (D) Entry of a sphere into a comparatively dense region that did not permit escape by Brownian motion. The network of gel (1.0% agarose) was obtained by, first, converting a digitized electron micrograph into a binary image and, then, skeletonizing and widening of the fibers. The computer-drawn objects in A-D are not drawn to the scale of the micrograph.

Figure 1.5 Trapping during gel electrophoresis[27]

streptavidin-DNA complex electrophoresis[30, 2, 33]. One therefore expects anomalous diffusion due to the random structure of the gel as well as the electric fields applied.

1.5 A New Algorithm

Our goal is to investigate the migration and the diffusion behaviours of particles moving through fixed particles (obstacles). Brownian-Dynamics (BD) is less efficient in dealing with long-time behaviour of particles. The diffusion process, however, is a long time process. Since it sometimes takes an exceedingly long time for the particles to attain the steady-state, especially in dense environments, BD is inefficient when applied to our problem.

The usual lattice Monte-Carlo (MC) algorithms, based on rejection methods, are widely used to simulate zero-field diffusion problems. However, when moving on a lattice, a particle must take different time durations to complete a step along the different axes (see chapter 2), due to the existence of external fields. In such cases, time is no longer "isotropic". The rejection method may not represent the dynamics correctly, even without obstacles. Therefore, it is necesary to develop a new computer simulation algorithm which is efficient and correctly generates the expected dynamics for all directions.

Our new algorithm, as we will see in chapter 2, is also based on MC. Unlike most MC algorithms, however, it does not employ rejection (so it is very fast). More than one clock is used: one for the motion along each fixed axis. Individual jumping times and individual jumping probabilities are analytically formulated by solving exactly the diffusion equation for the local environment. The new algorithm is then applied to periodic as well as random obstacle systems.

In the simulations, ensembles of up to 10^6 particles are followed for up to 10^6 time units. The computers used to carry out these simulations are two IBM and three SUN unix workstations.

Chapter 2

Theory and Algorithm

In this chapter, we introduce some general concepts, then we describe the details of the new Monte-Carlo algorithm that we have designed to study the problem of the electrodiffusion of a hard sphere moving in immobile obstacle systems.

2.1 The Ogston Model

By using the Poisson distribution, Ogston[18] originally derived the distribution of spaces available to a hard sphere placed in a random network of long fibres. It is an exponential function of the fibre concentration. Morris[14], Rodbard and Chambach[21] (the MRC model) proposed that, in electrophoresis, the electrophoretic mobility μ of a sphere is proportional to the volume available to the sphere. This assumption yields that for random gels, the mobility, normalized by its free solution value μ_0, is equal to the Ogston probability:

$$\frac{\mu}{\mu_0} = e^{-c\phi} \tag{2.1}$$

where ϕ is the concentration of gel fibers and c is a constant related to the radius of the sphere.

2.2 The Einstein Relation

A particle suspended in a stationary liquid performs a "pure" Brownian motion if there are no external fields. Einstein[3] derived a relationship between the diffusion coefficient D and the microscopic friction coefficient ξ of the particle:

$$D\xi = kT \tag{2.2}$$

where k is Boltzmann's constant and T is the temperature. On the other hand, when the particle (with a charge q) moves in an electric field (with a uniform intensity E) and attains a steady-state in the liquid, we have

$$qE = \xi v \tag{2.3}$$

where v is the drift velocity of the particle due to the electric field. We can thus rewrite the Einstein relation (2.2) as

$$\frac{D}{\mu} = \frac{kT}{q} \tag{2.4}$$

where μ=v/E is the defining relation for the electrophoretic mobility.

2.3 One-dimensional Biased Random Walks

The Brownian motion of a sphere in gels can be reasonably described by the random-walk model on a square or cubic lattice. In this section, we present the analytical results of the jumping probabilities and the mean jumping times as well as the fluctuations of the jumping time for a one-dimensional random walk.

2.3.1 Free Motion

Consider a charged particle carrying out a random walk on a one-dimensional lattice. The lattice parameter is d. The electric field points to the positive (+) direction of the axis, and it biases the random walk. The probabilities of jumping forward (+) and backward (-) over a distance d are (see Appendix, Eqs. (A.24) and (A.25)):

$$p_{\pm} = \frac{1}{1 + e^{\mp 2\varepsilon}} \tag{2.5}$$

where

$$\varepsilon = \frac{dqE}{2kT} \tag{2.6}$$

is the scaled (or dimensionless) electric field intensity; and the mean jumping time (forward or backward) is (see Eq. (A.27))

$$\langle \tau \rangle = \frac{\tanh(\varepsilon)}{\varepsilon} \tau_B \tag{2.7}$$

where

$$\tau_B = \frac{d^2}{2D} \tag{2.8}$$

is the Brownian time (the time required to complete one jump in the absence of fields). It is interesting to note that the time duration of a jump is the same whether the jump is made parallel or antiparallel to the field direction. However the probabilities are strongly biased by the field. Equations (2.5) and (2.7) are fundamentals of the biased reptation model[28, 17, 29, 22] for DNA gel

electrophoresis. When $\varepsilon \to 0$, Eqs. (2.5) and (2.7) yield the proper limits

$$p_{\pm}\,|_{\varepsilon \to 0} = \frac{1}{2} \tag{2.9}$$

and

$$\langle \tau \rangle\,|_{\varepsilon \to 0} = \tau_B \tag{2.10}$$

which correspond to the "pure" Brownian motion.

Slater[31] has shown that, when the Brownian motion is affected by an external field, the diffusion results from both spatial and temporal fluctuations:

$$D = \frac{\langle (\Delta x_d)^2 \rangle}{2\langle \tau \rangle} + \frac{v^2 \langle (\Delta \tau)^2 \rangle}{2\langle \tau \rangle} \tag{2.11}$$

where $\langle (\Delta x_d)^2 \rangle$ is the variance of the distance migrated in a single jump, v is the steady-state velocity, and $\langle (\Delta \tau)^2 \rangle$ is the variance of the time taken to do a single jump. Therefore, in order to obtain the proper diffusion coefficient, we must also take $<(\Delta \tau)^2>$ into account (see Appendix, Eq. (A.30)):

$$\langle (\Delta \tau)^2 \rangle \equiv \sigma_\tau^2 = \frac{\tanh(\varepsilon) - \varepsilon\, sech^2(\varepsilon)}{\varepsilon^3}\, \tau_B^2 \tag{2.12}$$

In the limit of $\varepsilon \to 0$, we have

$$\sigma_\tau^2\,|_{\varepsilon \to 0} = \frac{2}{3}\, \tau_B^2 \tag{2.13}$$

Figure 2.1 shows the jumping probabilities p_+ and p_- as functions of the scaled field intensity ε;

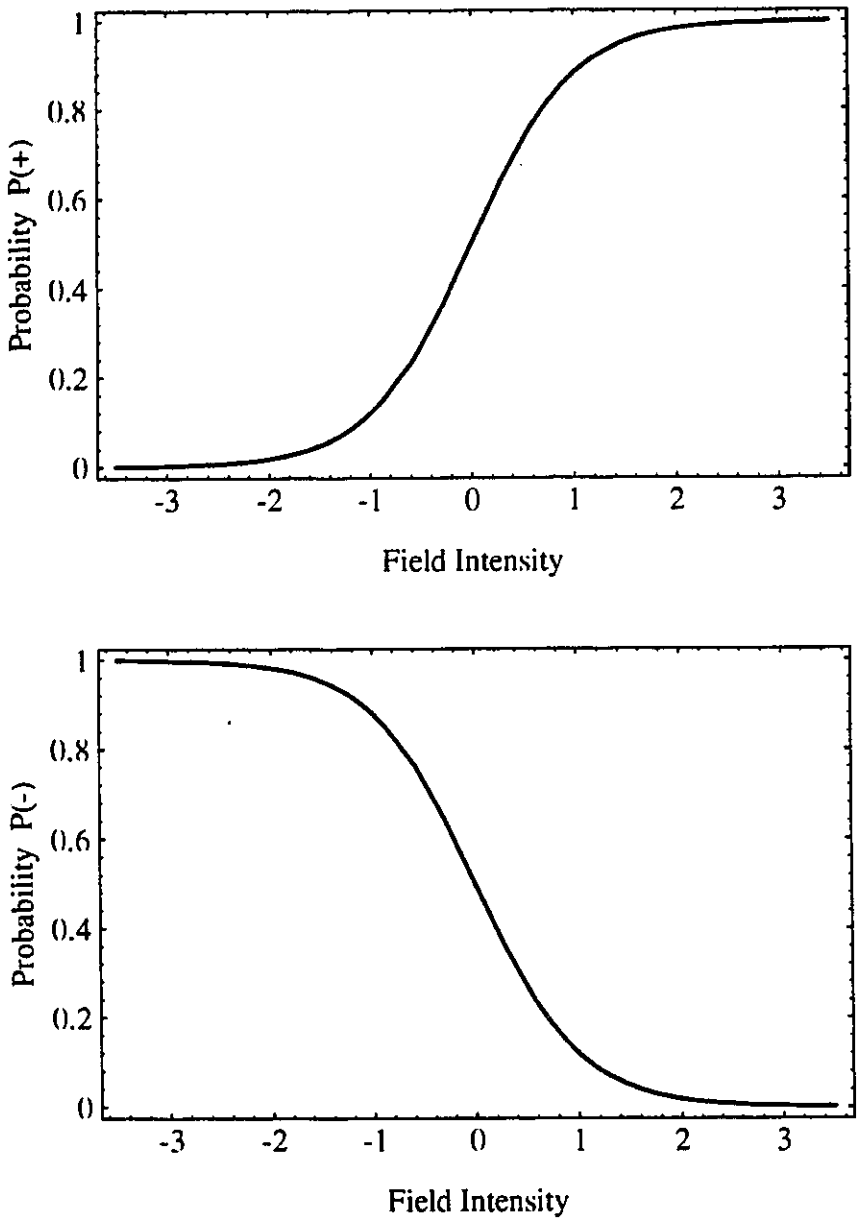

Figure 2.1 p_+ and p_- as functions of scaled field intensity ε for a free particle

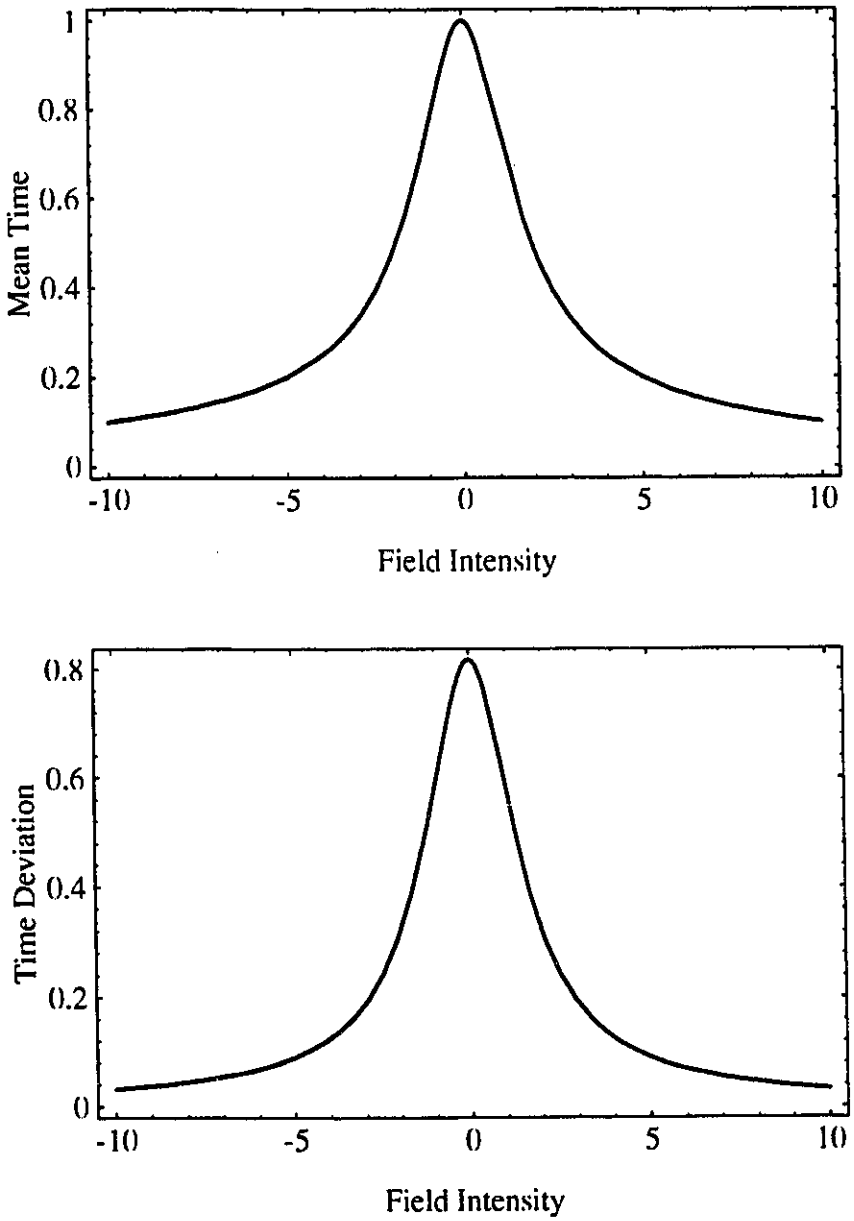

Figure 2.2 $\langle\tau\rangle$ and σ_τ as functions of ε for a free particle

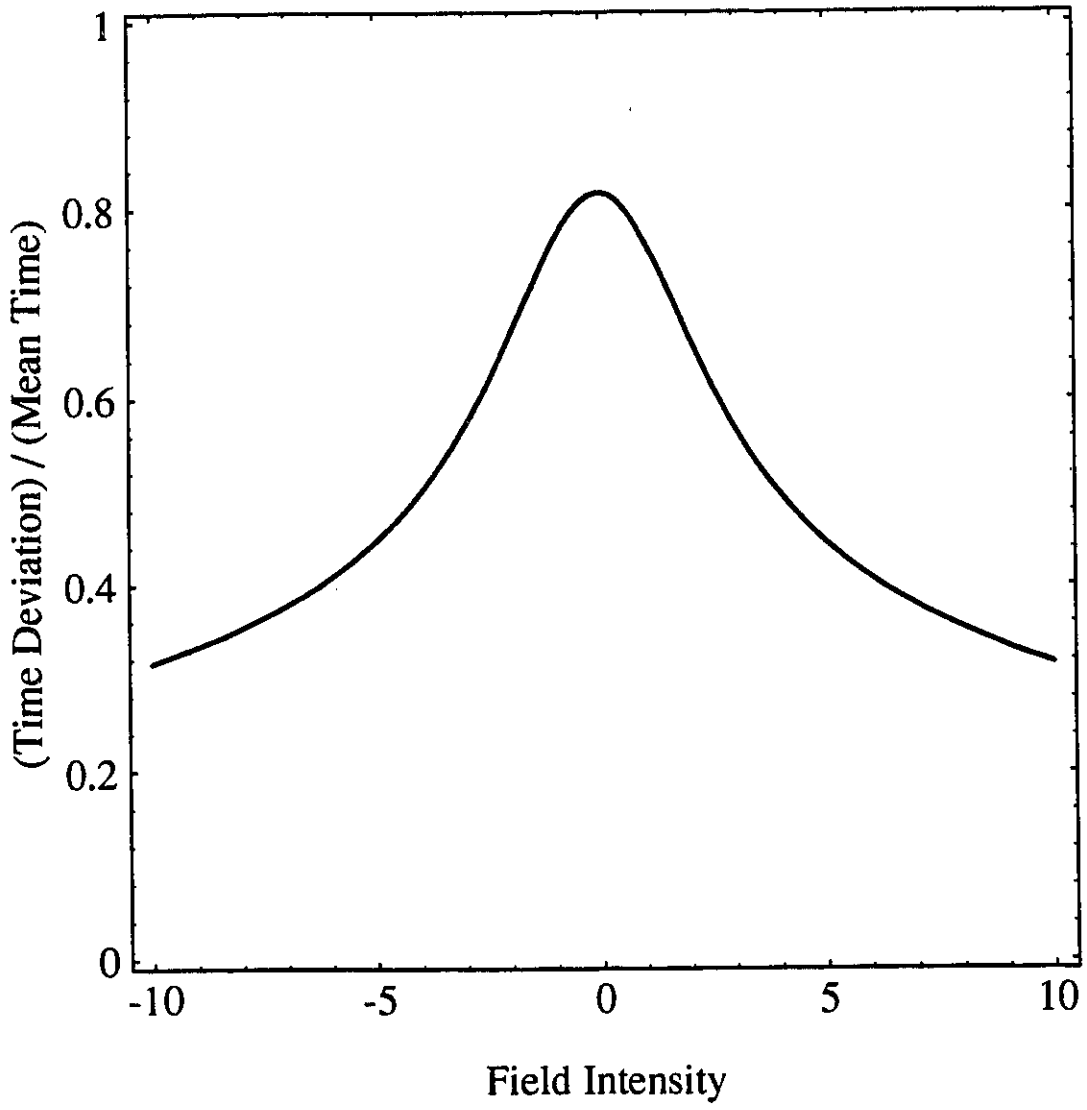

Figure 2.3 $\sigma_t/\langle t \rangle$ **as a function of** ε **for a free particle**

Fig. 2.2 shows $<\tau>$ and σ_τ as functions of ε; Fig. 2.3 shows $\sigma_\tau/<\tau>$ as a function of ε. Note that σ_τ is always smaller than $<\tau>$ for any value of ε. This will be very useful for our algorithm (see Sec. 2.4).

2.3.2 With Obstacles

If a Brownian particle meets an immobile obstacle in the path of a jump, the only possible alternative for the particle is to jump backward away from the obstacle. Under this circumstance, the probability of jumping backward must be (see Eq. (A.33))

$$p = 1 \tag{2.14}$$

and the mean time of jumping backward (or the "waiting time") is (see Appendix, Eq. (A.40))

$$\langle\tau\rangle = \frac{e^{2\varepsilon} - 2\varepsilon - 1}{2\varepsilon^2}\,\tau_B \tag{2.15}$$

Notice that $<\tau>$ is very sensitive to the field intensity ε. When $\varepsilon\to 0$, Eq. (2.15) provides a reasonable limit

$$\langle\tau\rangle\,|_{\varepsilon\to 0} = \tau_B \tag{2.16}$$

We see that the obstacle acts as a mirror: it always "reflects" the particle but, when there is no field, it yields the same time duration as if the mirror did not exist.

Similarly, we have the variance of the "waiting time" (see Appendix, Eq. (A.46)):

$$\sigma_\tau^2 = \frac{e^{4\varepsilon} + 4(1 - 2\varepsilon)\, e^{2\varepsilon} - 4\varepsilon - 5}{4\varepsilon^4}\, \tau_B^2 \qquad (2.17)$$

and its limiting value is

$$\sigma_\tau^2 \,|_{\varepsilon \to 0} = \frac{2}{3}\, \tau_B^2 \qquad (2.18)$$

Equations (2.16) and (2.18) yield the same results as those without obstacles (see Eqs. (2.10) and (2.13)), as expected. Figure 2.4 shows $<\tau>$ and σ_τ as functions of ε; Fig. 2.5 shows $\sigma_\tau/<\tau>$ as a function of ε. We see again that σ_τ is always smaller than $<\tau>$.

2.4 The New Algorithm

To take into account the temporal fluctuations, we should not simply take the mean jumping time $<\tau>$ as the time duration of a jump; instead, we pick up $<\tau>+\sigma_\tau$ and $<\tau>-\sigma_\tau$ randomly as time steps:

$$\Delta t = \langle \tau \rangle \pm \sigma_\tau \qquad (2.19)$$

where Δt is always non-negative (see last section). In simulations, a random number is used for each jump to choose the ($\pm$) sign of σ_τ. In Eq. (2.19), Eqs. (2.7) and (2.12) are used to yield $<\tau>$ and σ_τ when there is no obstacle; Eqs. (2.15) and (2.17) are used if there is an obstacle.

We now consider a particle jumping on a two-dimensional square lattice. Let the electric field E point to the +x direction (we use this convention throughout the thesis). Notice that due to the existence of the field, the mean time for jumping along one axis differs from that along

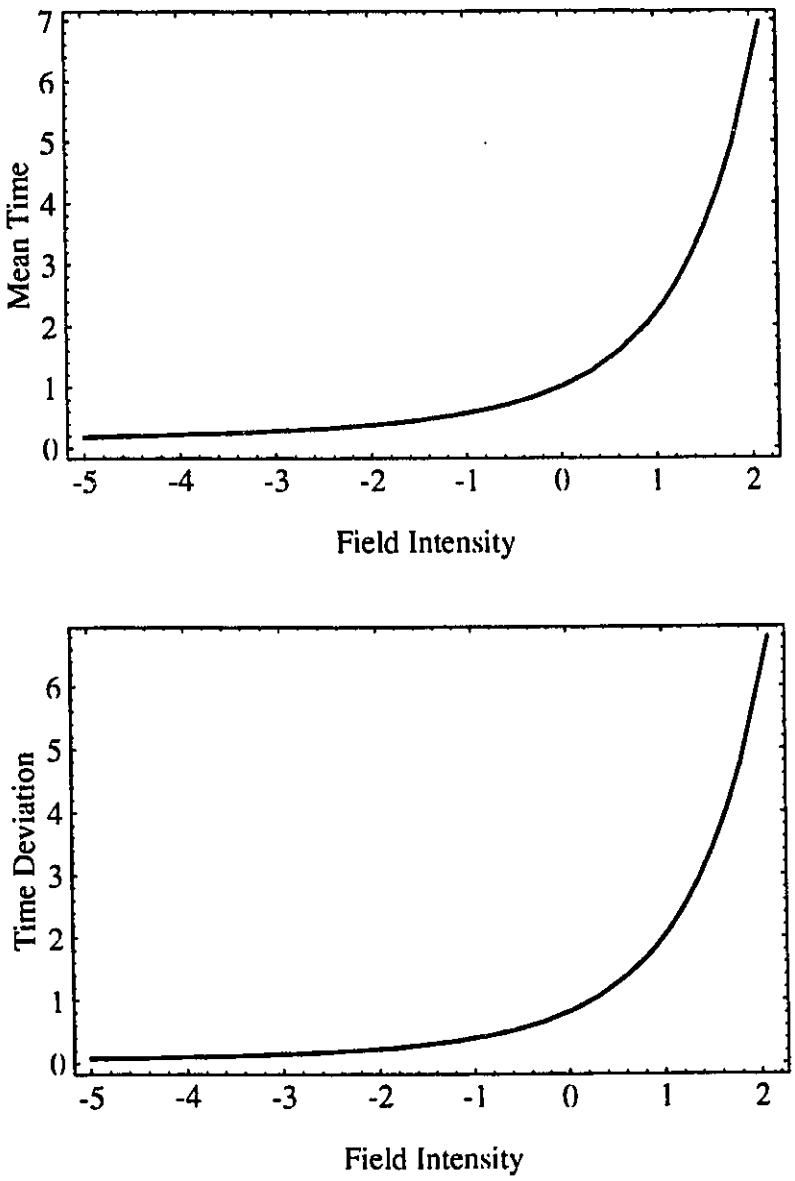

Figure 2.4 $\langle\tau\rangle$ and σ_τ as functions of ε for the case with an obstacle

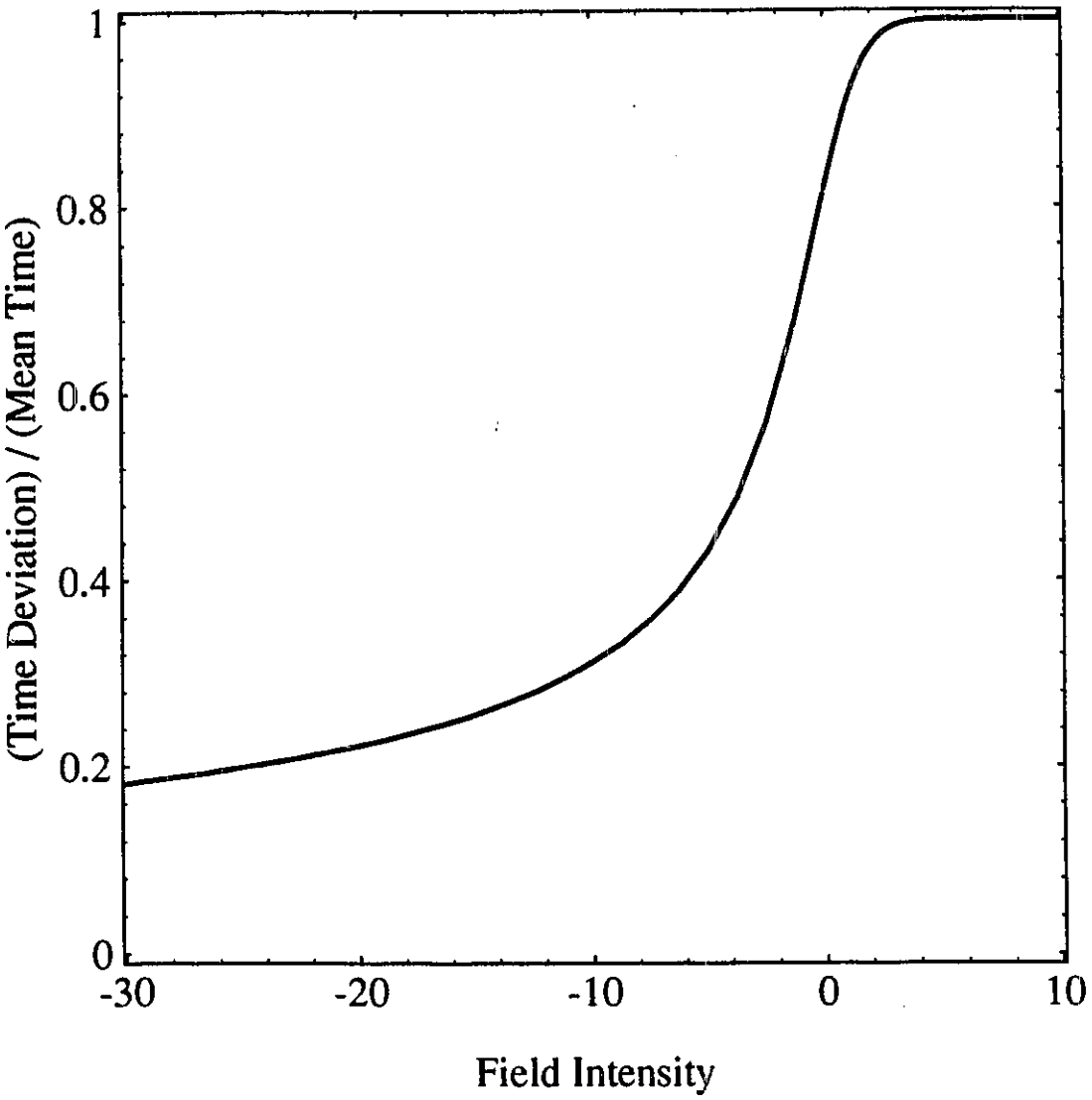

Figure 2.5 $\sigma_\tau/\langle\tau\rangle$ **as a function of** ε **for the case with an obstacle**

the other (see Eqs. (2.7) and (2.15)). The time is no longer "isotropic" in these two dimensions. In other words, there is no such thing as the uniform time-step used widely in the normal MC for zero-field diffusion. To overcome this "non-isotropic" problem, we introduce two clocks in correspondence with motions along the two different axes. In general, the two clocks are used seperately: the x-clock works if the motion is along the ±x directions; and the y-clock, if the motion is along the ±y directions. In some special cases, however, we synchronize both clocks; see details below.

At each step of the simulation, the particle may face one of the following two possible situations:

(i) **The no-tunnel case**: The particle may jump along either the x- or the y-axis (see Fig. 2.6); the x- and y-clock are then totally independent.

In the two-clock system, we have to define a reasonable rate of jumping along a particular axis in order to render the two clocks nearly synchronous when the particle gets to a steady-state since, in reality, we should have only one clock. Let $<\tau_x>$ and $<\tau_y>$ be the mean time durations required to complete one jump along x- and y-axes, respectively. The mean jumping frequencies in the ±x and ±y directions are then $1/<\tau_x>$ and $1/<\tau_y>$, respectively, and the total jumping frequency is $1/<\tau_x> + 1/<\tau_y>$. The net probability of jumping along a particular axis is thus defined as the individual jumping frequency devided by the total jumping frequency:

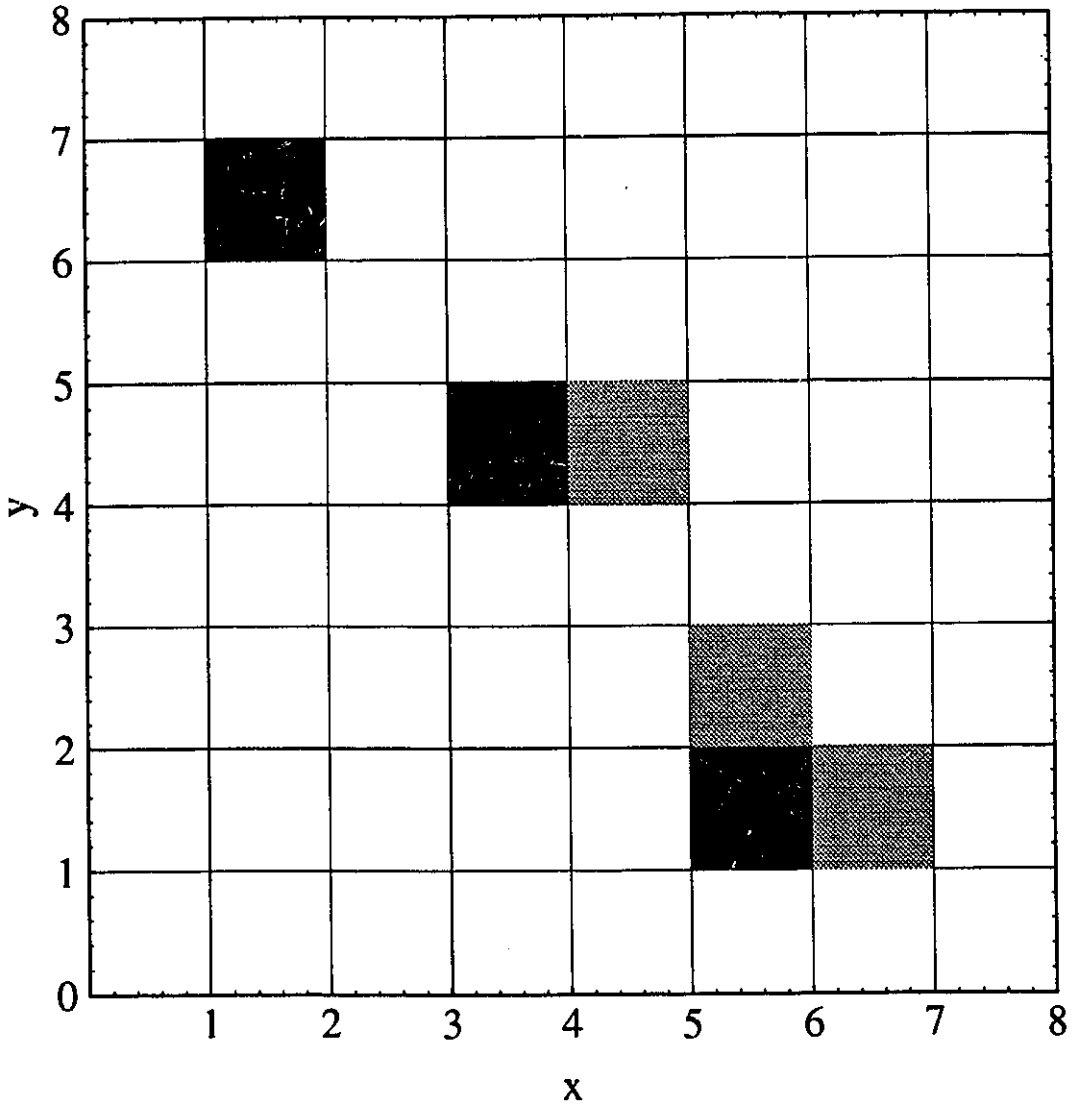

Figure 2.6 Particles (black squares) can jump along any of the two axes; gray squares represent immobile obstacles.

$$p_x = \frac{\langle \tau_y \rangle}{\langle \tau_x \rangle + \langle \tau_y \rangle} \tag{2.20}$$

or

$$p_y = \frac{\langle \tau_x \rangle}{\langle \tau_x \rangle + \langle \tau_y \rangle} \tag{2.21}$$

Notice that we have $p_x<\tau_x> = p_y<\tau_y>$ as required. This natural choice ensures that the two clocks will remain synchronized.

Equation (2.20) or (2.21) enables us to use a random number to decide along which axis the particle will jump next. After a particular jump axis is chosen, the clock corresponding to that axis "hops" by a time step given by Eq. (2.19) while the other clock stays at rest. Then the direction of the jump along this axis is selected: when there is no obstacle, another random number is used to choose the (±) direction acccording to Eq. (2.5); if there is an obstacle, the particle always moves away from it according to Eq. (2.14). Notice that we do not reject any attempted jumps when a particle hits an obstacle, i.e., all jumps are accepted (recall that rejection is usually employed in MC). Examples are given in Fig. 2.6:

(a) There are no obstacles on the adjacent sites. In this case, Eq. (2.7) is used for $<\tau_x>$ and $<\tau_y>$ in Eq. (2.20) or Eq. (2.21) to choose an axis; after an axis is chosen, Eq. (2.5) is used to determine the (±) direction along that axis. Finally, Eqs. (2.7), (2.12) and (2.19) are used to choose the time duration of the jump.

(b) There is a single obstacle. In this case, Eq. (2.7) and (2.15) are used for $<\tau_x>$ and $<\tau_y>$ in Eq. (2.20) or Eq. (2.21) to choose an axis. Then, Eq. (2.5) is used to choose the (±) direction

provided the particle can jump freely along that axis (again, if there is an obstacle, the particle always move away from it according to Eq. (2.14)). Finally, we use Eqs. (2.7) or (2.15), (2.12) or (2.17), and (2.19) to calculate the time duration of the jump.

(c) Two obstacles forming a corner. In this case, Eq. (2.15) is used in Eq. (2.20) or (2.21) to choose an axis. The particle then moves away from the obstacle along the chosen axis according to Eq. (2.14). Finally, Eqs. (2.15), (2.17) and (2.19) are used to compute the time duration of the jump.

(ii) **The tunnel case**: A particle can jump along only one axis (see Fig. 2.7); both clocks then move simultaneously by the same amount.

The axis, along which the motion is made, is now definitely fixed. When the clock corresponding to the chosen axis hops a time step, the other one is forced to move exactly the same time-step as the first one made. Here are examples:

(a) Two obstacles form a tunnel. In this case, Eq. (2.5) is used to decide the (±) direction toward which the particle jumps. Equations (2.7), (2.12) and (2.19) are used to determine the time duration of the jump.

(b) Three obstacles around. In this case, the particle has only one choise of moving out of the "trap". Equations (2.15), (2.17) and (2.19) are used to compute the time duration of the jump.

The advantage of moving the two clocks simultaneously is that this new algorithm can also be used to investigate the behaviour of a particle moving in a narrow tube, i.e., the algorithm

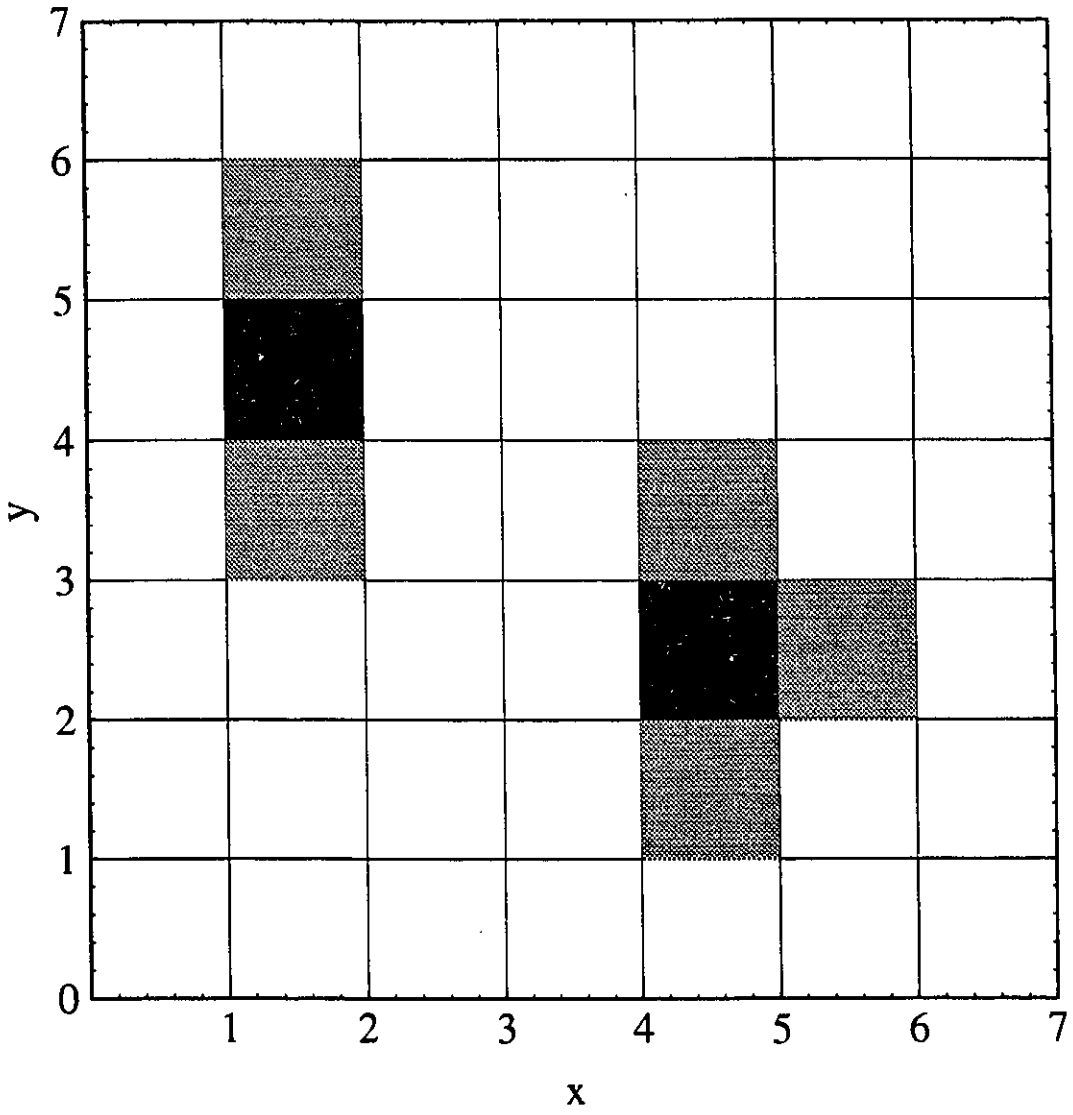

Figure 2.7 Particles (black squares) can jump only along the x-axis; gray squares represent immobile obstacles.

is also applicable for the one-dimensional motion; or for the cases where the obstacles are pipes or cylinders.

2.5 Implementation to Computer Simulations

A two-dimentional infinite square lattice is used for calculations. Charged particles carry out biased random walks on it. The field is always directed to +x direction. There are no periodic boundary conditions due to the infinite size of the lattice. Each particle occupies one lattice site. Interactions among particles are not considered, and there are no excluded-volume effects; two or more particles can occupy a same lattice site. Each obstacle occupies one lattice site. Obstacles are initially distributed periodically or randomly on the lattice at the required concentration (see Chaps. 3 and 4). Sites occupied by obstacles are not changed during a simulation.

A particle is then allowed to move, through a biased random walk, to one of the 1-4 empty adjacent sites. Particles form an ensemble moving independently through the same set of obstacles. At each jump, the mean time plus/minus the standard deviation is chosen randomly as the time duration, as stated before. The electrophoretic mobility μ is defined by

$$\langle x \rangle = A + \mu \varepsilon \langle t_x \rangle \tag{2.22}$$

where <x> is the mean displacement of the particles of the ensemble after an average time $<t_x>$ and A is a constant for the fit. The diffusion coefficients D_x and D_y are defined by

$$\langle (\Delta x)^2 \rangle = B_1 + 2D_x \langle t_x \rangle \tag{2.23}$$

and

$$\langle (\Delta y)^2 \rangle = B_2 + 2D_y \langle t_y \rangle \tag{2.24}$$

where $<(\Delta x)^2>$ and $<(\Delta y)^2>$ are the variances of the displacements x and y after average times $<t_x>$ and $<t_y>$, and B_1 and B_2 are constants for the fits. Note that t_x and t_y are recorded by two different clocks as described before.

In the simulations, the zero-field Brownian time $\tau_0=d^2/(2D)$ is chosen as the unit of time. The mean displacement $<x>$ and the variances $<(\Delta x)^2>$ and $<(\Delta y)^2>$ are recorded periodically. The mobility and the diffusion coefficients are obtained from the least-square fit of the simulation data to Eqs. (2.22)-(2.24). Examples of fits will be shown in Chap. 4.

Chapter 3

Simulation of Periodic Systems

The MRC model[14, 21] states that the electrophoretic mobility μ of a rigid particle is proportional to the fractional volume (the volume available to the particle in a gel divided by the total gel volume). In a periodic "gel" (gel molecules are placed periodically as obstacles), the only volumes unavailable to the particle are those occupied by the obstacles themselves. One can thus predict a relationship

$$\frac{\mu}{\mu_0} = 1 - \phi \tag{3.1}$$

for this simplest system where μ_0 is the free-solution mobility, $1-\phi$ is the fractional volume, and ϕ is the concentration of the gel. Moreover, if one assumes that the Einstein relation holds, i.e., the mobility μ and the longitudinal diffusion coefficient D_x are proportional to one another, one then expects

$$\frac{D_x}{D_0} = 1 - \phi \tag{3.2}$$

where D_0 is the free-solution diffusion coefficient.

In this chapter, we use a two-dimensional periodic "gel" to carry on computer simulations since, as we have just seen, the MRC model becomes trivial in this case. We are going to

investigate if the MRC hypothesis is valid for the periodic "gel" and if the Einstein relation applies to this obstacle system. Although it may not exist in the nature, the periodic system provides us a significant test of our new algorithm described in Chap. 2.

3.1 Implementation

To form a periodic "gel", the gel molecules are placed periodically and isotropically (same periodicity along both the x- and the y- directions) as immobile obstacles on a two-dimensional square lattice (see Fig. 3.1). The isotropy is required to avoid any entropic force generated by a concentration gradient: a moving spherical particle (tracer) will thus "see" the same structure in either the x- or the y- direction. If the periodicity (the distance between the two consecutive obstacles) is pxd (d is the lattice parameter), i.e., one site is occupied by an obstacle out of p×p sites, $\phi=1/p^2$ is the concentration of obstacles. Clearly, for such a simplified system, the fractional volume f available to a tracer is simply

$$f = \frac{p^2 - 1}{p^2} = 1 - \phi \qquad (3.3)$$

The minimun periodicity is selected to be p=3 (but in the special zero-field case, the minimun value p=2 is chosen). Tracers are initially placed randomly in a approximately 4000d×4000d area inside the "gel". Calculations of the mobility and the diffusion coefficients from the simulation data are carried out as described in Sec. 2.5.

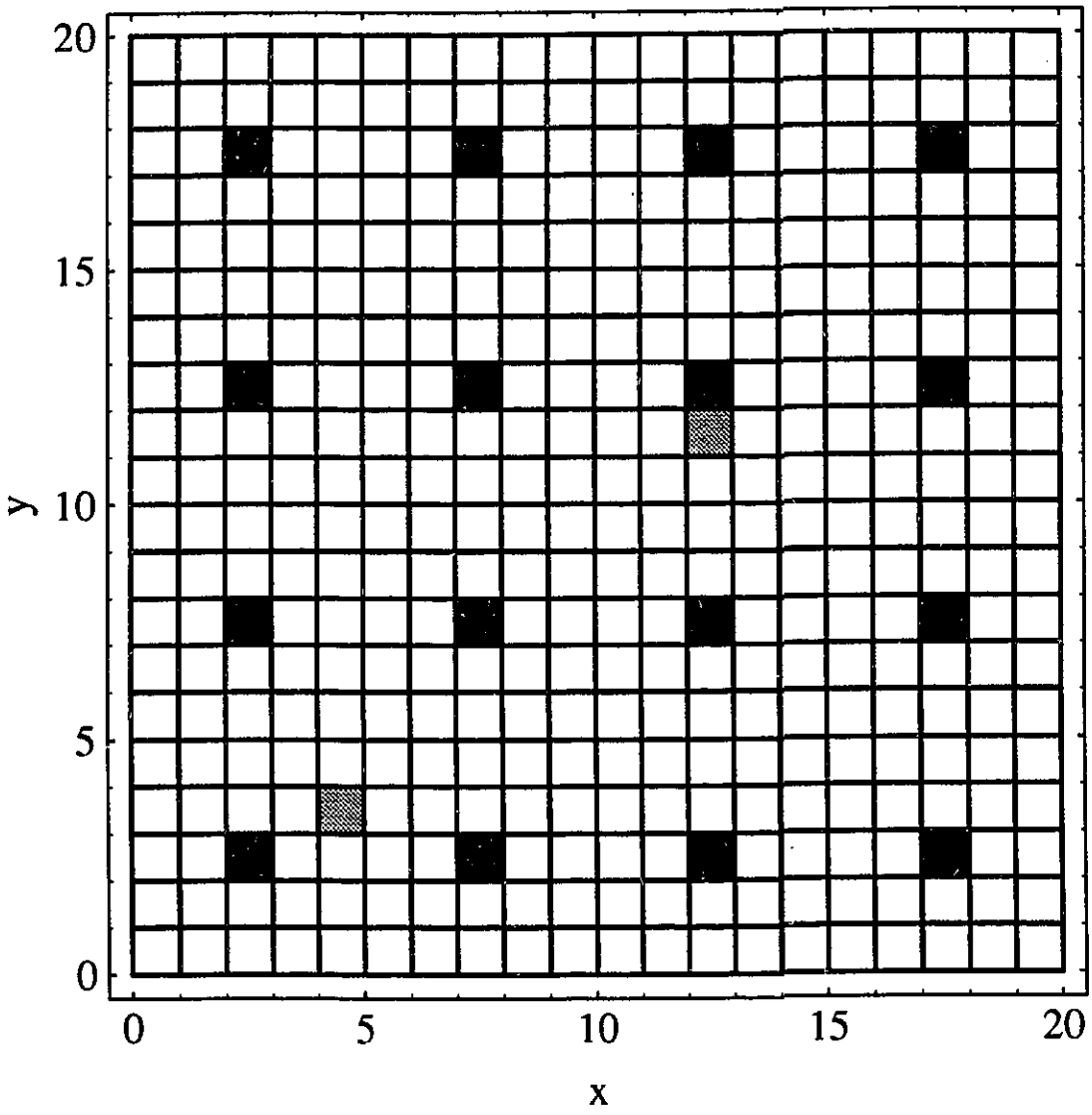

Figure 3.1 Schematic view of a periodic system with p=5. Black squares represent obstacles while gray ones are particles.

3.2 Drift in a Free Solution

We first consider a trivial case where there are no obstacles in the system (this is also the case of $p \to \infty$). An electric field is applied to drive the tracers through the system. In this case, the mobility and the diffusion coefficients can be expressed rigorously from Eqs. (2.5), (2.7) and (2.12) as

$$\mu = \frac{1}{E} \frac{(p_+ - p_-)\, d}{\langle \tau \rangle}$$

$$= 1 \ (\textit{scaled units}) \tag{3.4}$$

$$D_x = \frac{d^2 - (p_+ - p_-)^2 \, d^2}{2\langle \tau \rangle} + \frac{v^2 \, \sigma_\tau^2}{2\langle \tau \rangle}$$

$$= \frac{1}{2} \ (\textit{scaled units}) \tag{3.5}$$

and

$$D_y = \frac{1}{2} \ (\textit{scaled units}) \tag{3.6}$$

Figures 3.2 and 3.3 show the mobility μ and the diffusion coefficients D_x and D_y as functions of the scaled electical field intensity ε. We can see that Eqs. (3.4)~(3.6) are satisfied for all field intensities. This shows that our algorithm correctly reproduces the dynamics of a free- drifting particle. Also, Figs. 3.2 and 3.3 indicate that the Einstein relation $D_x/\mu=1/2$ (in scaled units) holds very well even at very high fields in this obstacle-free case. It was verified

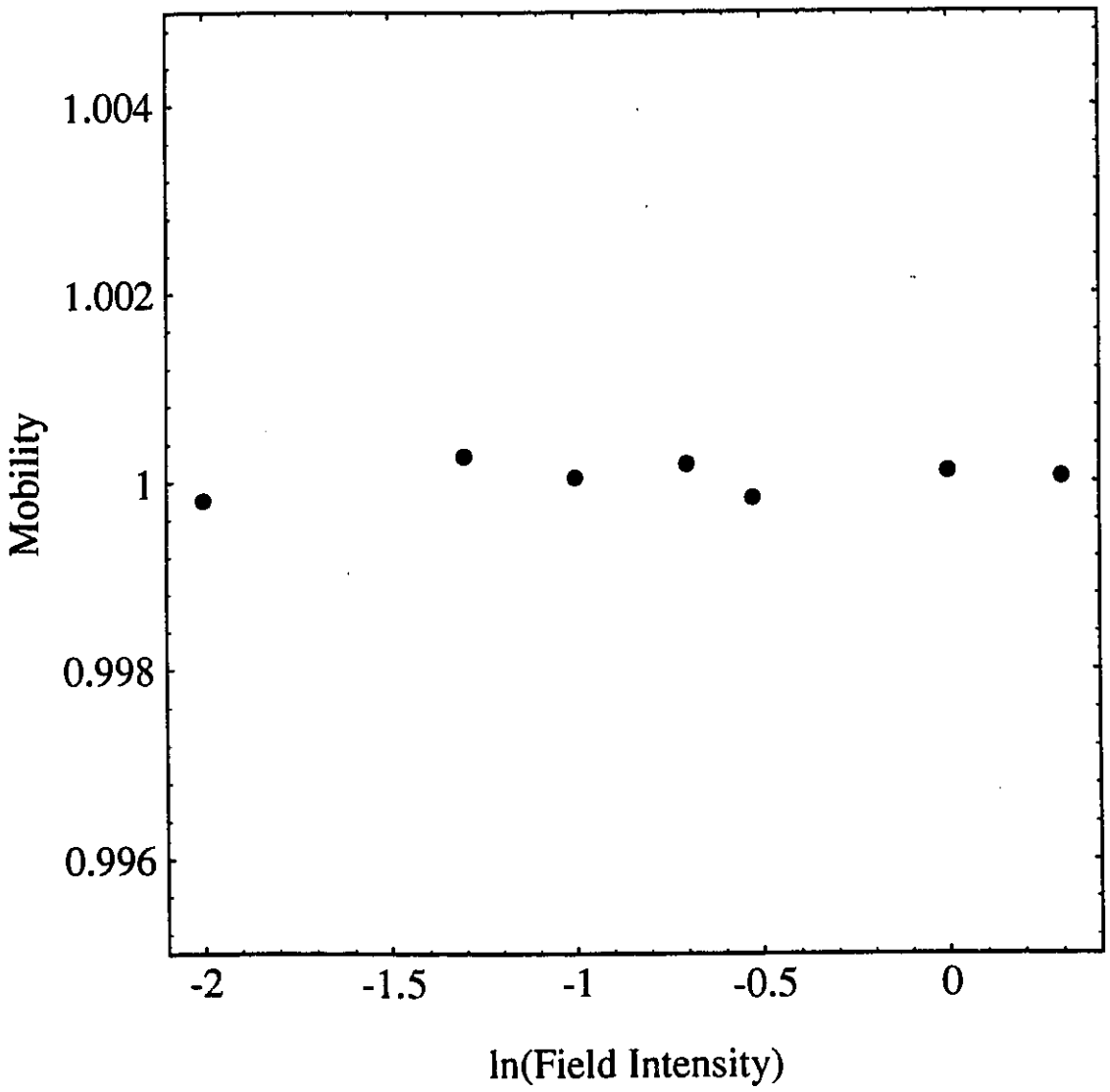

Figure 3.2 Mobility μ as a function of field intensity ε for a free solution

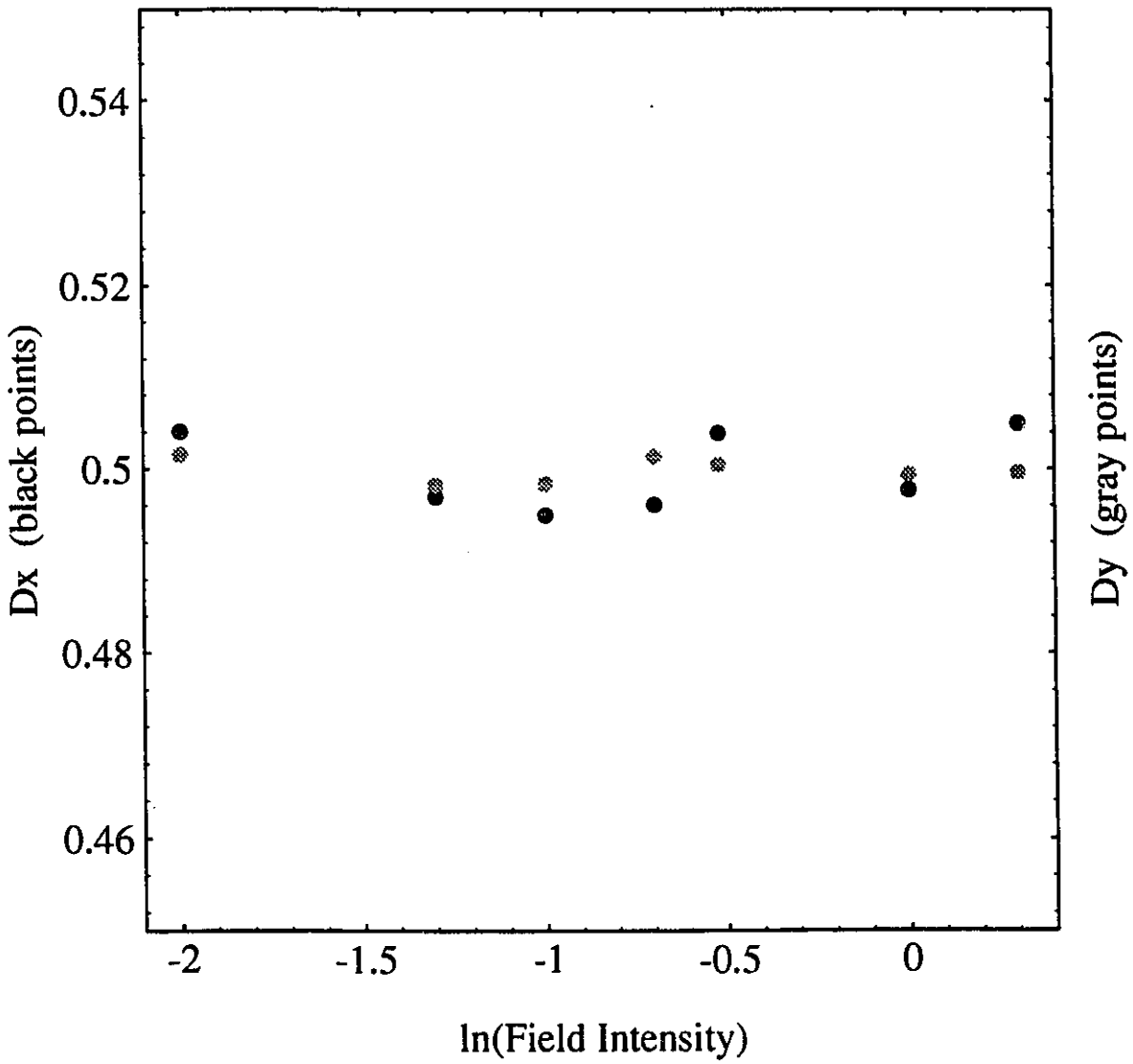

Figure 3.3 Diffusion Coefficients as functions of field intensity for a free solution

simulation (results are not shown) that one would have $D_x \to 0$ for very large field intensities if the time fluctuations (see Sec. 2.3, Eq. (2.19)) were not taken into account.

3.3 Zero-Field Diffusion: With Obstacles

We now place obstacles (periodically) onto the lattice but without electric fields. In this zero-field case, we only compute the diffusion coefficients. Since there are no differences between the x- and the y- directions, the global diffusion coefficient D is thus defined as:

$$D = \frac{1}{2} \frac{\langle (\Delta x)^2 \rangle + \langle (\Delta y)^2 \rangle}{\langle t_x \rangle + \langle t_y \rangle} \tag{3.7}$$

Simulation data are fitted to Eq. (3.7). Figure 3.4 shows the relation between the diffusion coefficient D and the gel concentration $\phi = 1/p^2$. Our results disagree with the straight-line approach suggested by Eq. (3.2): the decrease of the relative diffusion coefficient is not proportional to the increase of the fractional volume taken by the obstacles. Instead, our result yields

$$\frac{D}{D_0} = \frac{1}{1 + K_D \phi} \tag{3.8}$$

where $D_0 = 1/2$ (in scaled units) is the free solution diffusion coefficient and K_D is the retardation coefficient with the value $K_D = 2.00 \pm 0.02$. This expression explains all of our data with excellent precision.

In fact, we can calculate the diffusion coefficient analytically for p=2 when $\varepsilon = 0$. In this special case, a diffusing particle can only stay either in a "free" site (no obstacle around) or in

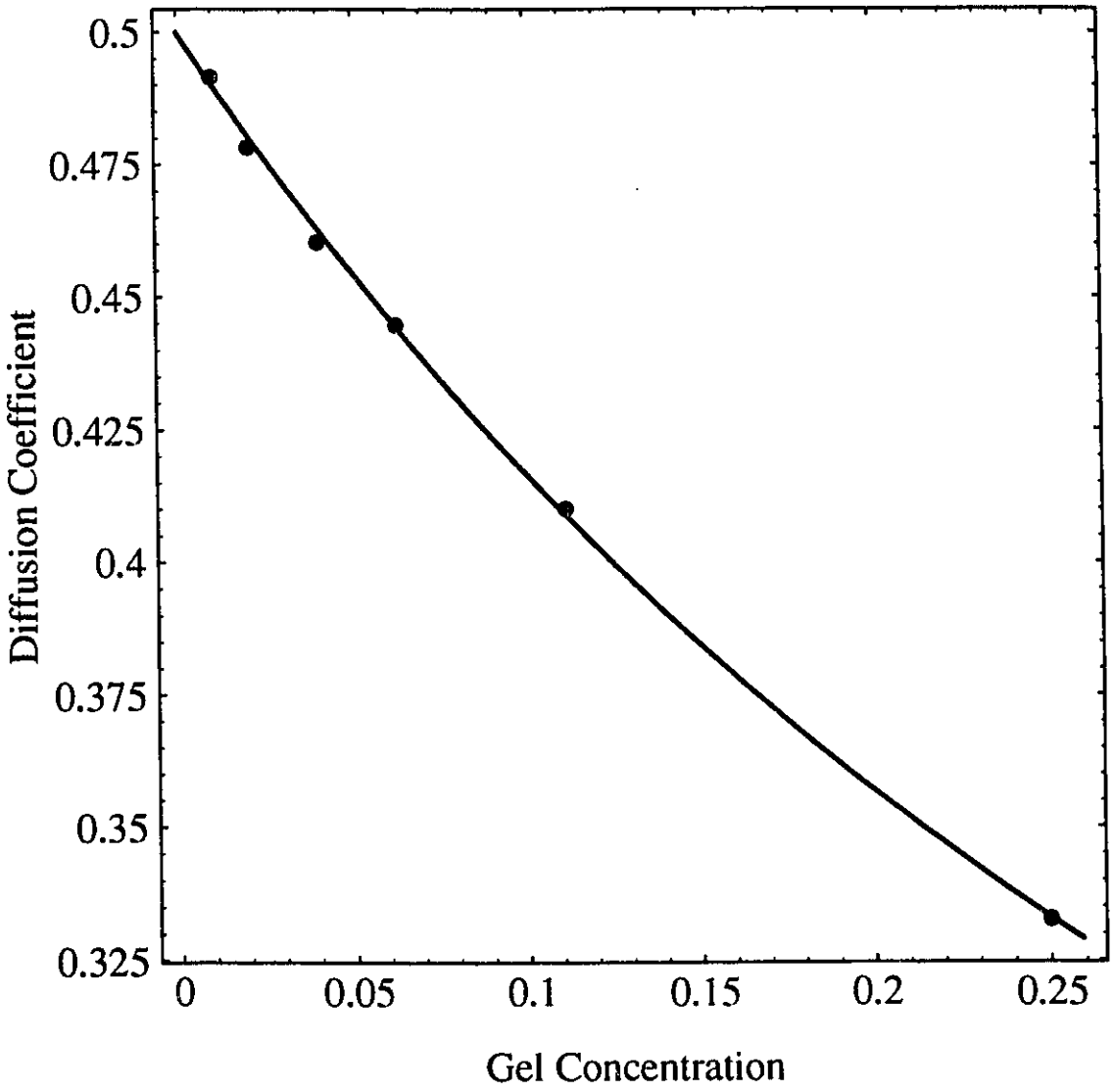

Figure 3.4 Zero-field diffusion coefficient as a function of the concentration: the solid curve shows the best fit D=0.5/(1+2.00ϕ)

a tight "tunnel". The particle visits the two sites alternatively, i.e., the probabilities of visiting both sites are equal. In other words, the particle spends 1/2 of its time in tunnels. Remember that in our algorithm, we employ two clocks to record the time. The two clocks are moved simultaneously if the particle jumps through a tunnel. So the diffusion coefficient can be expressed as

$$D = \frac{1}{2}\left[\frac{\langle(\Delta x_d)^2\rangle}{2\langle\tau\rangle + \langle\tau\rangle} + \frac{\langle(\Delta y_d)^2\rangle}{2\langle\tau\rangle + \langle\tau\rangle}\right]$$

$$= \frac{1}{3} \textit{ (scaled units)} \qquad (3.9)$$

where $\langle(\Delta x_d)^2\rangle$, $\langle(\Delta y_d)^2\rangle$ and $\langle\tau\rangle$ are the same as those in Eq. (2.11). This implies that for p=2, the theoretical value of the retardation coefficient is exactly K_D=2. Our simulation result Eq. (3.8) agrees with the theoretical analysis.

3.4 Effect of Electric Fields

We now study the mobility and the diffusion coefficients as functions of the electric field intensity when the gel concentration is fixed (here p=3 is selected). Figure 3.5 shows that the mobility μ remains a constant for the field intensities used here ($\varepsilon \leq 0.22$). Figure 3.6 shows that the transverse diffusion coefficient D_y does not change with the field intensity ε; and the longitudinal diffusion coefficient D_x does not change much for $\varepsilon < 0.15$, but increases with the field intensity when $\varepsilon > 0.15$.

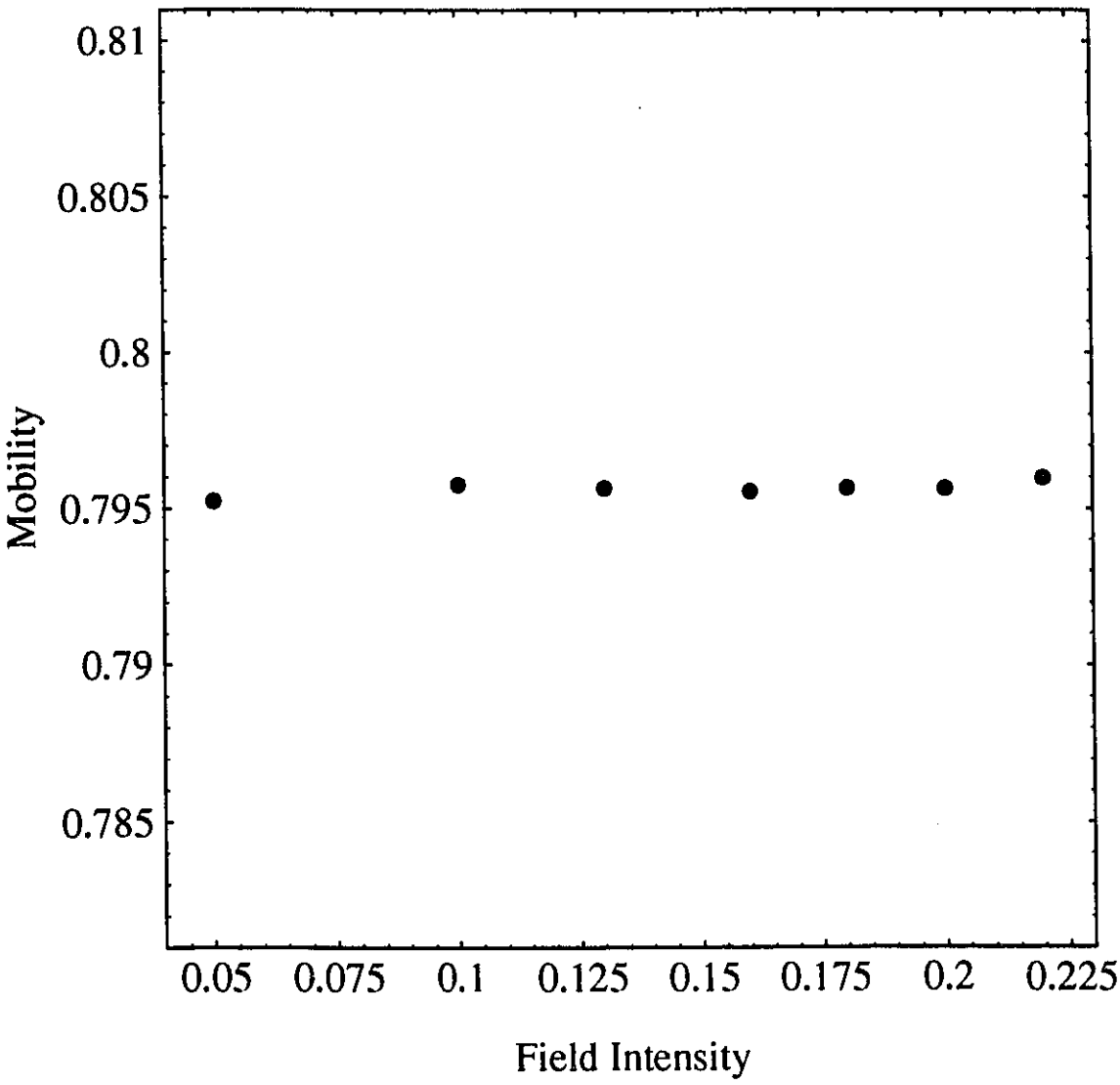

Figure 3.5 μ as a function of ε, with p=3

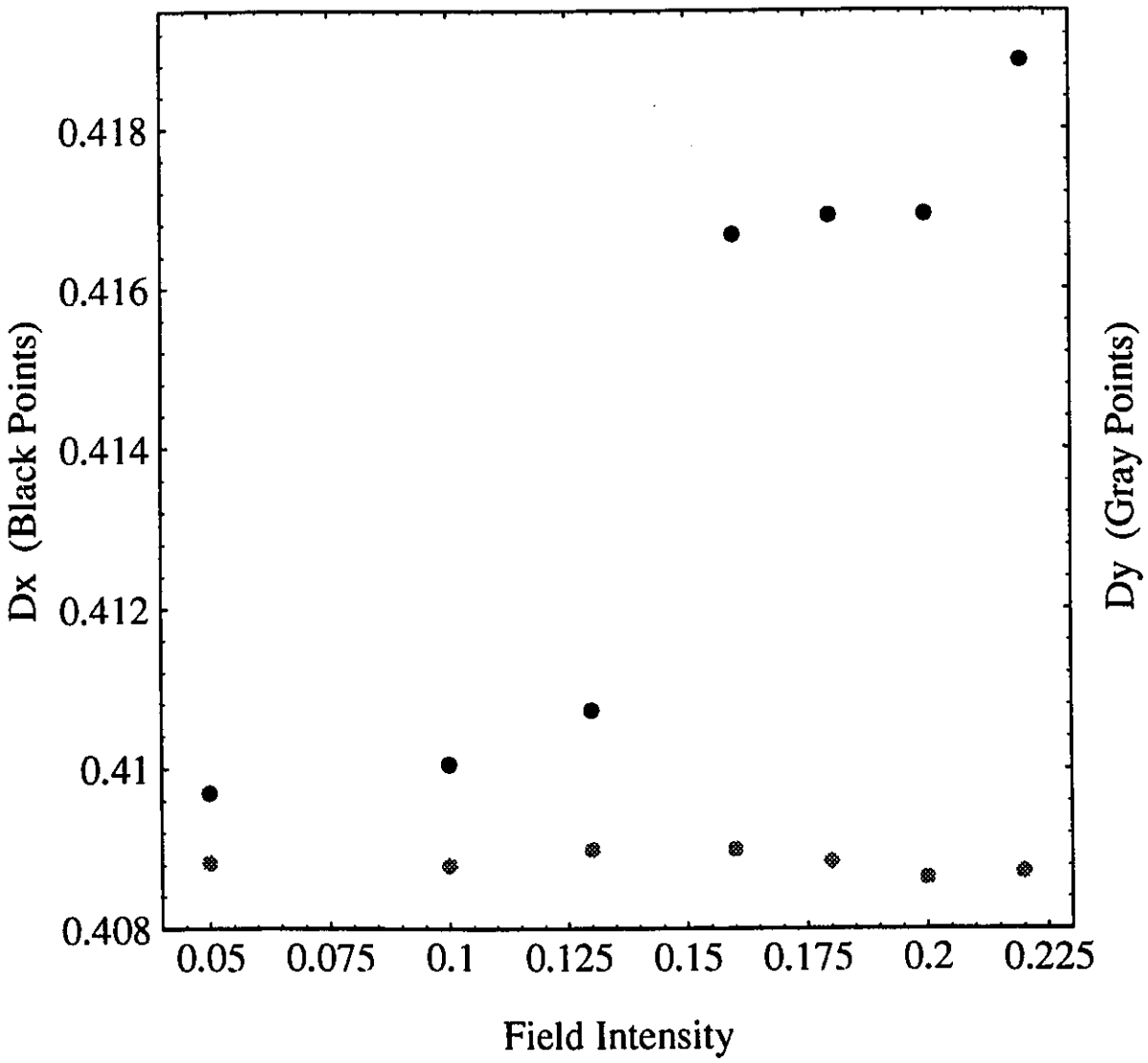

Figure 3.6 Diffusion coefficients as functions of ε, with p=3

The increase of the longitudinal diffusion coefficient at relatively high fields (ε>0.15) can be interpreted by the collision effect. When a moving particle collides with an obstacle, it stops there for a period of "waiting time" which becomes very large at high fields (see Eq. (2.15)). During that period of time, the other particles, which do not undergo collisions, move away at a large speed due to the high field. This effect increases the spatial dispersion of the particles, and hence the diffusion coefficient in the longitudinal direction.

3.5 Effect of Obstacles

Figures 3.7 shows how the relative mobility varies with the gel concentration at different field intensities. Over the range of field intensities (ε=0.05~0.2), the mobility is strictly field-independent. The data do not fall onto a straight line as Eq. (3.1) would predict, but can be described by

$$\frac{\mu}{\mu_0} = \frac{1}{1 + K_\mu \phi(1 - \phi)} \qquad (3.10)$$

where μ_0=1 is the free solution mobility and K_μ is the retardation coefficient with a value K_μ=2.60±0.05.

We then present the variation of the diffusion coefficients with the gel concentration at different field intensities. Our simulations show that the transverse diffusion coefficient D_y is field-independent. The results for D_y agree with Eq. (3.8), as shown in Fig. 3.8. The transverse diffusion coefficient behaves as if there were no fields. This is because (i) in y- direction the waiting time (when a particle hits an obstacle) and the jumping time (when there is no obstacle)

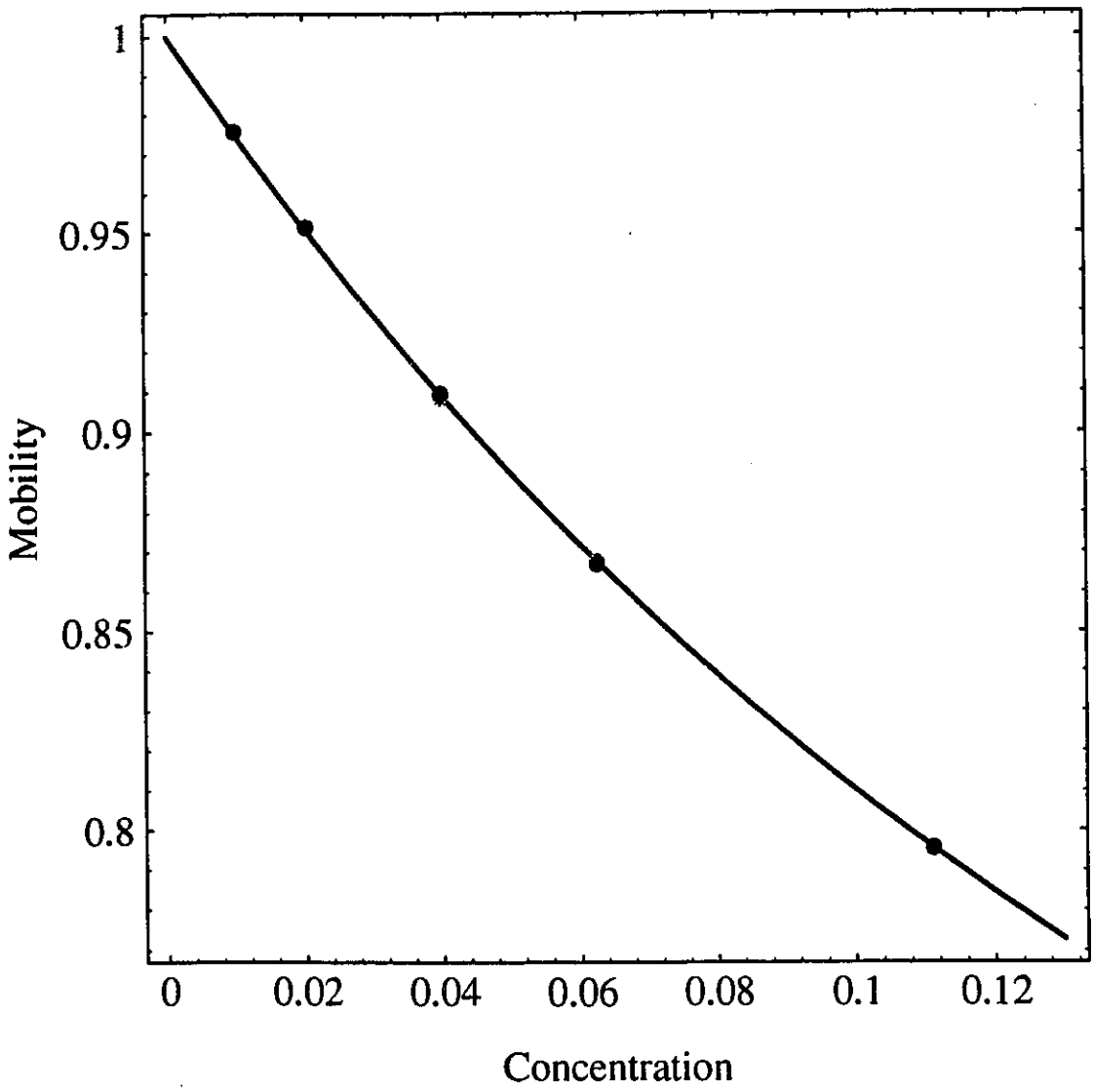

Figure 3.7 μ as a function of ϕ (gray points: ε=0.05; black points: 0.2): the solid curve represents the best fit $\mu=1/(1+2.60\phi(1-\phi))$. The two sets of points overlap almost perfectly.

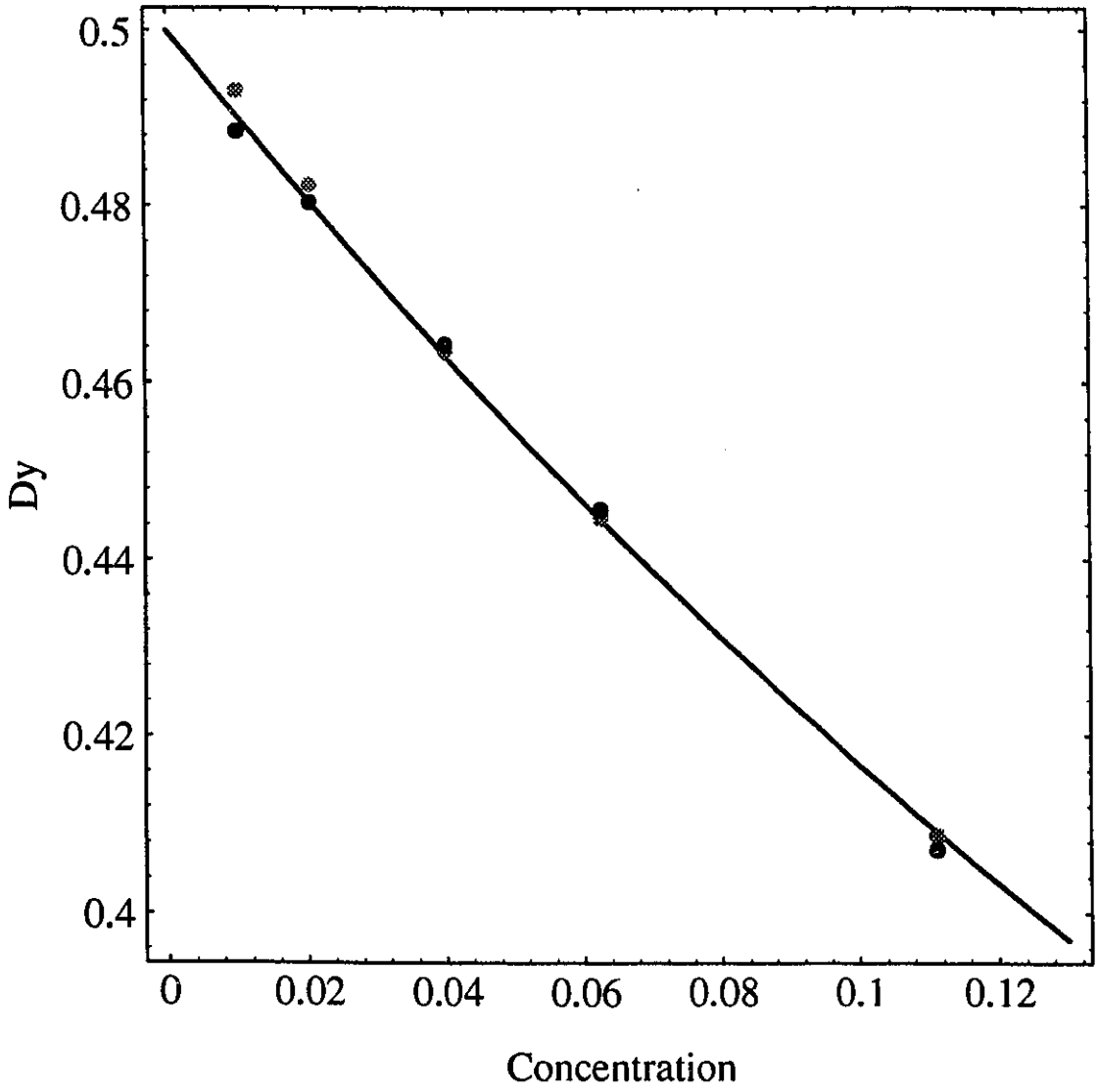

Figure 3.8 D_y **as a function of** ϕ **(gray points:** ε**=0.05; black points:** ε**=0.2): the solid curve represents the best fit** $D_y=0.5/(1+2.00\phi)$

are the same, so there are no collision effects in that direction; (ii) we use two clocks separately; and there are no tight tunnels because of the geometry of the periodic system (i.e., motions in x- direction do not affect those in y- direction).

The longitudinal diffusion coefficient D_x is different. At low field (ε=0.05), the data for D_x still agree with Eq. (3.8). But for non-negligible field intensities, our simulation indicates that D_x varies with both the gel concentration and the field intensity. For example, Fig. 3.9 shows that D_x decreases linearly with the gel concentration at ε=0.2. In fact, D_x even becomes an increasing function of the gel concentration at very high fields (data are not shown; such high fields are probably irrelevant for standard gel electrophoresis). This is due to the collision effect as explained in last section. Since the frequency of collisions increases with gel concentration, the field dependence of D_x is stronger at high gel concentrations. We can see from Fig. 3.9 that the difference between D_x and D_y increases with the concentration.

Figure 3.10 plots the Einstein ratio D_x/μ vs. the concentration ϕ at different field intensities. We can see that the value of D_x/μ increases with the concentration ϕ, and is always larger than 1/2 even at low concentrations. This indicates that the Einstein relation is invalid as long as the gel concentration is non-negligible. And we can see from Fig. 3.10 that the high fields enlarge the invalidity of the Einstein relation.

Even at low fields, predictions by Eqs. (3.10) and (3.8) are fundamentally different from those prediced by Eqs. (3.1) and (3.2): firstly, the mobility does not decrease linearly with the gel concentration, which makes the MRC model invalid; secondly, we do not find $D/D_0=\mu/\mu_0$ since the two retardation coefficients K_D and K_μ are different, which means that the Einstein

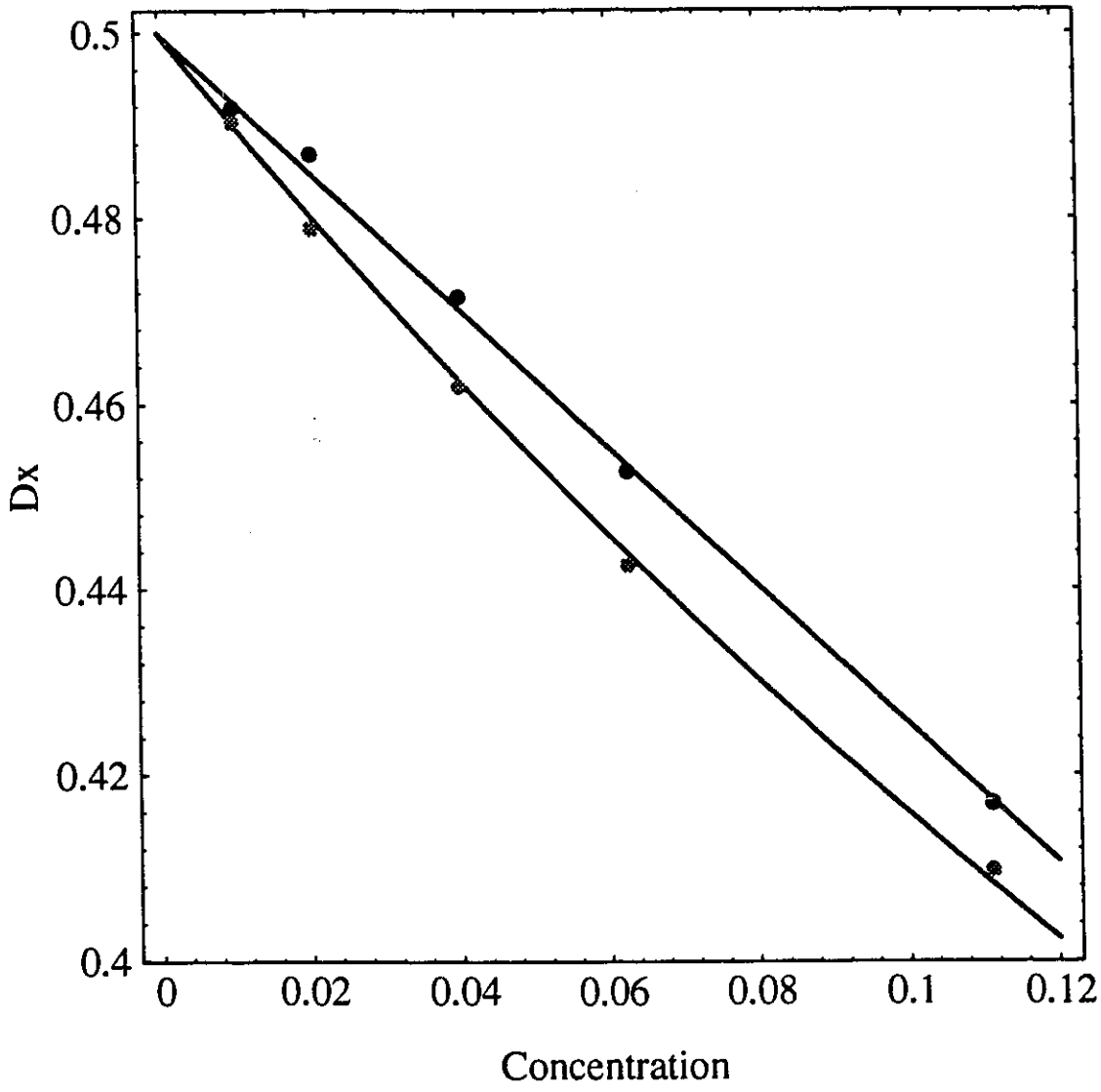

Figure 3.9 D_x as a function of ϕ. Gray points: ε=0.05, the solid curve shows the best fit $D_x=0.5/(1+2.00\phi)$; black points: ε=0.2, the solid line shows the best fit $D_x=0.5-0.745\phi$

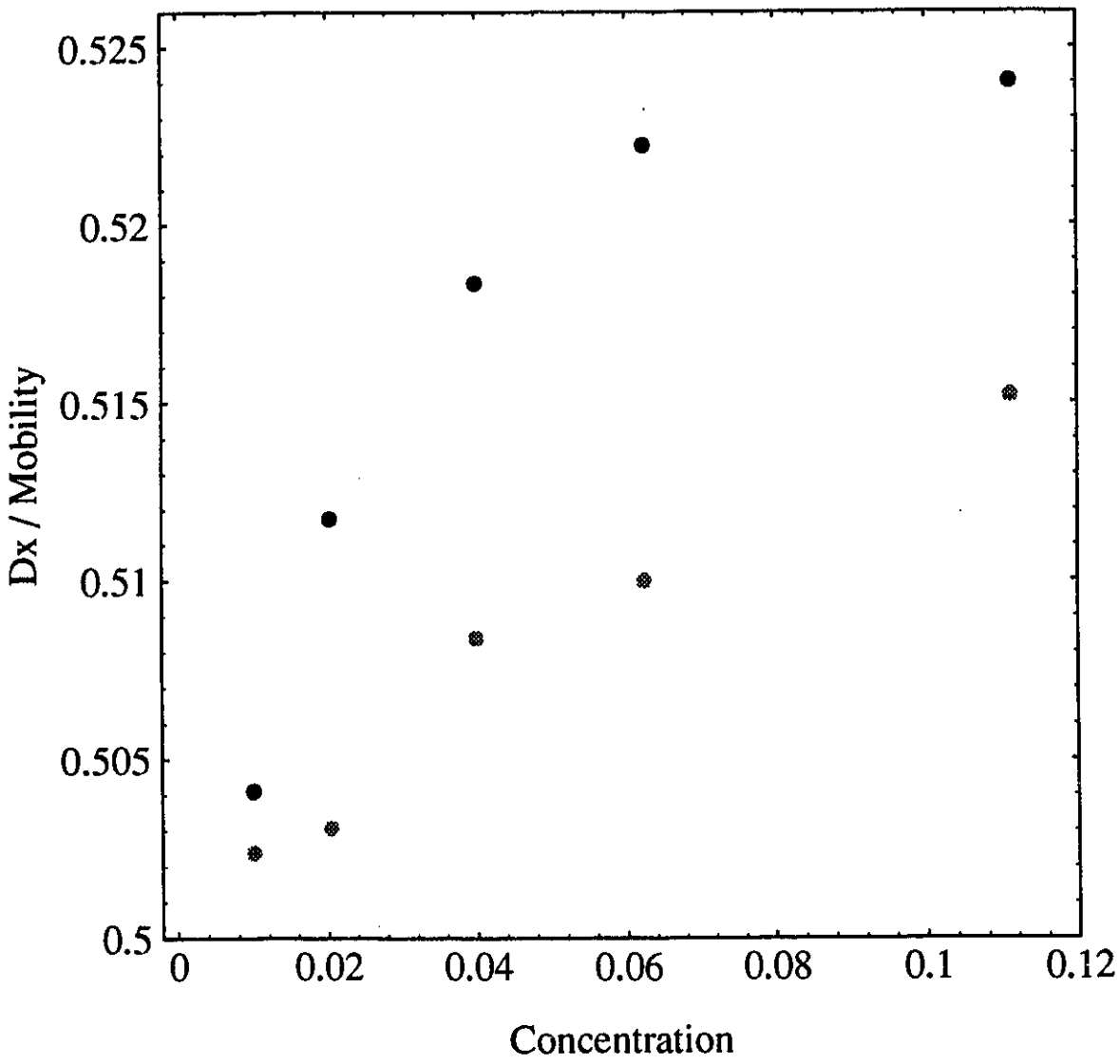

Figure 3.10 D_x/μ as a function of ϕ, with ε=0.05 (gray points) and 0.2 (black points)

relation is violated; finally, even at small concentrations where Eqs. (3.10) and (3.8) can be expanded in series, one fails to obtain the function 1-ϕ as that in Eq. (3.3) since the retardation coefficients are not equal to 1.

In order to understand these results, we compute and plot the fractional time that the moving particles spent on different sites of a 20d×20d periodic cell of the lattice. Figure 3.11 shows the case of ε=0. We can clearly see that a particle does not visit the available sites uniformly, or various sites are non-equivalent: the particle tends to avoid the sites located immediately ajacent to an obstacle (black areas), but visit the next sites (white areas) more often than the average. These results indicate that the MRC hypothesis fails: one cannot simply take the fractional volume as the relative mobility; one must instead weight sites according to the probability of occupation. Figure 3.11 also shows that the obstacle itself acts as a special "field". This "field" breaks the ergodic hypothesis which was the basic one in Einstein's Brownian motion theory. The Einstein relation no longer applies as long as there are obstacles. Figure 3.12 shows that the probability of site occupation becomes highly anisotropic in the presence of a field ε=0.2. The drift of the particles in the field direction creates a shadow behind the obstacles which more or less masks some of the sites. This shadow effect strongly affects the longitudinal diffusion coefficient and increases the invalidity of the Einstein relation. At very high fields the shadow even masks the next obstacle (results are not shown).

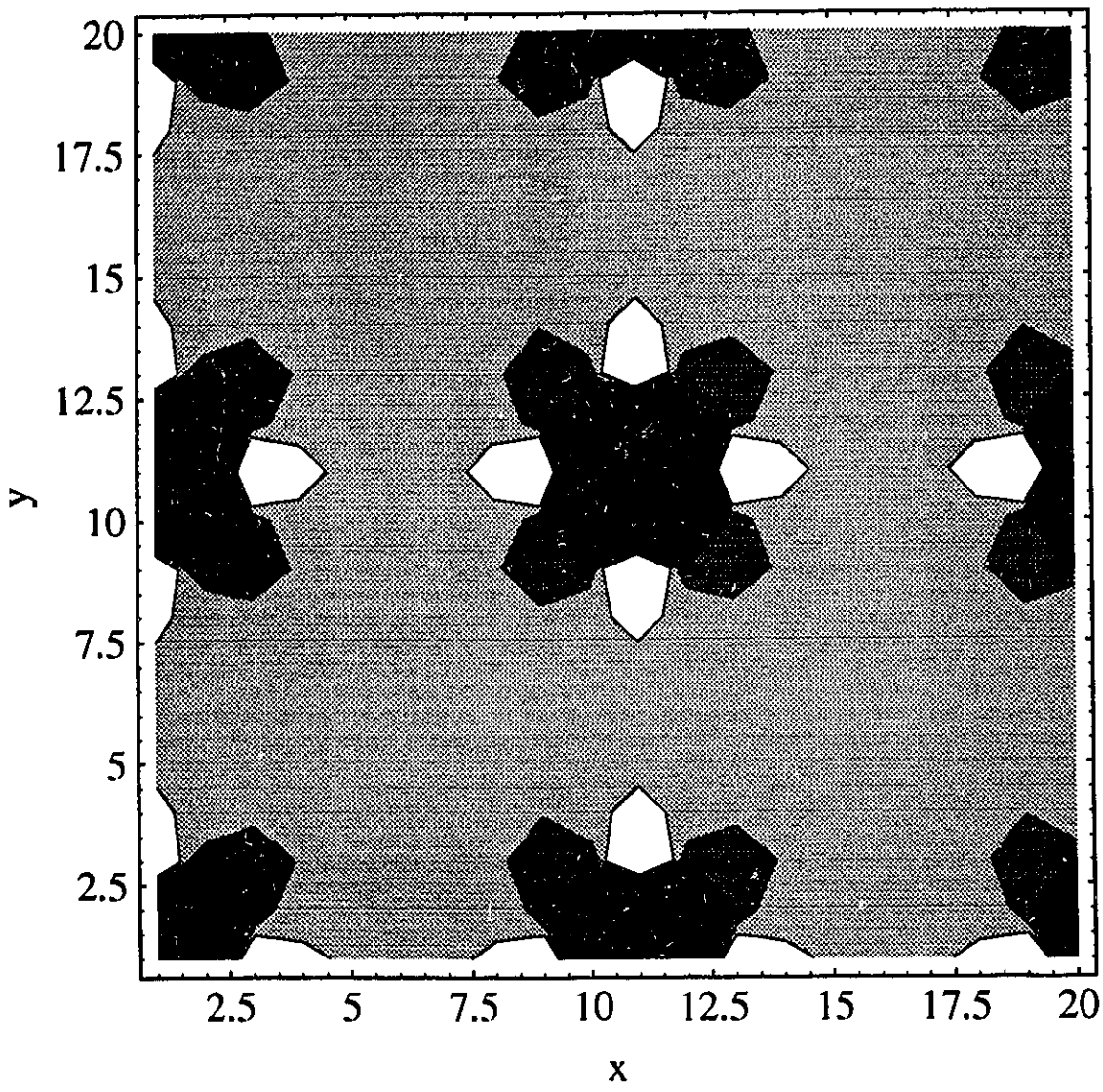

Figure 3.11 Contour plot of the occupation probability for ε=0. White areas are visited about 1.6 and 1.1 times more often than dark and background areas, respectively.

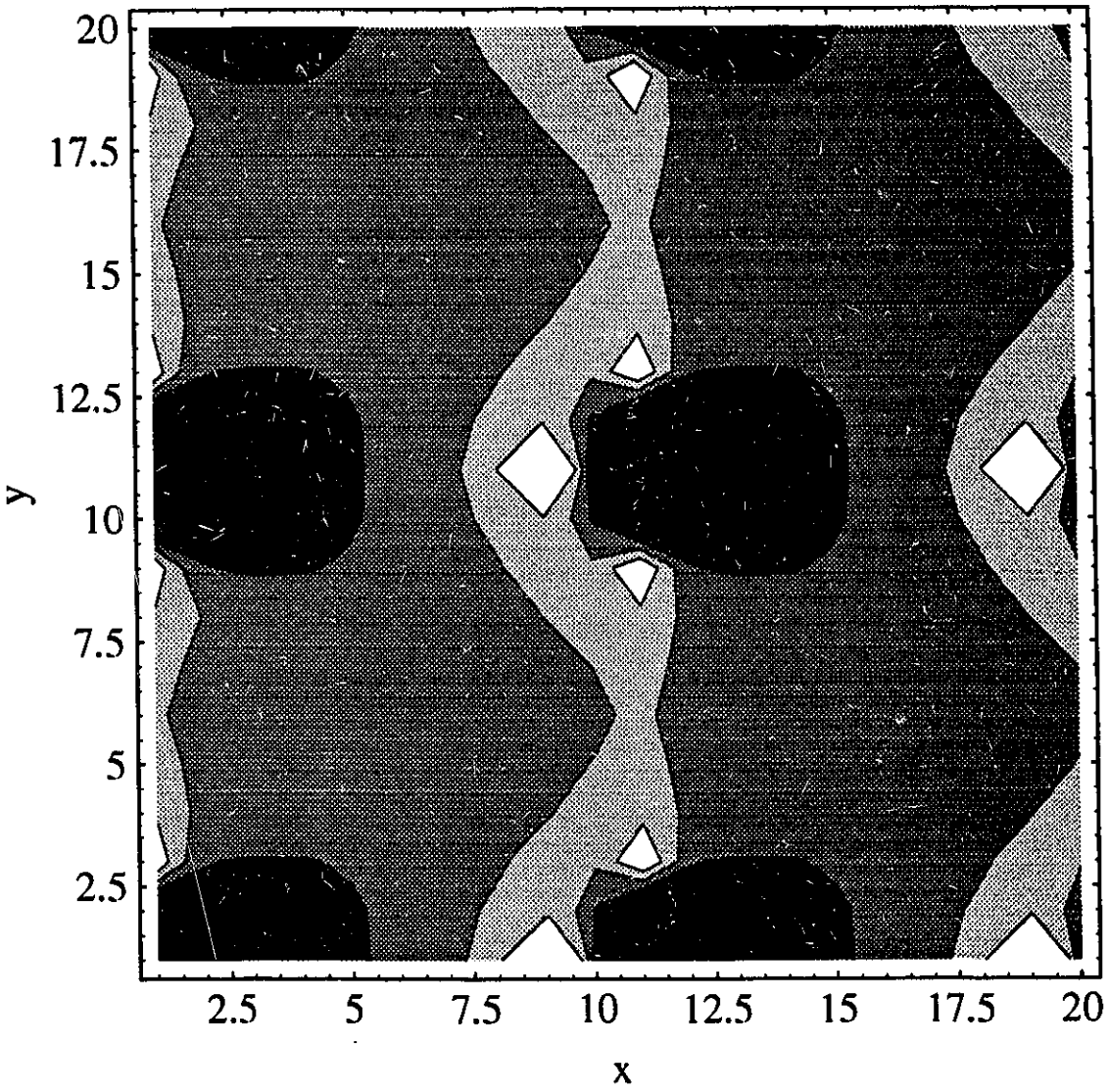

Figure 3.12 Contour plot of the occupation probability for ε=0.2. White areas are visited about 1.9 and 1.3 times more often than dark and background areas, respectively.

Chapter 4

Simulation of Random Systems

In gel electrophoresis, the gel molecules are supposed to be randomly distributed. Particles are driven by an electric field through this random gel system. The MRC model predicted that the relative electrophoretic mobility μ/μ_0 is equal to the Ogston probability, an exponential function of the gel concentration ϕ (see Eq. (2.1)). One thus expects a straight line if one plots $\ln(\mu/\mu_0)$ vs. ϕ (the Ferguson plots). One also expects another straight-line relationship between $\ln(D_x/D_0)$ and the gel concentration ϕ if one assumes that the Einsten relation (see Eq. (2.4)) holds.

We have seen in Chap. 3 that the MRC model does not apply to the periodic obstacle system, and that the Einstein relation never holds because of the existence of the obstacles. In this chapter, we are going to investigate if the MRC hypothesis is valid in the random gel system (for which the MRC model was originally proposed), i.e., if we can simply formulate the relative mobility only as a function of the fractional volume available to the particle being separated. Noticing that the field intensity plays no role in the MRC model, we are also going to study the effect of the fields on both the mobility and the diffusion coefficients. Finally, due to the appearance of traps (see Sec. 1.4) at high gel concentrations, we expect anomalous diffusion behaviour resulting from both the randomness of the gel molecules and the external fields.

4.1 Implementations

In computer simulations, we use a two-dimensional random system of obstacles to simulate gel electrophoresis. In this two-dimensional system, gel molecules are deemed as points randomly distributed on a plane. According to the Poisson distribution, the probability that a circle can be placed into the random point system (without overlaps), or the fractional area that is available to the circle, is

$$f = e^{-\pi R^2 \Phi} \tag{4.1}$$

where Φ is the density (number of points per unit area) of the points, and R the radius of the circle. Equation (4.1) can be regarded as the two-dimensional form of the Ogston probability.

The new simulation algorithm, the structure of the lattice and the calculation of the mobility and diffusion coefficients have been described in Secs. 2.4 and 2.5. Great efforts have been made to generate random immobile obstacles onto the infinite lattice. Briefly, we first create a column containing 2^{20} ($\sim 10^6$) lines. According to a given ratio, a logical constant (TRUE or FALSE) is randomly generated. It is then sequentially put into the column. The procedure continues until the column is filled. In our simulations, a TRUE or FALSE is in correspondence to a vacant or occupied site, and the probability of generating a FALSE is the gel concentration. We then use the position (x, y) of a lattice site as the seed of a "random" number generator to generate an interger (which is set to be between 1 and 2^{20}). This integer is introduced as the number of the line in the column. Thus each lattice site corresponds to a certain logical constant. By this way, obstacles are distributed randomly on the infinite lattice at the required

concentration. Figure 4.1 gives examples of the distribution of random obstacles in a 100d×100d area for different concentrations.

In the zero-field case, the diffusing particles are initially placed randomly on the unocupied sites within an approximately 4000d×4000d area inside the gel. But when the electric field is applied, we cannot start the particles inside the gel since some of the particles may get completely trapped in closed traps while others drift under the field. In fact, a particle should not start in a closed trap. For this reason, we open a slit inside the gel where there are no obstacles (this is very close to what is being done in a laboratory). The width (in x- direction) of the slit is 2d, the length (in y- direction) is infinite. Particles are initially distributed in this narrow slit, and then start to enter the gel. The mobility and diffusion coefficients are computed after the particles get to the steady-state.

4.2 Zero-field Diffusion

The global diffusion coefficient D is computed by Eq. (3.7) for various concentrations after the system reaches the steady-state. It takes a relatively long time ($t>2\times10^4\tau_B$) for the diffusing particles to get to a steady-state at high concentrations ($\phi>20\%$). Figures 4.2~4.4 give examples of the behaviour of 10^4 particles diffusing in a gel with the concentration $\phi=25\%$. The time used here is $t=2.5\times10^5\tau_B$. Figures 4.2 shows that the global variance $\langle(\Delta r)^2\rangle=\langle(\Delta x)^2\rangle+\langle(\Delta y)^2\rangle$ varies linearly with the time $\langle t\rangle=\langle t_x\rangle+\langle t_y\rangle$. Figure 4.3 shows the final positions of the 10^4 particles. They form a circlar spot as expected. Figure 4.4 shows that the position distribution, in the x- or y- direction, is a Gaussian. It is also as expected.

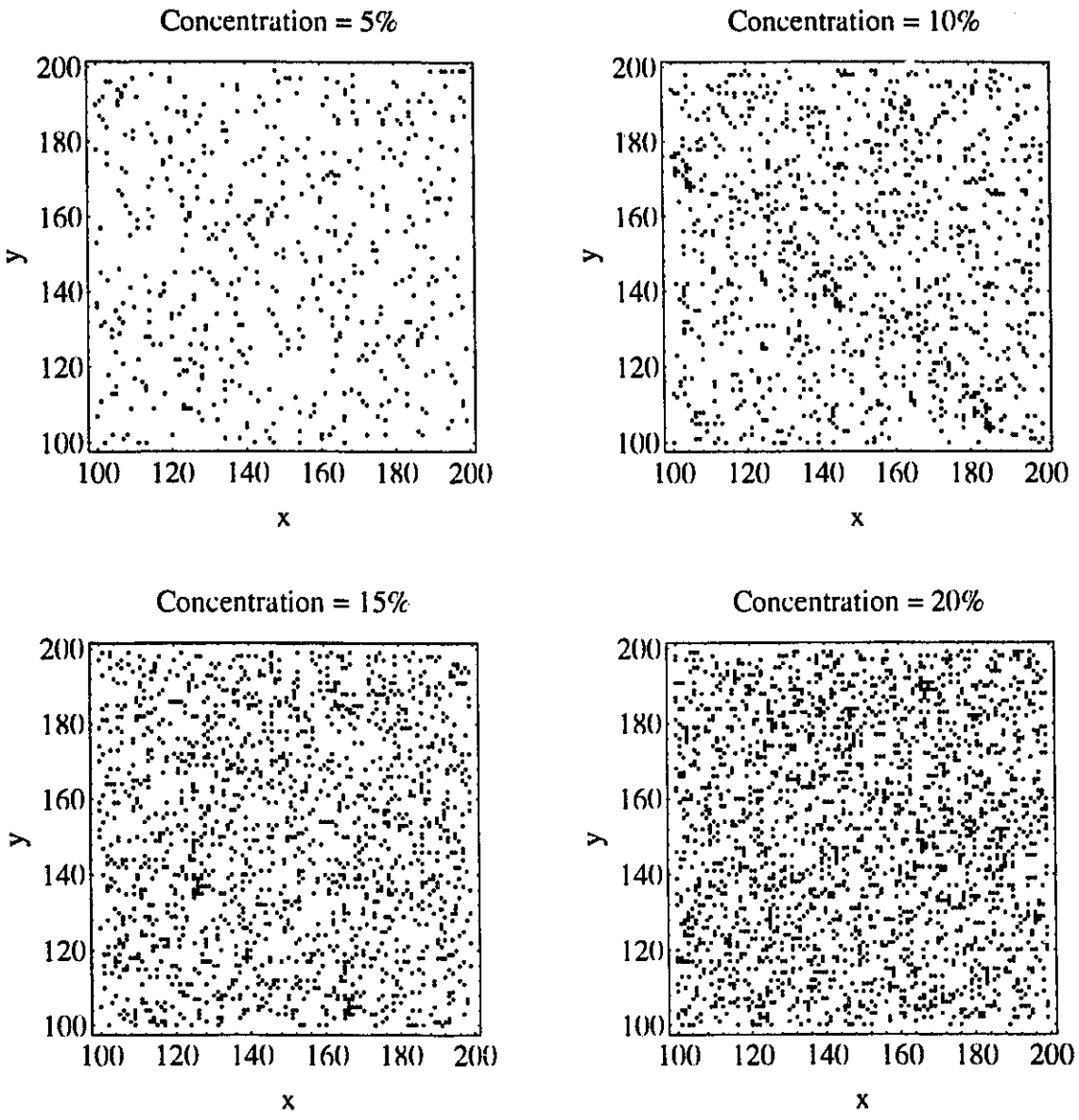

Figure 4.1 Distribution of random obstacles

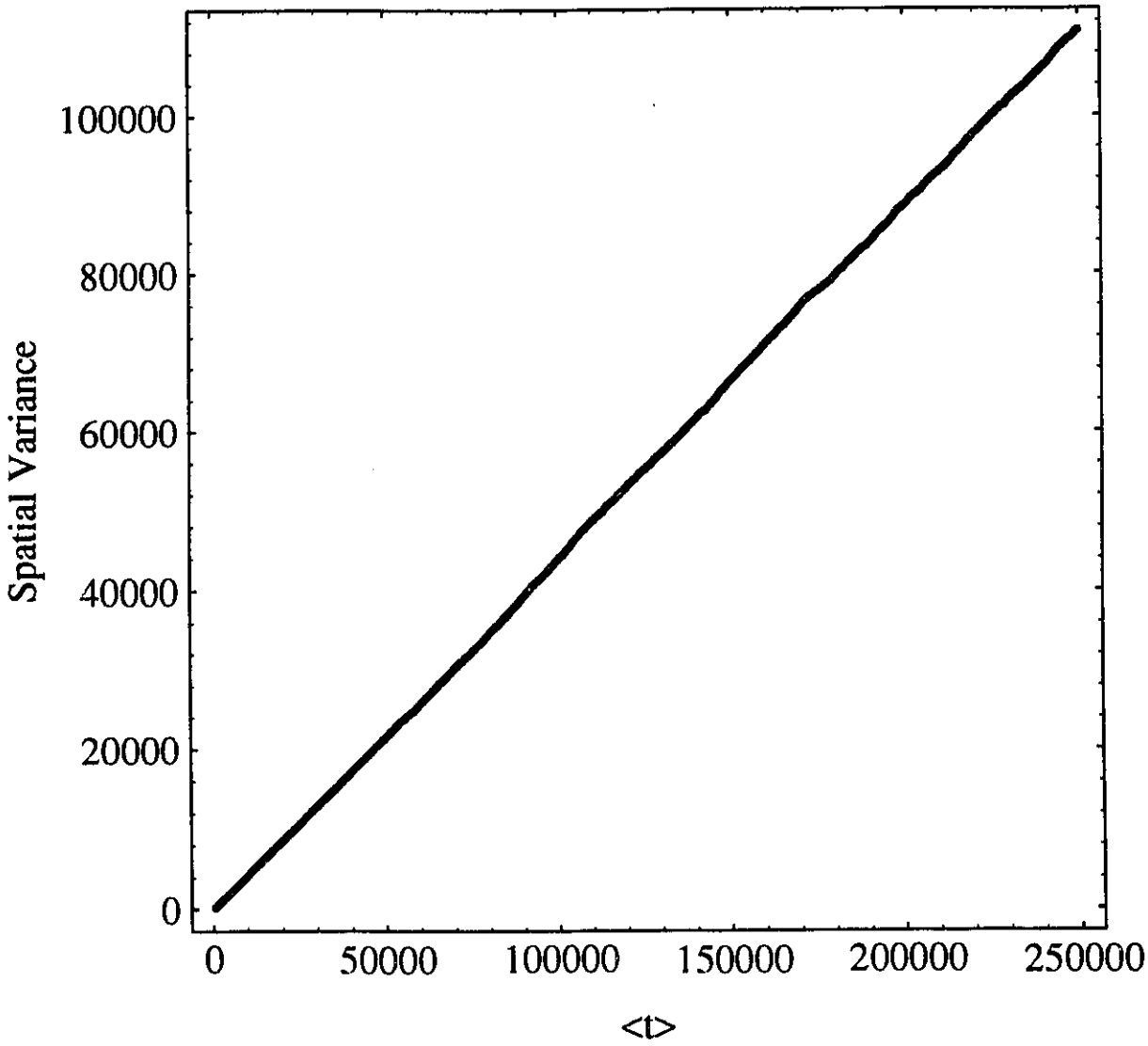

Figure 4.2 Spatial variance $\langle(\Delta r)^2\rangle$ vs. time $\langle t\rangle$, with ϕ=25%

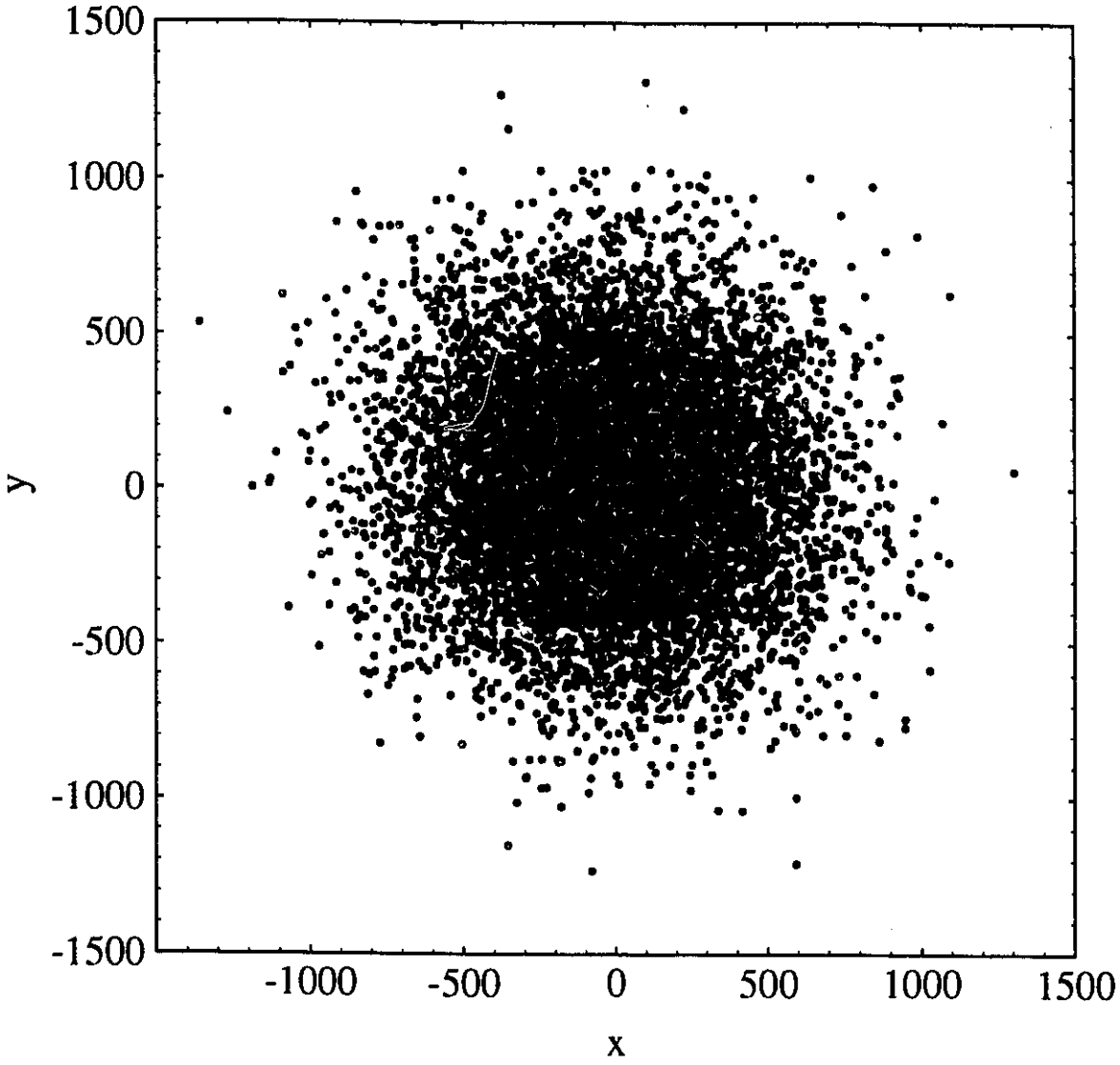

Figure 4.3 Final positions of 10^4 particles with $t=2.5\times10^5\tau_B$ and $\phi=25\%$

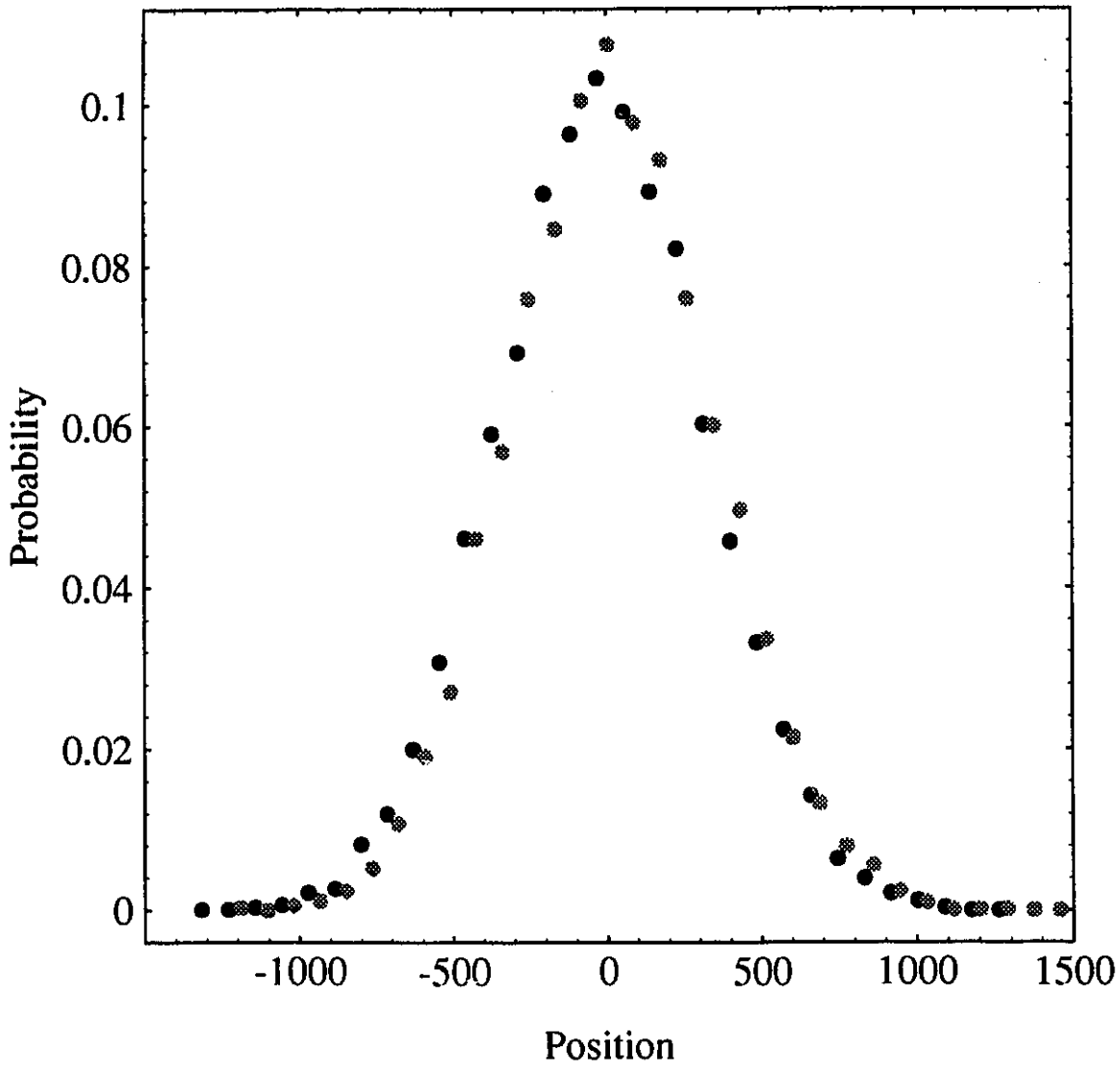

Figure 4.4 Position distribution of the 10^4 particles in Fig. 4.3. Black points for x-direction; gray points for y-direction.

Figure 4.5 shows our simulation results of the diffusion coefficient D as a function of concentration ϕ. We fit our data to a quadratic function which has two parameters. Our results agree with

$$\frac{D}{D_0} = 1 - A_D\phi - B_D\phi^2 \qquad (4.2)$$

where A_D=1.97 and B_D=1.23. This expression is very similar to Nieuwenhuizen's[15] theoretical formula $D/D_0=1-(\pi-1)\phi-0.85571\phi^2$. Saxton[23-26] has done a series of MC simulations on different (square, triangular, ...) lattices to study the zero-field diffusion (but he did not give a mathematical expression). Our results qualitatively agree with his square lattice results. The computation of the zero-field diffusion coefficient verifies again that our algorithm correctly represents the dynamics of hard particles diffusing through immobile obstacle systems. Equation (4.2) predicts that D=0 occurs at ϕ=40.5%. This is in agreement with Saxton's results[23]: the lattice of obstacle forms a percolating cluster for $\phi>\phi_c$=0.40723 which prohibits any long range diffusion.

4.3 Effect of Electric Fields

We now study the effect of an electric field on both the mobility and the diffusion coefficients when the gel concentration is fixed (for instance, ϕ=25%). When the field is on, it takes an extremely long time ($t>2\times10^5\tau_B$) for the system to get to the steady-state at high concentrations (ϕ>20%). Results for 10^4 particles moving through the gel (with the concentration ϕ=25%) are shown in Figs. 4.6~4.9. The time and the field intensity used here are $t=10^6\tau_B$ and

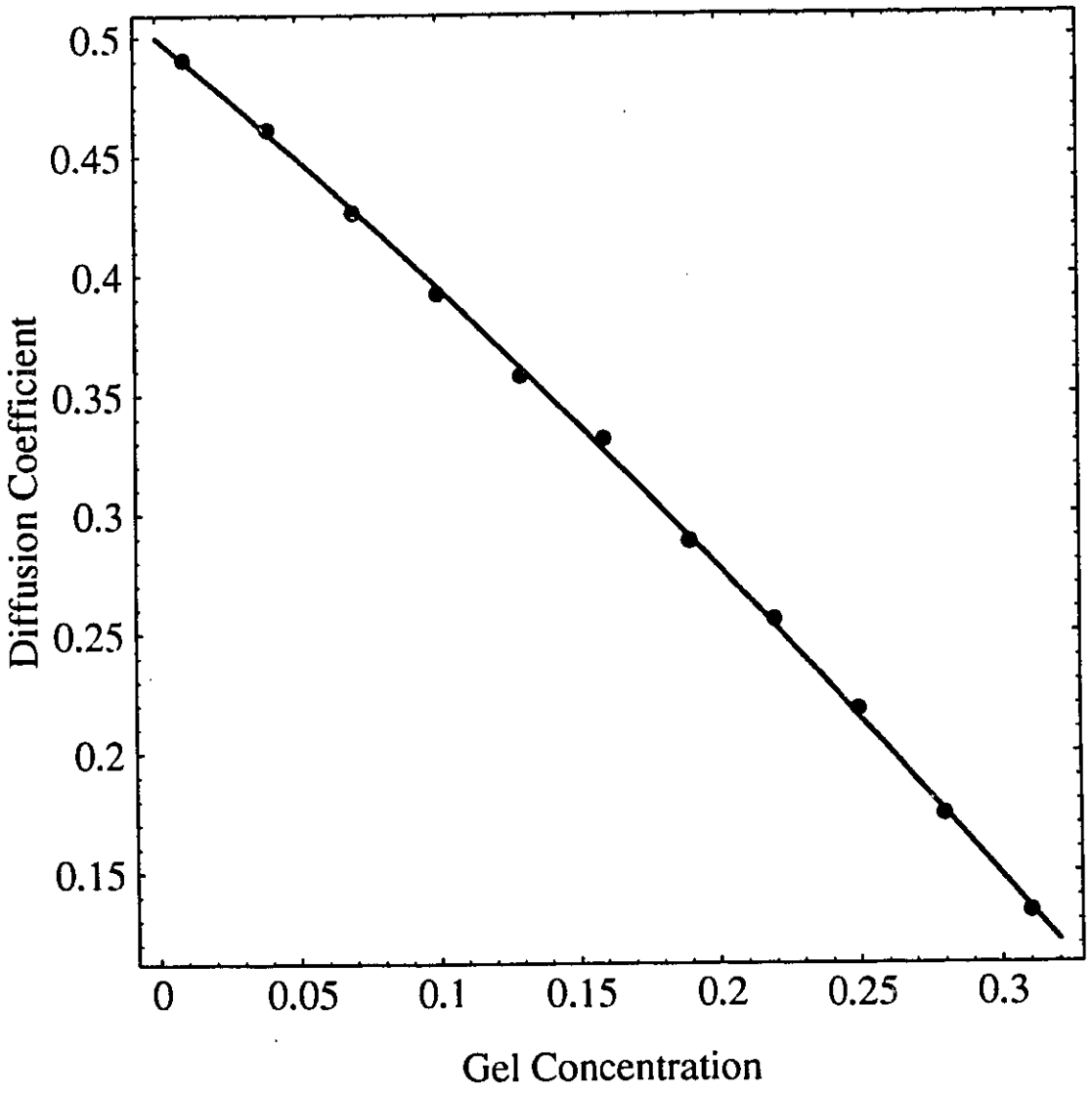

Figure 4.5 D vs. ϕ for $\varepsilon=0$. The solid curve gives the best fit $D=0.5-0.986\phi-0.615\phi^2$

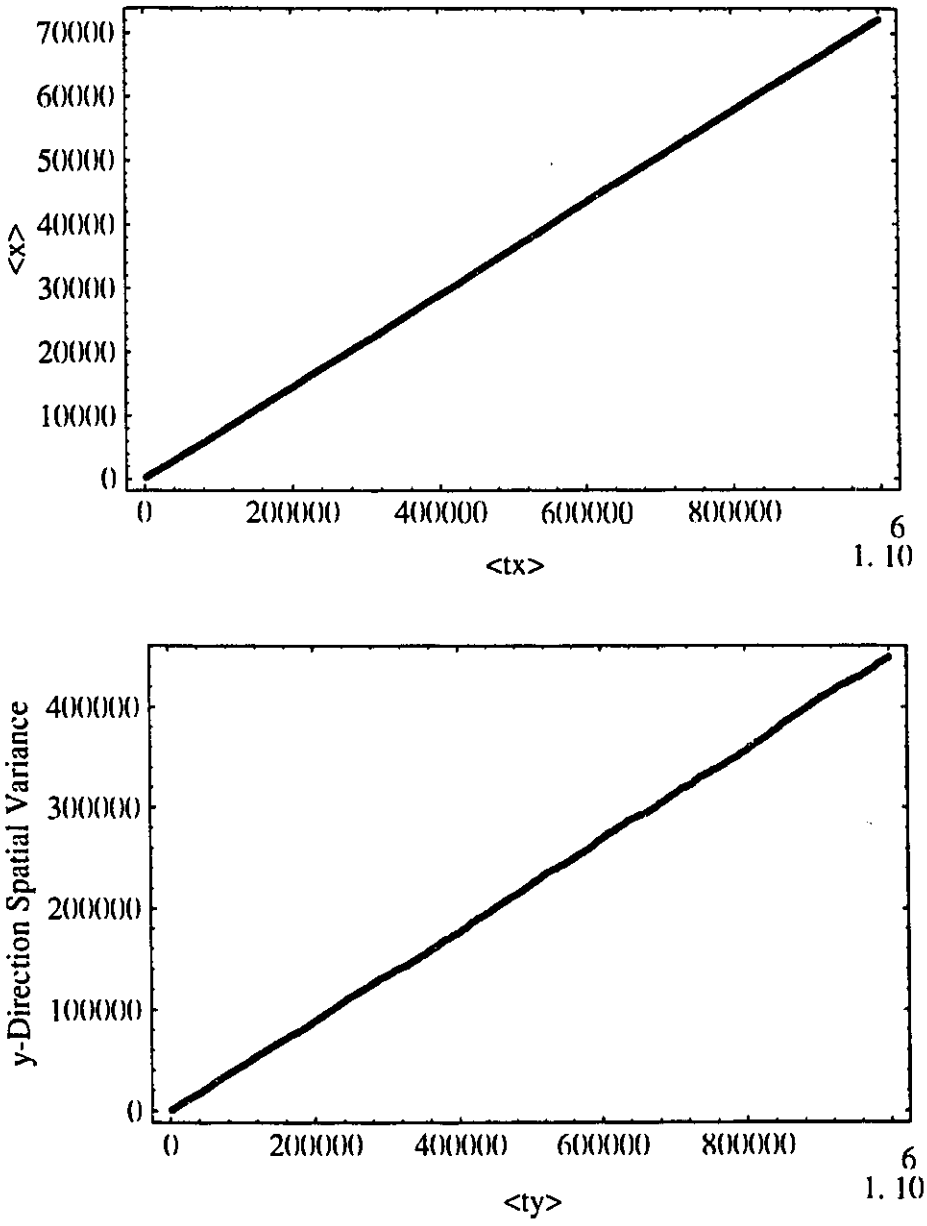

Figure 4.6 $\langle x \rangle$ vs. $\langle t_x \rangle$ and $\langle (\Delta y)^2 \rangle$ vs. $\langle t_y \rangle$

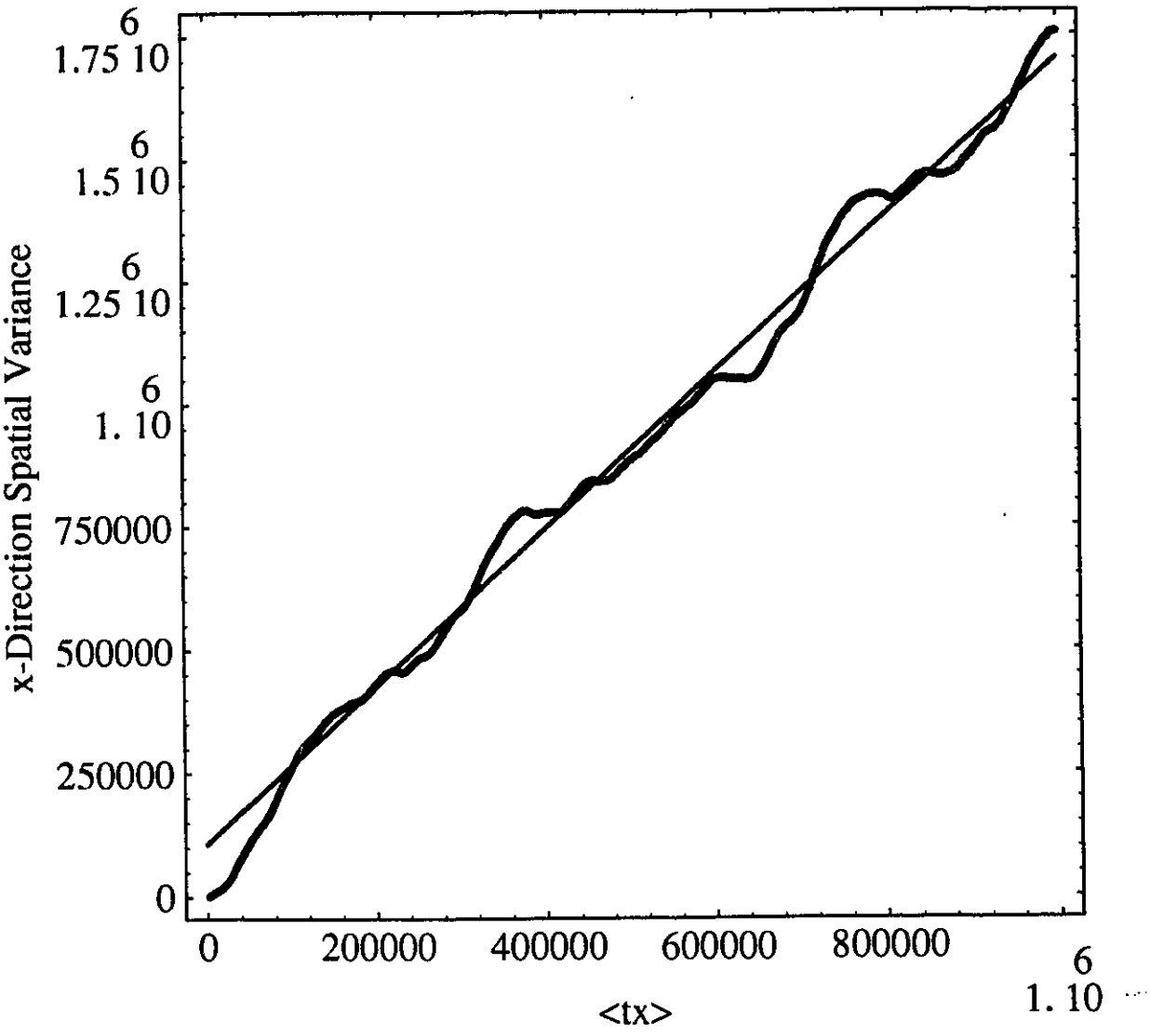

Figure 4.7 $\langle(\Delta x)^2\rangle$ vs. $\langle t_x\rangle$. **The solid straight line gives the best fit to the data.**

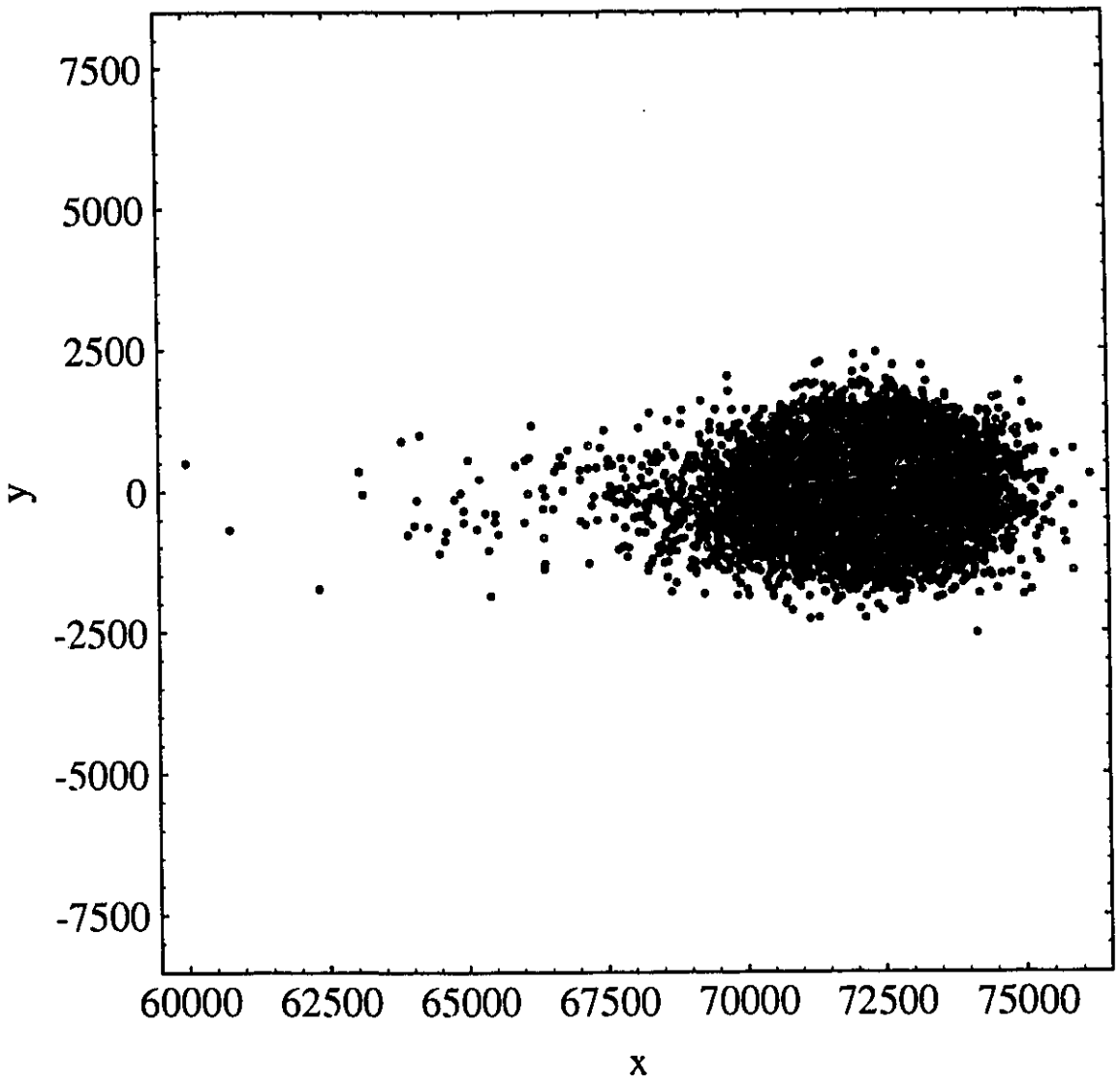

Figure 4.8 Final positions of 10^4 particles for ε=0.2 and ϕ=25%

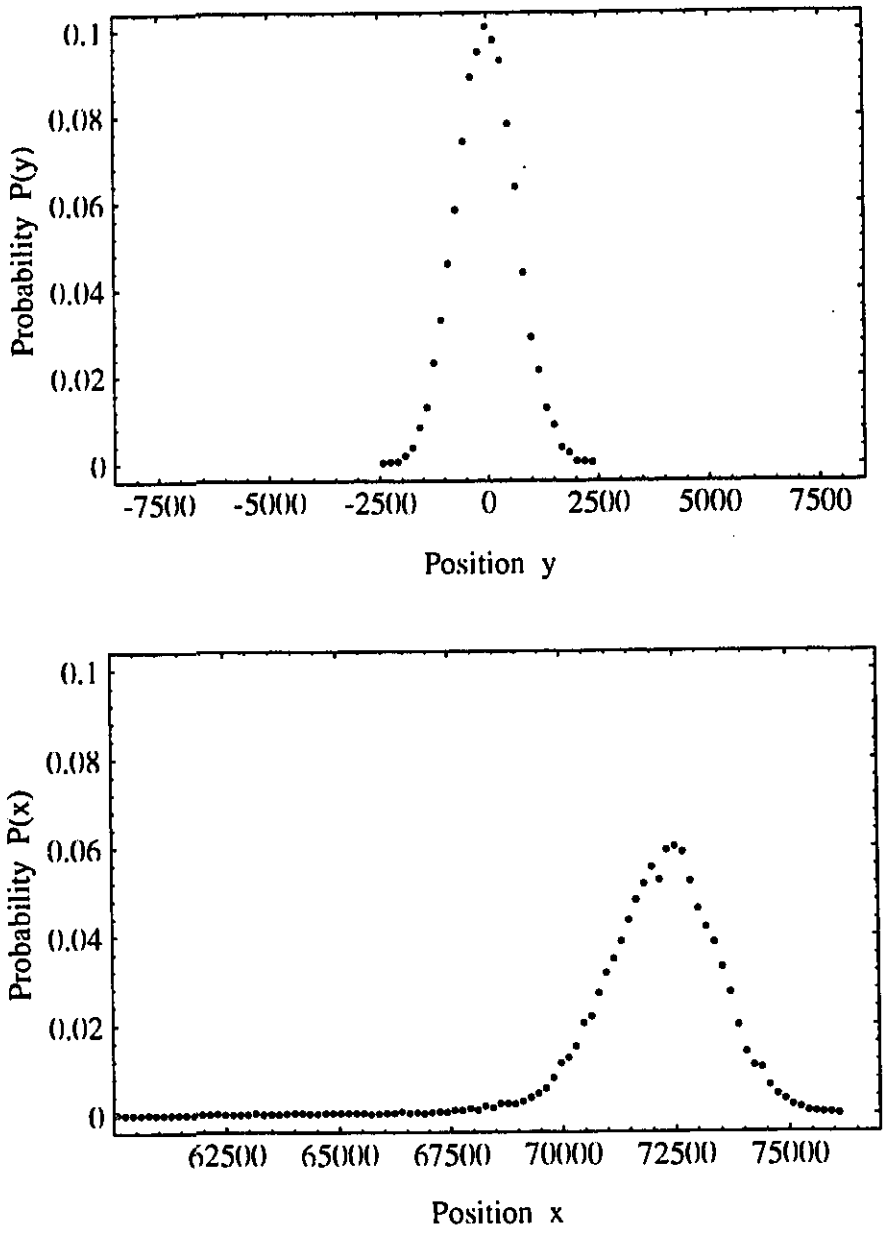

Figure 4.9 Position distributions for the particles shown on Fig. 4.8

ε=0.2 (scaled unit), respectively. Figure 4.6 shows linear relationships between $\langle x \rangle$ and $\langle t_x \rangle$ as well as $\langle (\Delta y)^2 \rangle$ and $\langle t_y \rangle$. Figure 4.7 shows that as a function of time, $\langle (\Delta x)^2 \rangle$ has more fluctuations. Figure 4.8 shows the final positions of 10^4 particles. They form a comet-like spot. It indicates that D_x is larger than D_y. Figure 4.9 shows that the position distributions are anisotropic in the presence of the field. The field results in a long tail in the longitudinal direction.

The effects of the field can be seen in Figs. 4.10 and 4.11. The gel concentration is ϕ=25%, the range of the field intensity used here is $0<\varepsilon<0.22$. Figure 4.10 shows that the mobility μ decreases slightly with the field intensity ε. Figure 4.11 shows how the diffusion coefficients vary with the field intensity. It seems that the transverse diffusion coefficient D_y does not change with the field intensity at this concentration, but the longitudinal diffusion coefficient D_x increases rapidly with ε.

In comparing the results with those of the periodic system (see Figs. 3.5 and 3.6), we find that there are two major differences: (i) the mobility decreases with the field intensity while in the periodic system it remains constant within the same range of field intensity, and (ii) the increase of D_x is much faster than that in the periodic system.

These phenomena can be interpreted as due to the trapping effect, in addition to the collision effect described in Sec. 3.4. As we can see from Fig. 4.1, the random obstacles may form $\supset$-shaped traps (especially at high concentrations ϕ>20%) which do not appear in the periodic system. When falling into such a trap (unfortunately!), a particle can only escape from it through the Brownian motion. It takes the trapped particle an extremely long time (detrapping

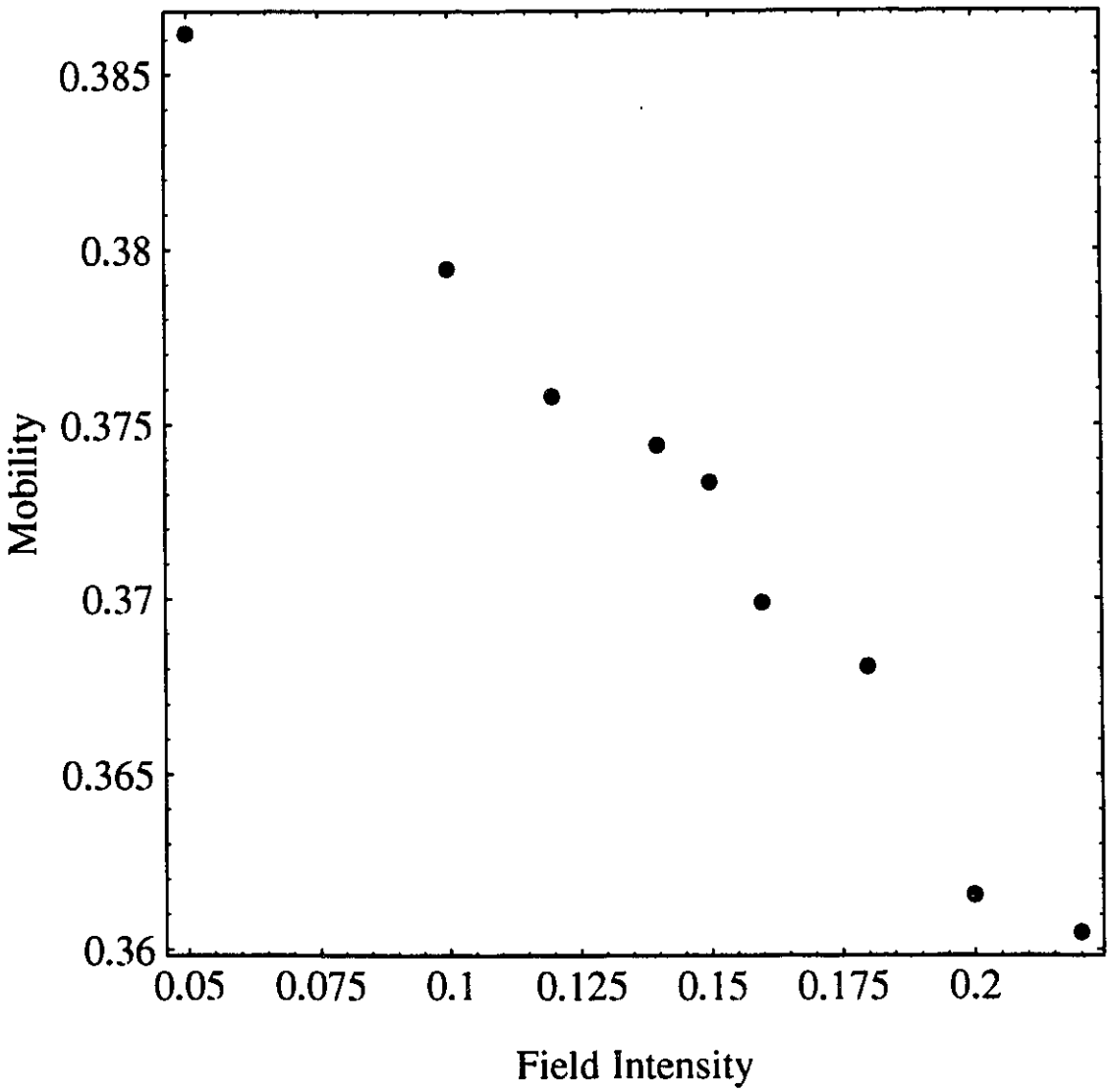

Figure 4.10 μ as a function of ε, for ϕ=25%.

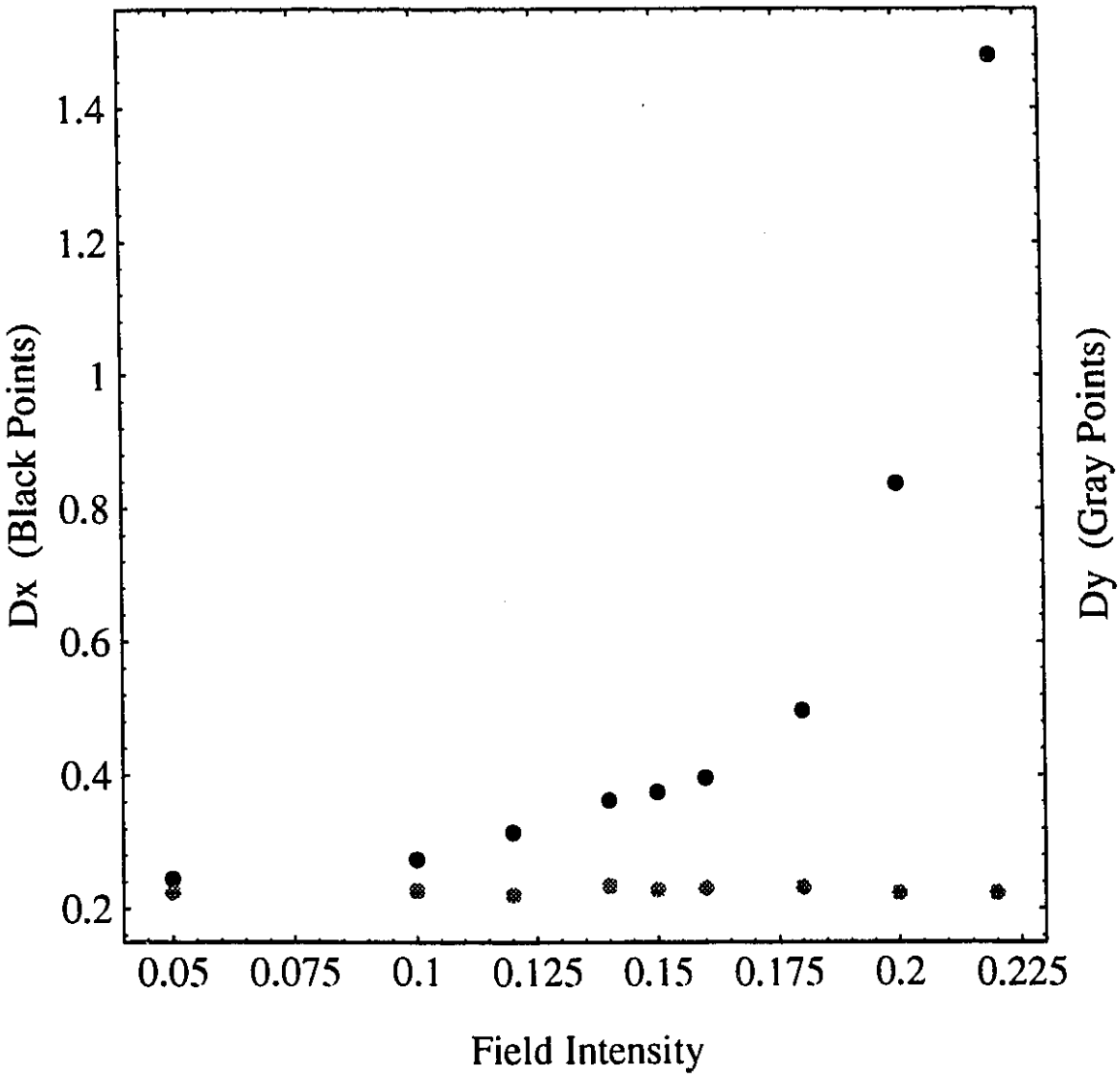

Figure 4.11 D_x and D_y as functions of ε, for ϕ=25%.

time) to get out of the trap if the field is non-negligable. This effect lowers the group velocity of the moving particles, and thus the mobility. And during the detrapping time, other particles which do not fall into traps may move far away under the electric field. It results in a exceedingly large spatial dispersion of the moving particles in the longitudinal direction (and thus a large longitudinal diffusion coefficient), much larger than that due to the normal diffusion processes and the collision effects. The deeper the ⊃-shaped traps and the stronger the electric field, the larger the longitudinal diffusion coefficient. The trapping effect also explains why there is a long tail in Fig. 4.9: the tail is formed by those trapped particles that have been left behind! Note that periodic boundary conditions would not permit an accurate estimation of the steady-state properties of such systems.

4.4 Effect of Obstacles

Figure 4.12 presents the mobility as a function of the gel concentration at different field intensities. When $\varepsilon \to 0$, the results agree with the relation

$$\frac{\mu}{\mu_0} = 1 - K_\mu \phi \qquad (4.3)$$

where K_μ=2.47. For a given concentration, higher fields decrease the mobility. We conclude from Fig. 4.12 that (i) the mobility is not an exponential function of the gel concentration as predicted by Eq. (4.1), and (ii) μ varies with both the gel concentration and the field intensity. These results disagree with what the MRC model predicted.

The decrease of the mobility with the field intensity can be interpreted as due to the

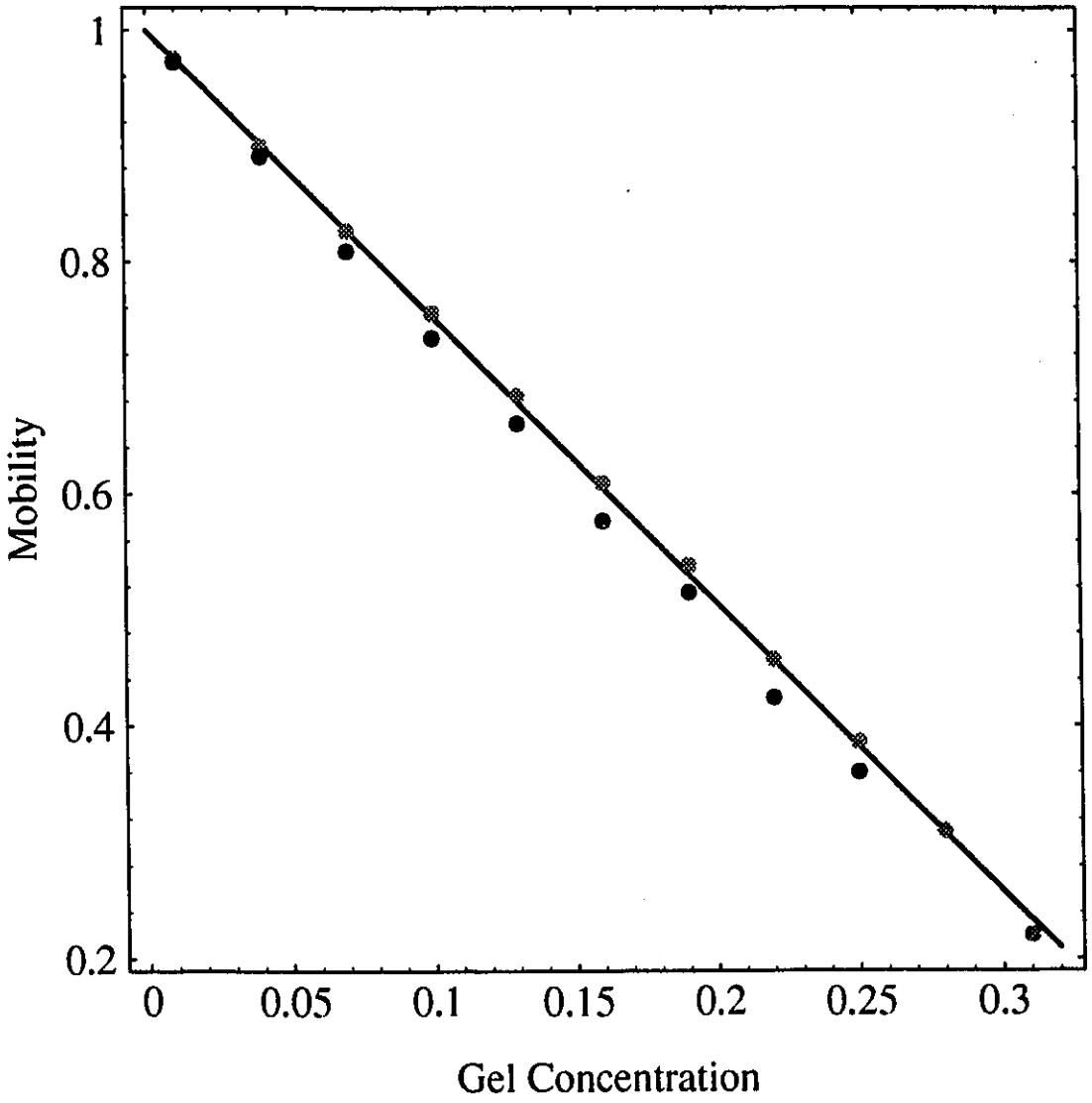

Figure 4.12 μ vs. ϕ for ε=0.05 (gray points) and ε=0.2 (black points); the solid line shows the relation μ=1-2.47ϕ.

trapping effect, as stated in Sec. 4.3. Notice that traps may appear for any concentration ϕ in random systems, but they do not exist in periodic systems. This is why we could not see the effect of the field on the mobility in the periodic system. This trapping effect predicts that for a given concentration, the mobility in the random system should be lower than that in the periodic system.

It is interesting to compare the present mobility with that obtained from the periodic system. Figure 4.13 is a plot of $\ln(\mu/\mu_0)$ vs. ϕ. The line is a "standard" Ferguson plot with the retardation coefficient K_μ=2.47; black and gray points represent random and periodic results, respectively. We can see that the periodic result bends up and the random result bends down. The MRC model predicts something in between. Our results indicate that the mobility is not simply proportional to the fractional volume. Other factors, such as the shadow effect (Fig. 3.11), the field intensity, etc., do affect the electrophoretic mobility during electrophoresis.

Figure 4.14 shows the transverse diffusion coefficient as a function of the concentration at different field intensities. The curve is given by Eq. (4.2). Gray and black points stand for ε=0.05 and ε=0.2 (scaled unit), respectively. At ε=0.05, D_y behaves as if there were no fields. At ε=0.2, the field affects D_y by increasing its value a little bit in the concentration range $7\%<\phi<20\%$. This increase can be interpreted as due to the tunnel effect. Lots of tunnels appear in random systems in that concentration range. Remember that the y-clock is moved if a particle goes through an x-tunnel. When there is an electric field, the time for passing through an x-tunnel is shorter than that in the zero-field case. But the dispersion in y-direction is not changed by the tunnel. So D_y increases due to the tunnel effect. The larger the field intensity, the stronger the

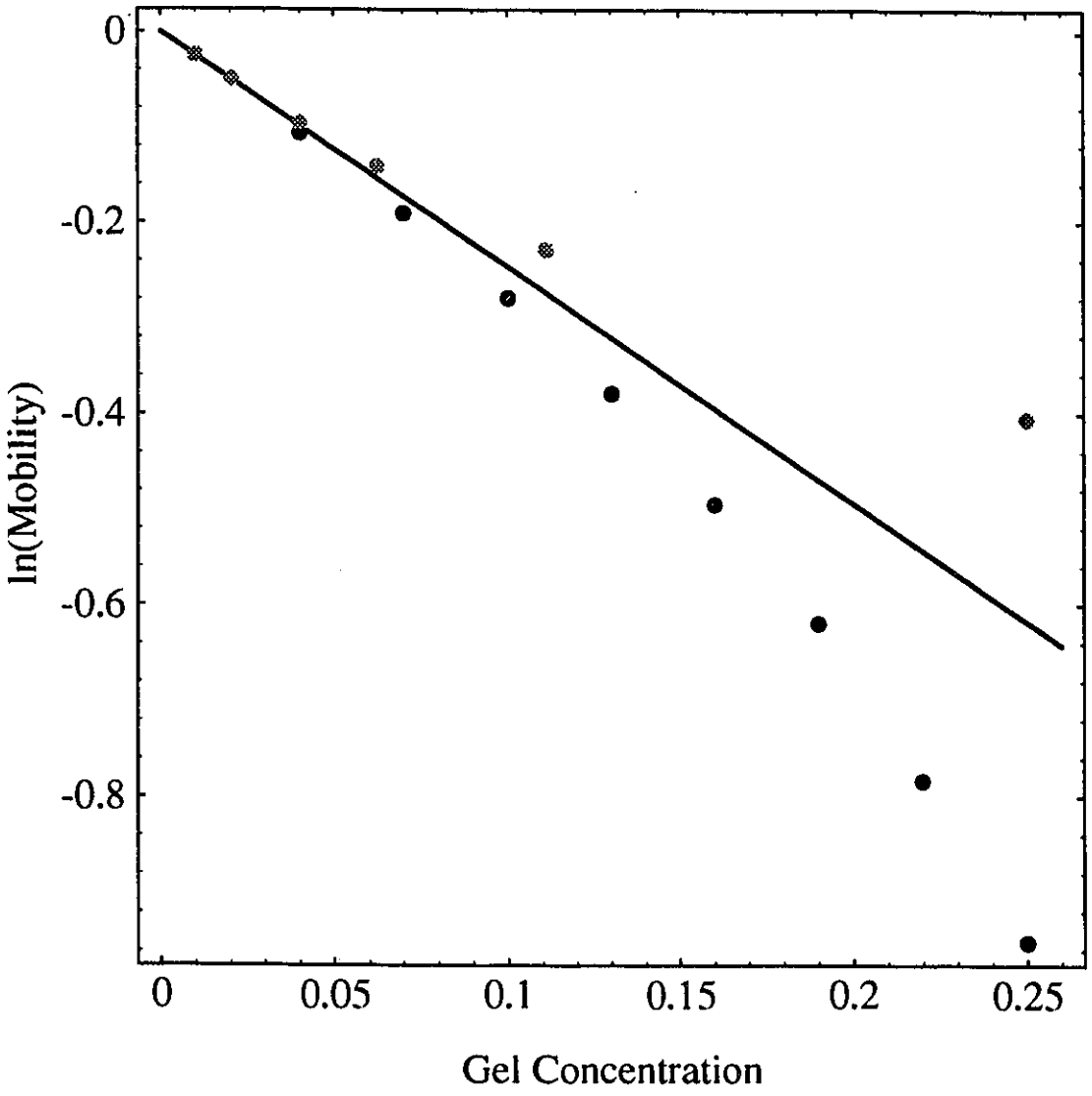

Figure 4.13 $\ln(\mu/\mu_0)$ vs. ϕ for ε=0.05; gray and black points are for the periodic and random systems, respectively; the solid line shows the relation $\ln(\mu/\mu_0)$=-2.47ϕ.

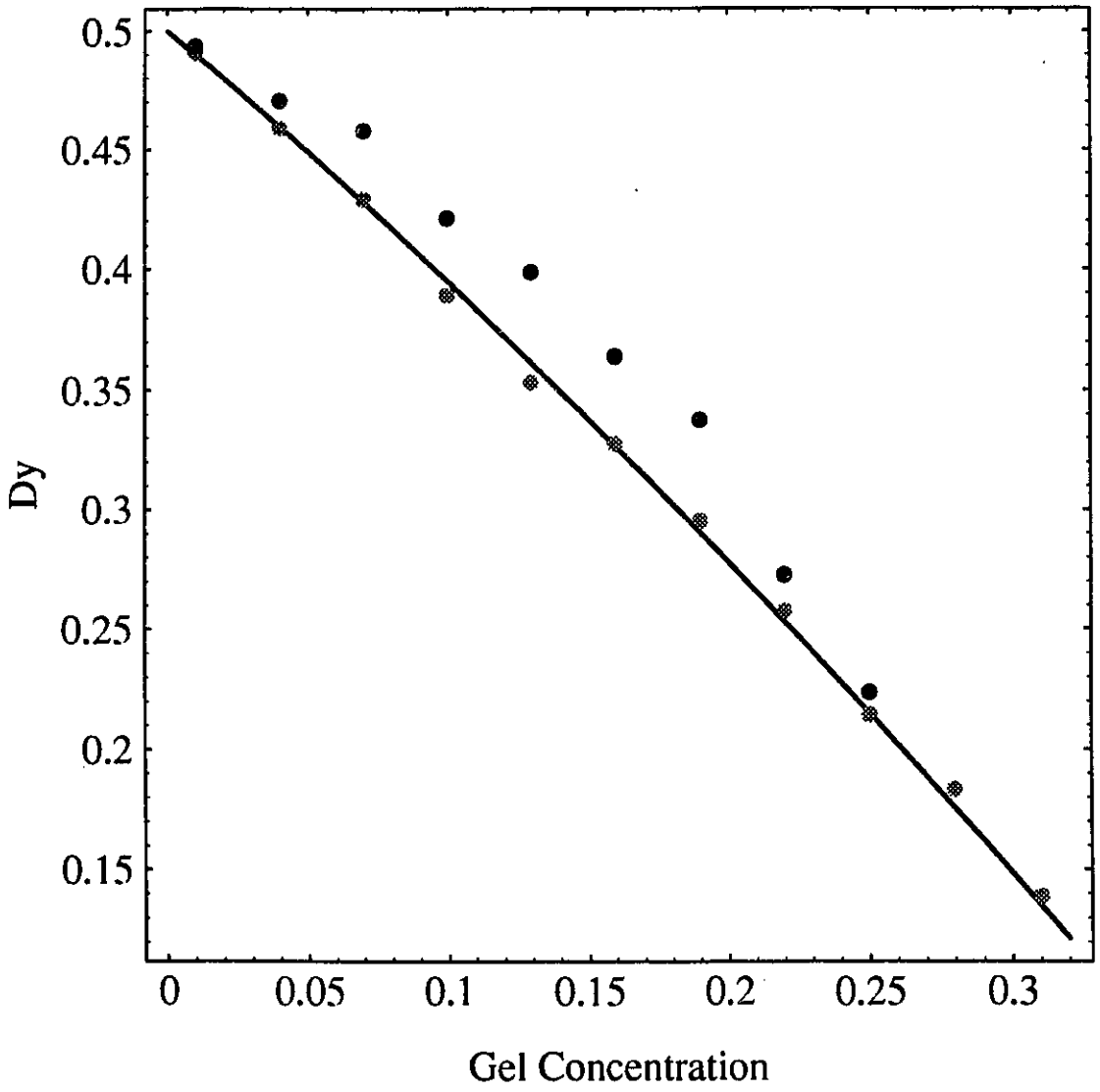

Figure 4.14 D_y **vs.** ϕ **for** ε**=0.05 (gray points) and** ε**=0.2 (black points); the solid curve is given by Eq. (4.2)**

tunnel effect. This effect does not appear in the periodic system since there are no tunnels in that system.

Figure 4.15 shows the longitudinal diffusion coefficient as a function of the gel concentration at different field intensities. The curve is from Eq. (4.2); Gray and black points are for ε=0.05 and ε=0.2, respectively. At low field, D_x bends up slightly only at high concentrations (ϕ>20%). At ε=0.2, D_x increases extremely fast with the concentration. This is definitely due to the trapping effect, as stated in Sec. 4.3. The large value of the longitudinal diffusion coefficient indicates that we cannot use such large field intensities as ε>0.2, and such dense gel systems as ϕ>20% to carry out molecular separations, since under such conditions the molecular bands become broadened, blurred, and they overlap with each other during gel electrophoresis.

Figure 4.16 shows again that even under low fields and low concentrations, the Einstein relation does not apply to the obstacle system. We can see this point from Eqs. (4.2) and (4.3) since the coefficients $A_{\parallel}$ and $K_{\parallel}$ are not equal. This conclusion agrees with experimental results[13].

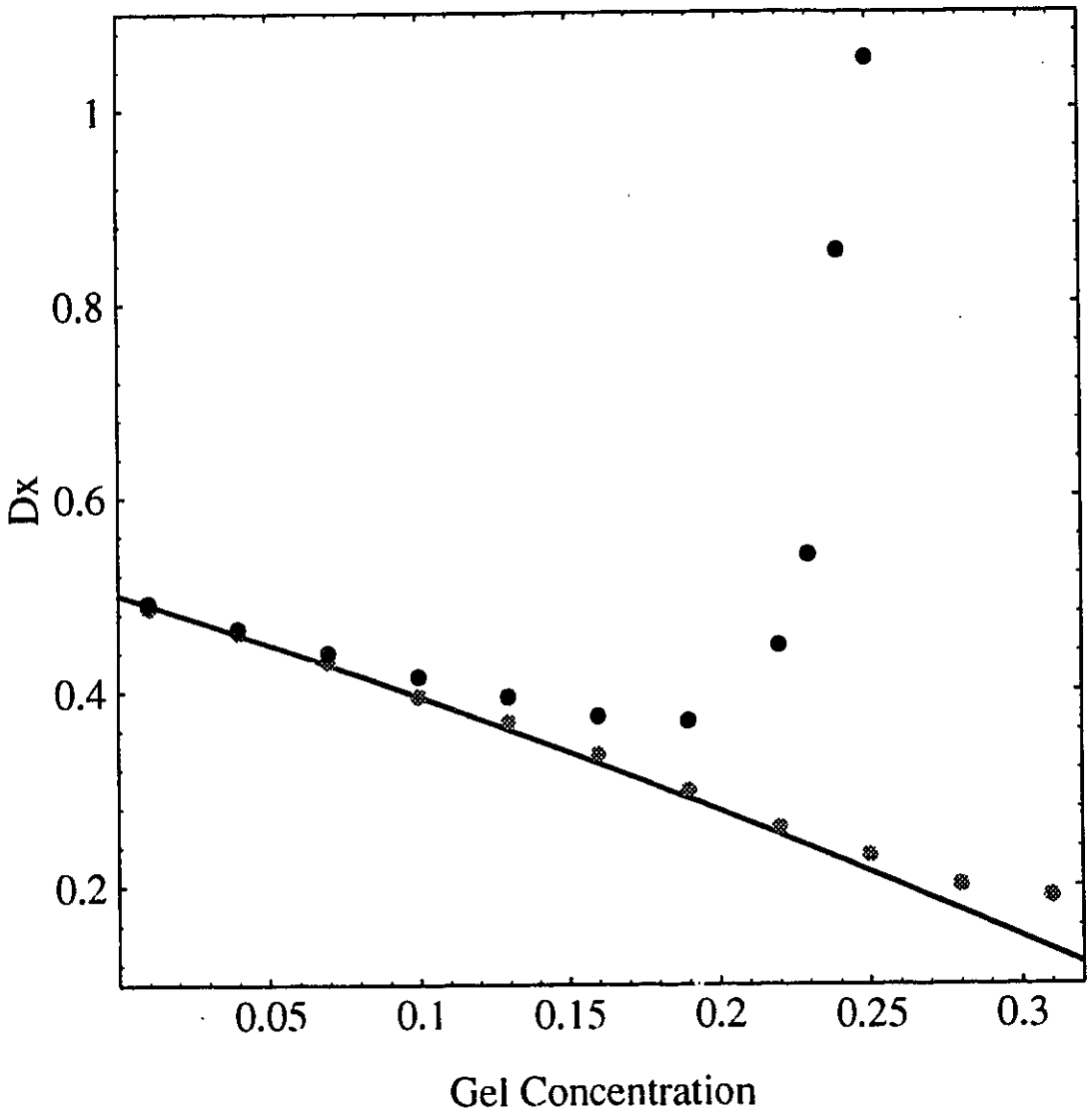

Figure 4.15 D_x vs. ϕ for ε=0.05 (gray points) and ε=0.2 (black points); the solid curve is given by Eq. (4.2)

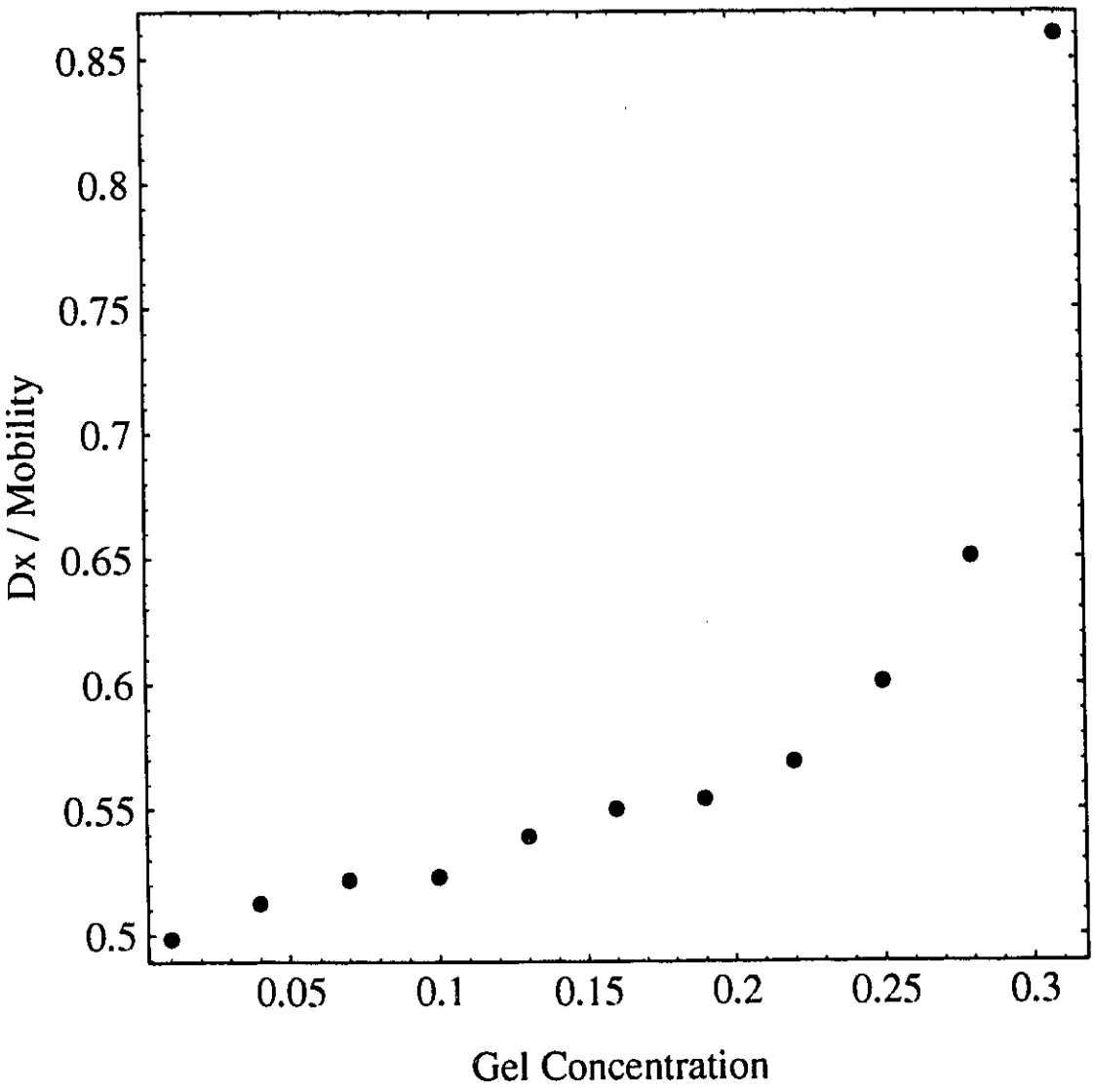

Figure 4.16 D_x/μ vs. ϕ, for ε=0.05

Chapter 5

Conclusions and Discussions

We developed a new Monte Carlo algorithm to simulate the behaviour of a hard particle during gel electrophoresis. The new algorithm is applied to the motion in periodic and random obstacle systems. The calculations of the electrophoretic mobility and diffusion coefficients lead to two main qualitative conclusions: the mobility is not proportional to the fractional volume available the particle, and the longitudinal diffusion coefficient is not proportional to the mobility. As far as quantitative results are concerned, we suggested Eqs. (3.8) and (3.10) for periodic "gels", and Eqs. (4.2) and (4.3) for random gels. These results declare the invalidity of both the MRC model and the Einstein relation for gel electrophoresis. The main consequence is that the Ferguson plot is not fundamentally linear, and that the diffusion coefficients must be measured and not inferred from the mobility data.

The reason of the invalidity of the MRC model and Einstein relation is that the obstacles change the dynamics of the Brownian motion by invalidating the ergodic hypothesis. Our simulations indicate that the electric field does play roles in electrophoresis, especially for the diffusing process in a random, dense environment. The mobility and diffusion coefficients are functions of both the gel concentration and the field intensity. The results predict that high electric fields and large gel concentrations are useless for molecular separations.

The new algorithm involves several approximatioms. First, a pure hard-core repulsive interaction between a particle and an obstacle is assumed. Attractive forces and long-range repulsive forces are neglected. Second, both the particles and the obstacles are considered point-like, i.e., they have the same size. Increasing the size of the particle and/or the obstacle will definitely change the migration and diffusion behaviours. Third, the model assumes that obstacles are immobile on the time scale of the migration and diffusion measurement. Mobile obstacles may have significant effects. Fourth, the model is two-dimensional. In three-dimension, the particle has more freedom and is not easy to get trapped. Finally, our model neglects hydrodynamic interactions among particles. All these limitations are more important than the statistical errors in the MC simulations.

Many possible research projects can follow this thesis. For instance, since it is not a rejection MC, the new algorithm allows us to add some forces to the interactions between a particle and an obstacle. In fact, there is a general method to solve the first-passage problem[5] for such situations. We can also change the size of the particle to study the size-dependence on the mobility and diffusion coefficients. We can use the stick gel model instead of point-like obstacles in order to extend the model to the three-dimensional case where we may employ three clocks. We can change alternatively the (±) directions of the field to simulate pulsed field gel electrophoresis[35]. Finally, we can study the effect of mobile obstacles or concentration gradients. These suggestions all have experimental importance and will be pursued for my Ph.D.

Appendix

One-Dimensional Brownian Motion

In this appendix, we study the Brownian dynamics of a particle that performs a one-dimensional random walk between two walls. We present explicit expressions for the probability of being absorbed by one of the walls, the mean (conditional) absorption time as well as the fluctuation of this absorption time.

A.1 Two Absorbing Walls

We first consider a particle performing a random walk between two absorbing walls. Suppose the particle has probabilities p and q of making a positive and a negative step, respectively. During each time duration t_0 the particle moves a step a_0 in either the positive or the negative direction. Let the two walls be located at 0 and L, and the initial position of the particle be at x ($0 \le x \le L$). The motion continues until the particle for the first time reaches either 0 or L.

Let P_- be the probability of the particle being absorbed at 0. Obviously, the probability P_- is a function of the initial position x. The difference equation for $P_-(x)$ is[4]:

$$P_{-}(x) = p\, P_{-}(x+a_0) + q\, P_{-}(x-a_0) \tag{A.1}$$

with the boundary conditions

$$P_{-}(0) = 1 \tag{A.2}$$

and

$$P_{-}(L) = 0 \tag{A.3}$$

Expanding Eq. (A.1) according to Taylor's theorem (up to terms of second order) when $a_0 \rightarrow 0$, we get the formal differential equation

$$D\, P_{-}''(x) + v\, P_{-}'(x) = 0 \tag{A.4}$$

where

$$D = \frac{a_0^2}{2\, t_0} \tag{A.5}$$

is the diffusion coefficient and

$$v = (p - q)\, \frac{a_0}{t_0} \tag{A.6}$$

is the drift velocity of the particle, in response to the Brownian motion and the electrophoretic drift. The solution to Eq. (A.4), with boundary conditions (A.2) and (A.3), is

$$P_{-}(x) = \frac{e^{-\frac{xv}{D}} - e^{-\frac{Lv}{D}}}{1 - e^{-\frac{Lv}{D}}} \tag{A.7}$$

Substituting x→L-x and v→-v into Eq. (A.7), we get the probability of the particle being absorbed at L:

$$P_{+}(x) = \frac{1 - e^{-\frac{xv}{D}}}{1 - e^{-\frac{Lv}{D}}} \tag{A.8}$$

One can easily verify that $P_{+}(x)+P_{-}(x)=1$ as expected.

The mean first passage time of the particle (or mean conditionnal absorbtion time) at 0 is given by[31, 41]

$$\left\langle t_{-}^{n}(x) \right\rangle = \frac{\int_0^{\infty} t^n f(t, x)\, dt}{\int_0^{\infty} f(t, x)\, dt} \tag{A.9}$$

where[41]

$$f(t, x) = \frac{2\pi D}{L^2} e^{-\frac{v}{4D}(vt+2x)} \sum_{k=1}^{\infty} k\, e^{-\frac{k^2\pi^2 Dt}{L^2}} \sin\left(\frac{k\pi x}{L}\right) \tag{A.10}$$

So that

$$\left\langle t_-^n(x) \right\rangle = \frac{\sum_{k=1}^{\infty} k \sin\left(\frac{k\pi x}{L}\right) \int_0^{\infty} t^n e^{-yt}\, dt}{\sum_{k=1}^{\infty} k \sin\left(\frac{k\pi x}{L}\right) \int_0^{\infty} e^{-yt}\, dt} \qquad \text{(A.11)}$$

where

$$y = \frac{v^2}{4D} + \frac{k^2\pi^2 D}{L^2} \qquad \text{(A.12)}$$

Let us define a function I(q)

$$I(q) = \sum_{k=1}^{\infty} k \sin\left(\frac{k\pi x}{L}\right) \int_0^{\infty} e^{-(y+q)t}\, dt \qquad \text{(A.13)}$$

$$= \frac{L^2}{\pi^2 D} \sum_{k=1}^{\infty} \frac{k \sin\left(\frac{k\pi x}{L}\right)}{k^2 + \left(\frac{v^2 L^2}{4\pi^2 D^2} + \frac{qL^2}{\pi^2 D}\right)} \qquad \text{(A.14)}$$

Using the identity[6]

$$\sum_{k=1}^{\infty} \frac{k \sin(kx)}{k^2 + b^2} = \frac{\pi}{2} \frac{\sinh[b(\pi - x)]}{\sinh(b\pi)} \qquad \text{(A.15)}$$

we obtain

$$I(q) = \frac{L^2}{2\pi D} \frac{\sinh\left[\sqrt{\frac{v^2L^2}{4D^2} + \frac{qL^2}{D}}\left(1 - \frac{x}{L}\right)\right]}{\sinh\left(\sqrt{\frac{v^2L^2}{4D^2} + \frac{qL^2}{D}}\right)} \tag{A.16}$$

From Eq. (A.13), <t_-^n> can be expressed as

$$\left\langle t_-^n \right\rangle = (-1)^n \frac{I^{(n)}(q) \mid_{q=0}}{I(q) \mid_{q=0}} \tag{A.17}$$

Substituting Eq. (A.16) into Eq. (A.17), we get

$$\left\langle t_-(x) \right\rangle = \frac{L}{v} \coth(u) - \frac{L}{v}\left(1 - \frac{x}{L}\right) \coth(u-z) \tag{A.18}$$

where

$$u = \frac{L\,v}{2D} \tag{A.19}$$

and

$$z = \frac{x\,v}{2D} \tag{A.20}$$

Similarly, we obtain the second moment

$$\left\langle t_-^2(x) \right\rangle = \frac{L}{v^3} \operatorname{csch}(u-z) \sinh(u) \cdot [\, 2\, D \coth(u) \operatorname{csch}(u) \sinh(u-z)$$

$$- 2 D \left(1 - \frac{x}{L}\right) \cosh(u-z)\ csch(u)$$

$$+ L \nu\ csch^3(u)\ \sinh(u-z)$$

$$+ L \nu \coth^2(u)\ csch(u)\ \sinh(u-z)$$

$$- 2 L \nu \left(1 - \frac{x}{L}\right) \cosh(u-z)\ \coth(u)\ csch(u)$$

$$+ L \nu \left(1 - \frac{x}{L}\right)^2 csch(u)\ \sinh(u-z)\ ] \qquad \textbf{(A.21)}$$

which will be used to calculate the variance of the mean first passage time.

The mean time of being absorbed at L can be obtained by substituting x→L-x and ν→-ν into Eqs. (A.18) and (A.21):

$$\langle t_+(x) \rangle = \frac{L}{\nu} \coth(u) - \frac{x}{\nu} \coth(z) \qquad \textbf{(A.22)}$$

and

$$\left\langle t_+^2(x)\right\rangle = \frac{L}{v^3}\, csch(z)\, \sinh(u) \cdot [\; 2\, D\, \coth(u)\, csch(u)\, \sinh(z)$$

$$- \frac{2Dx}{L} \cosh(z)\, csch(u)$$

$$+ L\, v\, csch^3(u)\, \sinh(z)$$

$$+ L\, v \coth^2(u)\, csch(u)\, \sinh(z)$$

$$- 2\, x\, v \cosh(z) \coth(u)\, csch(u)$$

$$+ \frac{x^2 v}{L} csch(u)\, \sinh(z)\;] \qquad \textbf{(A.23)}$$

In our simulation model, the particle jumps freely on a one-dimensional lattice with the lattice parameter d. It moves a distance d in either the +x or the -x direction to complete a jump. To obtain the probabilities and the mean times for jumping forward and backward, we must use L=2d and x=d in the equations above. Equations (A.7) and (A.8) then yield

$$P_- = \frac{1}{1 + e^{2\varepsilon}} \qquad \textbf{(A.24)}$$

and

$$P_{+} = \frac{1}{1 + e^{-2\varepsilon}} \tag{A.25}$$

where

$$\varepsilon = \frac{dqE}{2kT} \tag{A.26}$$

is the scaled field intensity. Here q is the electric charge of the particle, E is the intensity of the external electric field, k is Boltzmann's constant, T is the temperature, and Eq. (2.4) is used.

Under the same conditions (L=2d and x=d), Eq. (A.18) and Eq. (A.22) yield the same expression

$$\langle t_{\pm} \rangle = \frac{\tanh(\varepsilon)}{\varepsilon} \tau_B \tag{A.27}$$

where

$$\tau_B = \frac{d^2}{2D} \tag{A.28}$$

is the Brownian time for one free jump; Eqs. (A.21) and (A.23) also yield the same expression:

$$\langle t_{\pm}^2 \rangle = \frac{\varepsilon \tanh^2(\varepsilon) + \tanh(\varepsilon) - \varepsilon \, sech(\varepsilon)}{\varepsilon^3} \tau_B^2 \tag{A.29}$$

From Eqs. (A.27) and (A.29), we obtain the variance

$$\sigma_{t_+}^2 \equiv \langle t_{\pm}^2 \rangle - \langle t_{\pm} \rangle^2 = \frac{\tanh(\varepsilon) - \varepsilon \, sech^2(\varepsilon)}{\varepsilon^3} \tau_B^2 \tag{A.30}$$

In our computer simulations, d, q, 2kT and τ_B are chosen as the units of the length,

charge, energy and time, respectively.

A.2 One Absorbing and One Reflecting Wall

Let us consider a random walk in the interval (0, L) as defined before but with the modification that whenever the particle is at L-a_0 it has probability q of moving to L-2a_0 and probability p to stay at L-a_0. We can imagine a wall placed at L-a_0/2 with the property that a particle moving from L-a_0 toward L is reflected at the wall and returns to L-a_0 instead of reaching L.

Let P(x) be the probability that a particle starting at x will get absorbed. Notice that the particle can only get absorbed at 0 now. P(x) satisfies difference equation (A.1) and the boundary condition (A.2) for the left wall but now with a different boundary condition for the right wall:

$$P(L) = P(L-a_0) \tag{A.31}$$

We expand Eq. (A.31) (up to terms of first order) when $a_0 \to 0$ and get

$$P'(L) = 0 \tag{A.32}$$

The solution to Eq. (A.4), under conditions (A.2) and (A.32), is

$$P(x) = 1 \tag{A.33}$$

as expected.

Now, let t(x) be the mean time required for absorption. The difference equation for t(x) is[4]

$$t(x) = p\ t(x+a_0) + q\ t(x-a_0) + t_0 \tag{A.34}$$

with boundary conditions

$$t(0) = 0 \tag{A.35}$$

and

$$t(L) = t(L-a_0) \tag{A.36}$$

By Taylor's expansion, Eqs. (A.34) and (A.36) become

$$D\ t''(x) + v\ t'(x) + 1 = 0 \tag{A.37}$$

and

$$t'(L) = 0 \tag{A.38}$$

where D and v are defined as before. The solution to Eq. (A.37), under conditions (A.35) and (A.38), is

$$t(x) = \frac{D}{v^2}\, e^{\frac{Lv}{D}} \left(1 - e^{-\frac{xv}{D}}\right) - \frac{x}{v} \tag{A.39}$$

When a particle moving on the lattice hits an immobile obstacle (suppose the obstacle is at the right-hand side of the particle), it cannot move forward anymore. The only possibility is to move backward a distance d. So we put L=d and x=d and get the mean time of absorption (or mean jumping time):

$$t = \frac{e^{2\varepsilon} - 2\varepsilon - 1}{2\varepsilon^2}\,\tau_B \qquad \text{(A.40)}$$

where ε and τ_B are defined as before.

To obtain the variance of the absorption time σ_t^2, we use the following interesting trick which we developed (other approaches can be used): Suppose the particle is initially at an arbitrary position x between two absorbing walls located at 0 and L, as described before. The probabilities of jumping backward and forward are $P_-(x)$ and $P_+(x)$ (Eqs. (A.7) and (A.8)), respectively; and the mean times of the particle being absorbed at 0 and L are $\langle t_-(x)\rangle$, $\langle t_-^2(x)\rangle$ and $\langle t_+(x)\rangle$, $\langle t_+^2(x)\rangle$ (Eqs. (A.18), (A.21) and (A.22) (A.23)). When it reaches the right wall, we replace the particle back to its initial position and let it diffuse again. Finally the particle will get absorbed by the left wall: it may be absorbed directly with probability $P_-(x)$; or absorbed after one replacement with probability $P_+(x)P_-(x)$; or absorbed after two replacements with probability $P_+^2(x)P_-(x)$; ...; and so on. Therefore, the variance of the absorption time for this curious (very artificial) process can be expressed as

$$\sigma_t^2(x) \sim P_-(x)\,\sigma_{t_-}^2(x) + P_+(x)\,P_-(x)\left[\sigma_{t_+}^2(x) + \sigma_{t_-}^2(x)\right]$$

$$+ P_+^2(x)\,P_-(x)\left[2\sigma_{t_+}^2(x) + \sigma_{t_-}^2(x)\right] + \cdots$$

$$= \sum_{n=0}^{\infty} P_+^n(x)\,P_-(x)\left[n\,\sigma_{t_+}^2(x) + \sigma_{t_-}^2(x)\right]$$

$$= \frac{P_+(x)}{P_-(x)}\,\sigma_{t_+}^2(x) + \sigma_{t_-}^2(x) \tag{A.41}$$

Besides, we must consider the variance of the number of times ($\sigma_n^2(x)$) that the particle is replaced to its initial position. Note that the particle "loses" a time duration $<t_+(x)>$ each time it is put back to its starting point. So we write

$$\sigma_t^2(x) \sim \sigma_n^2(x)\,\langle t_+(x)\rangle^2$$

$$= \left[\langle n^2(x)\rangle - \langle n(x)\rangle^2\right]\langle t_+(x)\rangle^2 \tag{A.42}$$

where

$$\langle n(x)\rangle = 0\,P_-(x) + 1\,P_+(x)\,P_-(x) + 2\,P_+^2(x)\,P_-(x) + \cdots$$

$$= \sum_{n=0}^{\infty} n\,P_+^n(x)\,P_-(x)$$

$$= \frac{P_+(x)}{P_-(x)} \tag{A.43}$$

and

$$\langle n^2(x)\rangle = \sum_{n=0}^{\infty} n^2\,P_+^n(x)\,P_-(x)$$

$$= 2\,\frac{P_+^2(x)}{P_-^2(x)} + \frac{P_+(x)}{P_-(x)} \tag{A.44}$$

Combining Eqs. (A.41) and (A.42), we obtain

$$\sigma_t^2(x) = \left[\frac{P_+(x)}{P_-(x)}\ \sigma_{t_+}^2(x) + \sigma_{t_-}^2(x)\right] + \left[\frac{P_+^2(x)}{P_-^2(x)} + \frac{P_+(x)}{P_-(x)}\right]\langle t_+(x)\rangle^2$$

$$= \left\langle t_-^2(x)\right\rangle - \langle t_-(x)\rangle^2 + \frac{P_+(x)}{P_-(x)}\left\langle t_+^2(x)\right\rangle + \frac{P_+^2(x)}{P_-^2(x)}\langle t_+(x)\rangle^2 \qquad \textbf{(A.45)}$$

Taking the limit $\sigma_t^2(x)|_{x\to l}$ and then putting L be equal to the lattice parameter d, we finally obtain

$$\sigma_t^2 = \frac{e^{4\varepsilon} + 4\,(1 - 2\,\varepsilon)\,e^{2\varepsilon} - 4\,\varepsilon - 5}{4\,\varepsilon^4}\,\tau_B^2 \qquad \textbf{(A.46)}$$

where ε and τ_B are defined as before.

Equations (A.24), (A.25), (A.27), (A.30), (A.33), (A.40) and (A.46) are used in our computer simulations (see Chapter 2).

References

[1] Arvanitidou, E., Hoagland, D. and Smisek, D., "Mobility Models for Stiff and Flexible Macromolecules in Dilute Gels", *Biopolymers*, **31**, 435 (1991).

[2] Desruisseaux, C. and Slater, G.W., "Simple Model of Trapping Electrophoresis with Complicated Transient Dynamics", *Phys. Rev. E*, **49**, 5885 (1994).

[3] Einstein, A., "On the Movement of Small Particles Suspended in a Stational Liquid Demanded by the Molecular-Kinetic Theory of Heat", *Ann. d. Phys.*, **17**, 549 (1905).

[4] Feller, W., *An Introduction to Probability Theory and Its Applications, Vol.1* (2nd ed., John Wiley & Sons, New York 1957), pp.311-327.

[5] Gardiner, C.W., *Hand book of Stochastic Methods for Physics, Chemistry and the Nature Sciences*, (Springer-Verlag, Berlin 1983), pp.118-143.

[6] Gradshteyn, I.S. and Ryzhik, I.M., *Table of Integrals, Series and Products*, (Academic, San Diego 1979), p.40.

[7] Griess, G.A., Moreno, E.T., Easom, R.A. and Serwer, P., "The Sieving of Spheres During Agarose Gel Electrophoresis: Quantitation and Modeling", *Biopolymers*, **28**, 1475 (1989).

[8] Griess, G.A., Moreno, E.T., Herrmann, R. and Serwer, P., "The Seiving of Rod-Shaped Viruses During Agarose Gel Electrophoresis: I. Comparison with the Sieving of Spheres", *Biopolymers*, **29**, 1277 (1990).

[9] Griess, G.A., Guiseley, K.B. and Serwer, P., "The Relationship of Agarose Gel Structure

to the Seiving of Spheres during Agarose Gel Electrophoresis", *Biophys. J.*, **65**, 138 (1993).

[10] Han, J. and Herzfeld, J., "Macromolecular Diffusion in Crowded Solutions", *Biophys. J.*, **65**, 1155 (1993).

[11] Johansson, L. and Lofroth, J.-E., "Diffusion and Interaction in Gels and Solutions: 4. Hard Sphere Brownian Dynamics simulations", *J. Chem. Phys.*, **98**, 7471 (1993).

[12] Jonsson, B., Wennerstrom, H.,Nilsson, P.G. and Linse, P., *Colloid Polym. Sic.*, **264**, 77 (1986).

[13] Lunney, J., Chrambach, A. and Rodbard, D., "Factors Affecting Resolution, Band Width, Number of Theoretical Plates, and Apparent Diffusion Coefficients in Polyacrylamide Gel Electrophoresis", *Anal. Biochem.*, **40**, 158 (1971).

[14] Morris, C.J.O.R., in: Peeters, H. (editor), *Protides of the Biological Fluids, Vol. 14* (Elsevier, New York 1967), p.543.

[15] Nieuwenhuizen, T.M., van Velthoven, P.F.J. and Ernst, M.H., "Diffusion and Long-time Tails in a Two-dimensional Site-percolation Model", *Phys. Rev. Lett.*, **57**, 2477 (1986).

[16] Nilsson, L.G., Nordenskiold, L., Stibs, P. and Braunlin, W.H., *J. Phys. Chem.*, **89**, 3385 (1985).

[17] Noolandi, J., Rousseau, J. and Slater, G.W., "Self-Trapping and Anomalous Dispersion of DNA in Electrophoresis", *Phys. Rev. Lett.*, **58**, 2428 (1987).

[18] Ogston, A.G., "The Spaces in a Uniform Random Suspension of Fibres", *Trans. Faraday Soc.*, **54**, 1754 (1958).

[19] Phillies, G.D.J. and Clomenil, D., "Probe Diffusion in Polymer Solutions under θ and

Good Conditions", *Macromolecules*, **26**, 167 (1993).

[20] Phillips, C.G., *J. Chem. Phys.*, **95**, 4593 (1991).

[21] Rodbard, D. and Chrambach, A., "Unified Theory for Gel Electrophoresis and Gel Filtration", *Proc. Nat. Acad. Sci.* (USA), **65**, 970 (1970).

[22] Rousseau, J., *A Generalized Reptation Model of DNA Gel Electrophoresis* (M.Sc. thesis, University of Waterloo 1988), pp.102-111.

[23] Saxton, M.J., "Lateral Diffusion in an Archipelago: The Effect of Mobile Obstacles", *Biophys. J.*, **52**, 989 (1987).

[24] Saxton, M.J., "Lateral Diffusion and Aggregation", *Biophys. J.*, **61**, 119 (1992).

[25] Saxton, M.J., "Lateral Diffusion in an Archipelago: Dependence on Tracer Size", *Biophys. J.*, **64**, 1053 (1993).

[26] Saxton, M.J., "Anomalous Diffusion Due to Obstacles: A Monte Carlo Study", *Biophys. J.*, **66**, 394 (1994).

[27] Serwer, P. and Griess G.A., "Large Particle Gel Electrophoresis", *Analusis Magazine*, **21**, M16 (1993).

[28] Slater, G.W., Rousseau J. and Noolandi J., "On the Stretching of DNA in the Reptation Theories of Gel Electrophoresis", *Biopolymers*, **26**, 863 (1987).

[29] Slater, G.W. and Noolandi J., "The Biased Reptation Model of DNA Gel Electrophoresis", in: Lee, L.-H. (editor), *New Trends in Physics and Physical Chemistry of Polymers* (Proceedings of the International Symposium, Plenum, New York and London 1989), pp.547-600.

[30] Slater, G.W. and Villeneuve, C., "A Computer Simulation of Trapping Electrophoresis",

J. Polym. Sci. B, **30**, 1451 (1992).

[31] Slater, G.W., "Theory of Band Broadening for DNA Gel Electrophoresis and Sequencing", *Electrophoresis*, **14**, 1 (1993).

[32] Slater, G.W. and Guo, H.L., "Ogston Gel Electrophoretic Seiving: How is the Fractional Volume Available to a Particle Related to its Mobility and Diffusion Coefficient(s)?", accepted for publication in *Electrophoresis*.

[33] Slater, G.W., Villeneuve, C., Guo, H.L., Desruisseaux, C and Drouin, G., "Trapping Gel Electrophoresis of End-labeled DNA: An Analytical Model for Constant Fields", submitted to *Electrophoresis*.

[34] Tietz, D., "Evaluation of Mobility Data Obtained from Gel Electrophoresis: Strategies in the Computation of Particle and Gel Properties on the Basis of the Extended Ogston Model", in: Chrambach, A., Dunn, M.J., and Radola, B.J. (editor), *Advances in Electrophoresis, Vol.2* (VCH, Weinheim 1988), pp.109-169.

[35] To, K.-Y. and Boyde, T.R.C., "Pulsed-field Acceleration: The Electrophoretic Behavior of Large Spherical Particles in Agarose Gels", *Electrophoresis*, **14**, 597 (1993).

[36] Wheeler, D. and Chrambach, A., "The Fractional Volume Available to Prolate Spheroids in a Network of Randomly Oriented Fibers Obtained by Computer Modeling: Correlation with the Ogston Equation", *Electrophoresis*, **14**, 993 (1993).